MAGNETOTELLURIC SURVEY

ON THE

GLASS BUTTES GEOTHERMAL EXPLORATION PROJECT

LAKE COUNTY, OREGON

FOR

ORMAT TECHNOLOGIES INC.

DATA ACQUISITION REPORT

ZONGE JOB# 2010.181

ISSUE DATE: 31 AUGUST 2011

ZONGE GEOSCIENCES INC.
924 Greg Street
Sparks, Nevada 89431

Table of Contents

LIST OF FIGURES (A5-A33 included in Appendix A)

MAGNETOTELLURIC SURVEY

ON THE

GLASS BUTTES PROJECT

INTRODUCTION

Zonge Geosciences, Inc. performed a magnetotelluric (MT) survey for the Glass Buttes Project at the request of Ormat Technologies Inc. The survey area is located in Lake County, Oregon. The objective of the survey was to collect deep electromagnetic data to assist Ormat Technologies in assessing potential geothermal resources in the area.

This survey was conducted during the period of 7 October 2010 to 8 November 2010 and is covered under Zonge job number 2010.181.

The survey area is located in T23S, R21-23E and lies within the Glass Butte and Hat Butte, Oregon 1:24,000 topographic sheets. Tensor magnetotelluric data were acquired at 30 stations in the eastern survey area and array MT data were acquired along one line, 6.8 kilometers in length in the western survey area. Station locations and location of cross-sections are shown in Figure 1 for the East Area, and in Figure 2 for the West Area.

Jerrod Davis, Geophysical crew chief for Zonge Geosciences Inc., supervised this survey in the field. A daily logistics and production log is listed in Appendix B.

SURVEY CONTROL

Zonge personnel established survey control for this project. Stations were located using Garmin hand-held GPS model GPSMAP 60CSx. These GPS receivers are Wide Area Augmentation System (WAAS) enabled and accuracy in the field typically ranged from 2-5 meters. Line control in the field utilized UTM, Zone 10N NAD83 coordinates. Survey coordinates for the stations are in Appendix B. All map products, however, are registered in UTM, Zone 11N, NAD83.

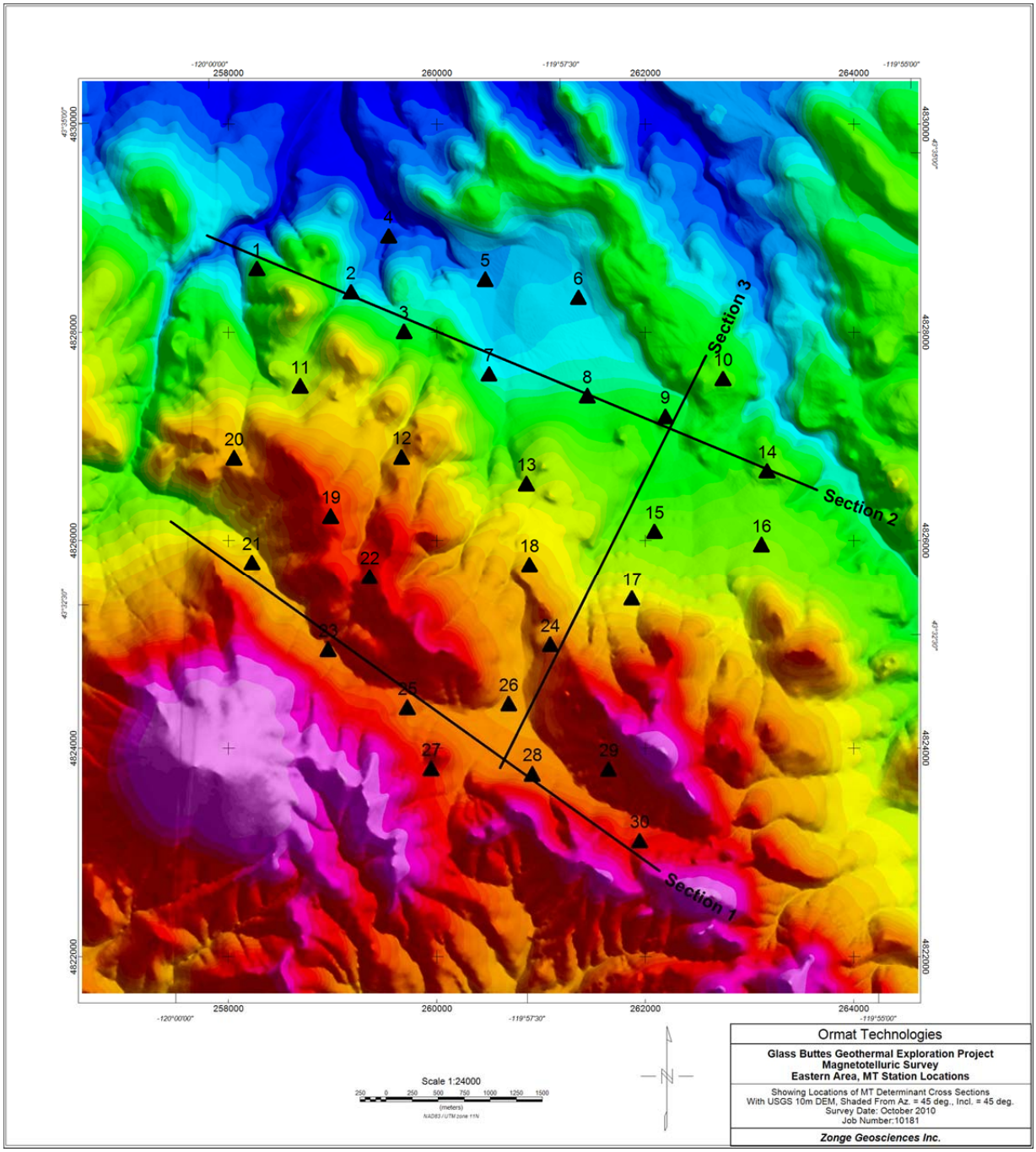

Figure 1. MT station locations overlain on topography, East Area.

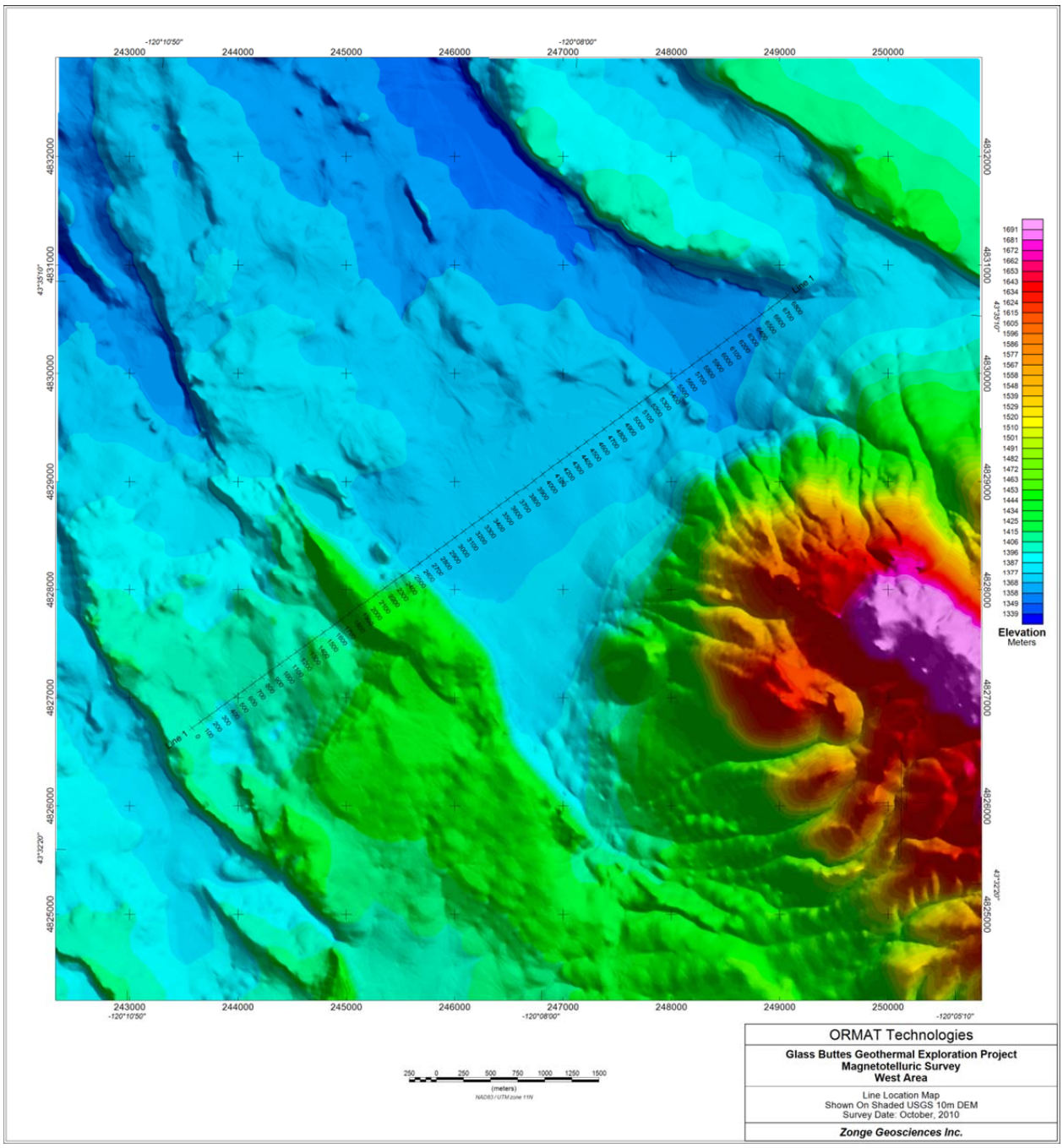

Figure 2. MT Line 1, West Area shown on USGS DEM.

DATA ACQUISITION

MT/AMT data were acquired over a frequency range of 0.0029 to 8192 Hz. The field notes in Appendix B refer to four frequency bands: low, medium, high, and very high bands.

There is some overlap in the frequency ranges. The bands are summarized in Table 1. The field crew also noted cultural features, such as fences, that could have an influence on data quality. These features are listed in Appendix B.

Table 1. AMT/MT frequency band designations.

Band Name	Designator	Frequency Range (hertz)
Low	L	0.0029 - 4
Medium	M	3 -64
High	H	48 - 1024
Very High	VH	384 - 8192

EAST AREA

Tensor MT data were acquired for the 30 stations in the East Area, shown in Figure 1. Each station consisted of two orthogonal electric-field dipoles, Ex and Ey and two magnetic antennas Hx and Hy, oriented in the East and North directions respectively. In addition a magnetic antenna (Hz) was oriented vertically.

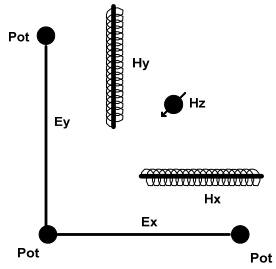

Figure 3. Tensor MT configuration.

WEST AREA

Magnetotelluric (MT) data were acquired along Line 1, shown in Figure 2, using 100-meter electric-field receiver dipoles. Measurements were made in spreads consisting of six electric-field dipoles (4 Ex/2 Ey) with the magnetic-field antennas (1 Hy/1 Hx) located in the center of the spread. The data were acquired with four electric-field dipoles (Ex) oriented along the survey line, and two electric-field dipoles (Ey) oriented perpendicular to the survey lines.

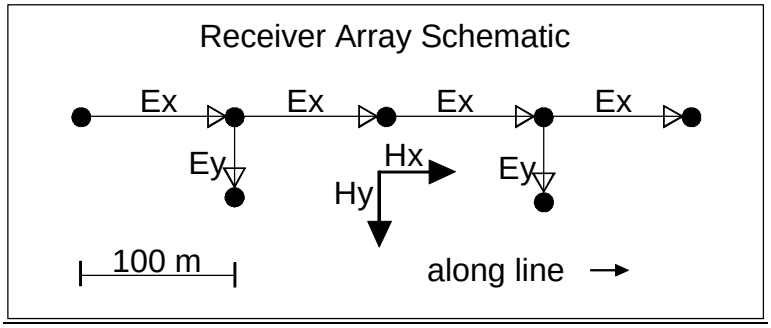

Figure 4. Tensor MT Receiver Array used for Line 1 in the Western Area.

INSTRUMENTATION

MT data were acquired with three Zonge model GDP-32/II multiple purpose receivers, serial numbers 3220, 32287, 32258 and SC-8 serial numbers SC31, SC33 and SC60. The Zonge GDP-32/II instrument is a backpack-portable, 16 bit, microprocessor-controlled receiver that can gather data on as many as eight channels simultaneously. The SC-8 is an external signal-conditioning instrument designed to provide the additional analog gain and filtering required to collect audiomagnetotelluric and magnetotelluric measurements.

The electric-field signal was measured at the receiver site using non-polarizing ceramic Cu-$CuSO_4$ porous-pot electrodes connected to the receiver with insulated 14-gauge wire. Magnetic field measurements were made with both Zonge ANT/4 and ANT/6 antennas, serial numbers 246, 276, 706, 1146, 1666, 1796, 1846, 2146, 1044, 1114, 1184, 1464, 1534, 1544, 1554, and 1564.

MT time-series data were simultaneously recorded with three GPS-synchronized GDP-32 receivers. Two of the three GDP receivers were on the site collecting data while the third receiver was at a stationary, low noise site approximately 15 km to the west of the survey area. The data acquired by each of the two on line GDP receivers was remote-referenced by the third remote GDP.

The magnetotelluric method relies on electric-field/magnetic-field ratios, termed impedances and symbolized as $Z = E/H$. Electric field values were measured as a potential difference between the endpoints of grounded dipoles. Magnetic field strengths were measured

with mu-metal-cored coils located near the receiver at the center of each sensor array. Zonge model ANT6 magnetic-field antennas were used for AMT frequencies above 3 hertz and ANT4 antennas for MT frequencies below 3 hertz. Both electric- and magnetic-field sensor signals were amplified and conditioned by a Zonge SC8 signal-conditioning preamplifier, followed by amplification, analog-to-digital conversion, processing and storage in GDP32/II geophysical data receivers.

A complete listing of instrument specifications can be found in Appendix D.

DATA PROCESSING

The MT data processing flow includes the following steps:

1. Fourier transform time-series data into the frequency domain with cascade decimation. Apply magnetic field antenna and analog gain calibration factors.
2. Group frequency domain data by frequency and presort by coherence.
3. Apply robust processing to estimate apparent resistivity, phase, coherence, and error.
4. Interactively review unaveraged data with apparent resistivity versus frequency sounding curve and complex plane point-cloud plots to deweight noisy outlier data before final averaging. Repeat values for each station are then averaged and written to ASCII avg-format files.
5. Group averaged data by line and read into program ASTATIC for further review. Interactive data review of pseudosections or individual sounding curves to set or clear skip flags marking outlier points in the averaged data.
6. Input .avg file into NSSKEW to compute tensor parameters including skew and determinant resistivity and plot impedance polar diagrams.
7. Two-dimension, smooth-model inversion of data for each line to model sections.
8 Plot data pseudosections and inversion-model sections for interpretation.

MT PARAMETER DEFINITIONS AND COMPUTATIONS

Impedance estimates for each pair of electric and magnetic field components are calculated. The impedance tensor $\overline{\overline{\mathbf{Z}}}$ relates horizontal electric and magnetic field components as

$$\begin{bmatrix} E_x \\ E_y \end{bmatrix} = \begin{bmatrix} Z_{xx} & Z_{xy} \\ Z_{yx} & Z_{yy} \end{bmatrix} \cdot \begin{bmatrix} H_x \\ H_Y \end{bmatrix}$$

or equivalently

$$E_x = Z_{xx} \cdot H_x + Z_{xy} \cdot H_y \text{ and } E_y = Z_{yx} \cdot H_x + Z_{yy} \cdot H_y .$$

Note that since E_x and E_y are associated with two different equations, estimates of Z_{xx} and Z_{xy} are separate from estimates of Z_{yx} and Z_{yy}.

Impedance magnitudes are transformed to Cagniard apparent resistivity values

$$\rho_{xy} = \frac{1}{\omega \cdot \mu} \left| Z_{xy} \right|^2 \text{ (ohm - meters)}$$

where ω is radial frequency in radians/second, μ is magnetic permeability in henries/m, and Z_{xy} is electrical impedance in ohms (Cagniard, 1953). The magnetic permeability is usually taken as the magnetic permeability of free space, μ_0.

Similarly, Z_{xx}, Z_{yx} and Z_{yy} magnitudes can be scaled to ρ_{xx}, ρ_{yx} and ρ_{yy}. The accepted scientific convention is to use SI units with electric field values in V/m and magnetic field values in A/m. But since geophysical signal strengths are so low, it is convenient to scale E-field values to nanoVolts/meter (nV/m) and H-field values to picoTesla (pT). Note that although pT values should be annotated as B-field magnetic flux density, H-field labels and pT units are used in most of Zonge's documentation and plot annotation.

Apparent resistivity and frequency can then be used to calculate an approximate depth of investigation:

$$z = 356 \cdot \sqrt{\rho / f} \quad \text{(meters)}$$

where ρ is resistivity in ohm-m and *f* is frequency in hertz, and the constant 356 comes from dividing the skin depth constant 503 by $\sqrt{2}$. Depth of investigation increases in proportion to $1/\sqrt{frequency}$ so measurements over a range of frequencies can be used to estimate resistivities over a range of depths.

Impedances are complex, therefore they have both magnitude |Z| and phase ϕ:

$$\phi_{xy} = \text{phase}\left(Z_{xy}\right) = 1000 \cdot \arctan\left(\frac{\text{imag}(Z_{xy})}{\text{real}(Z_{xy})}\right) \text{ mrad}.$$

Impedance phase is related to the change in apparent resistivity as a function of frequency:

$$\phi = 1000\frac{\pi}{4}\left(1 + \frac{\partial \log(\rho)}{\partial \log(f)}\right) \text{ mrad}.$$

Impedance phase is a measure of the slope of the apparent resistivity sounding curve, adding information about sounding curve shape at each data point. Plots of apparent resistivity sounding curves, produced by Zonge, often include impedance phase information represented as a vector posted at each data point. If impedance phase values are consistent with apparent resistivity curve shape, the posted vectors are tangent to the sounding curve.

In addition to apparent resistivity and impedance phase representations of each impedance tensor element, additional derived parameters can be constructed (Vozoff, 1987, Simpson and Bahr, 2005), of which a subset is described below.

The impedance tensor coordinate system can be rotated to generate an impedance tensor for an arbitrary (x, y) electromagnetic component orientation. Impedance tensor rotation is used to estimate electrical strike by finding an (x, y) orientation for which the magnitude of the tensor's diagonal trace is minimized, in effect identifying the EM component orientation for which the geological structure appears to be most two-dimensional. In this fashion, the strike direction θ_{min} is the E_x azimuth that minimizes $|Z_{xx}|^2 + |Z_{yy}|^2$ and maximizes $|Z_{xy}|^2 + |Z_{yx}|^2$. (In data files on the CD accompanying this report, the quantity θ_{min} is denoted MaxResEAzm.) It should be noted that the strike direction calculated in this manner is non-unique to 90 degrees.

In addition to information describing the electrical strike, parameters derived from the impedance tensor can be used to estimate the degree of multidimensionality, namely with the rotationally-invariant parameter skew:

$$skew = \frac{\left|Z_{xx} + Z_{yy}\right|}{\left|Z_{xy} - Z_{yx}\right|}$$

In one- and two-dimensional geology, the skew is near 0. Values of 0.2 or less have been used to imply one- or two-dimensional geologic structure, while areas with skew values greater than 0.3 indicate measurements near the corners of three-dimensional structure. Simpson and Bahr, (2005) argue that while values of 0.2 and greater are indicators of influence of 3D structure, values of less 0.2 cannot be used to infer that the geologic structure is two-dimensional. Skew values are shown on the data plots in Appendix B and are tabulated in the Tensor_Data.csv file, which is included on the CD-ROM.

Rotationally-invariant versions of the apparent resistivity and phase can be used to average the multidimensional information into single pseudosections and plan view presentations. The determinant apparent resistivity and phase combine impedance tensor elements into a single apparent resistivity and impedance phase values:

$$\rho_{\det} = \frac{1}{\omega \cdot \mu}\left|Z_{\det}\right|^2 \quad \text{(ohm - meters)}$$

$$\phi_{\det} = 1000 \cdot \arctan\left(\frac{imag\left(Z_{\det}\right)}{real\left(Z_{\det}\right)}\right) \text{ (mrad)}$$

where $Z_{det} = (Z_{xx}Z_{yy}\text{-}Z_{xy}Z_{yx})^{1/2}$.

Ranganayaki (1984) concluded that determinant apparent resistivity and impedance phase were the best summary parameters to use for one-dimensional, layered-earth modeling in areas with complex two- and three-dimensional geology (in the absence of more sophisticated inversion algorithms or sufficient data density). 1D inversion of the determinant resistivity are presented as plans and depth sections of the inversion resistivity.

Small-scale, near-surface resistivity structure and topography can cause a frequency independent effect termed “static shift”. Static effects shift the entire apparent resistivity sounding curve up or down without changing sounding curve shape (in log(frequency) versus

log(apparent resistivity) plots). For line-oriented surveys with continuous coverage along line static shift and topographic effects are partially accounted for by the two-dimensional smooth-model inversion algorithm. Two-dimensional topographic effects are explicitly modeled by shaping the forward-model finite-element mesh to match the along-line topographic profile. The inversion program can model small static offset effects by adding near-surface resistivity structure to the inversion model section.

Tensor parameters are calculated using Zonge's NSSKEW algorithm and are output in csv file format which is included on the data CD-ROM.

Impedance polar diagrams are presented in map view plots along with the determinant resistivity for selected frequencies. The outer curve of this plot represents the magnitude of $|Z_{xy}|$ as it is rotated through 360 degrees in 4 degree increments. The inner curve represents the magnitude of the diagonal element $|Z_{xx}|$ as described above. A circular polarization is usually considered as evidence of 1-D structure.

More detail on the MT method can be found in Appendix E: Overview of magnetotellurics. This section also includes more information on tipper quantities and phase tensors.

Static corrections to the MT data were made using transient electromagnetic (TEM) data. TEM data were acquired at each MT station for the purpose of making corrections for static shift. A 100m transmitter loop was used for the survey, with the Ex and Ey dipoles forming two sides of the square transmitter loop. Measurements of the decaying magnetic field (dB/dt) were made in the center of the loop with a Zonge TEM3 coil.

TEM in-loop sounding data were transformed into an equivalent MT sounding using a layered-earth model to link the TEM and MT geophysical data (Sternberg et al, 1988; Pellerin and Hohmann, 1990). The TEM transient is first converted into a layered-earth model using the smooth-model TEM inversion program STEMINV. STEMINV sets model layer thicknesses by calculating source-field penetration depths for each TEM time window. Layer resistivities are then iteratively adjusted until the calculated TEM response for the model is as close as possible to observed TEM data, consistent with smooth resistivity variation from one layer to the next. Results are also output as plots showing the observed and calculated transient voltage on the left

side of the plot and a curve showing the inversion results as a smoothly-varying resistivity versus depth. These plots are included on the Data CD-ROM.

STEMINV outputs the layered model parameters to a text file with the filename extension *.m1d. Program TEM2AVG reads layer thicknesses and resistivities from the *.m1d file and calculates the model MT response as Cagniard resistivity and impedance phase over a range of frequencies consistent with the transient sounding.

These converted TEM data were combined with the determinant resistivity and input into the ASTATIC program. The determinant resistivity was then shifted to match TEM curve in the range of frequency overlap. In many cases the TEM resistivity were not parallel with the MT data and the match was made to maximize the agreement over the frequency range considered to be the best quality.

The static-corrected resistivity values are saved in the *Det.avg files along with the uncorrected resistivity values. Plots of the combined and adjusted data along with the results of the one-dimensional smooth-model inversion are included on the CD-ROM.

DATA QUALITY

Several measures of data quality are recorded in the averaged data files. Natural source signal strengths were sufficient to get good quality data over most of the survey's MT frequency range extending from .0029 to 8192 hertz. The magnetotelluric data collected during this survey are considered of generally good quality. Other than a few fences, there were few cultural noise sources in the survey areas.

Plots of the observed Cagniard resistivity and impedance phase are included in Appendix B. These plots show error bars and allow a visual evaluation of the data quality.

The Geomagnetic indices, as provided by NOAA, are included in Appendix G. These data provide information on the strength of the Geomagnetic field variations, the primary signal source at frequencies below approximately 1 hertz. The indices indicate low to moderate signal levels during the course of the survey. Very low levels (A=0) are reported for 14 October, which encompassed stations 2 and 3. A review of the curves for these stations show acceptable data quality.

1-D INVERSION

The static-corrected determinant resistivity and impedance phase data for each station were inverted to one-dimensional resistivity-depth sections using Zonge's 1-D MT inversion algorithm. The 1-D depth inversion results for several stations were then projected onto the six profile lines, and contoured to produce resistivity sections. Smooth-model 1-D inversion uses an iterative procedure to improve the match between measured field data and values calculated using a layered-earth forward model algorithm. At each iteration, layer resistivities are adjusted to improve the fit with field data, while maintaining a smoothly varying layer-to-layer resistivity structure. The results of the smooth-model inversion are intentionally gradational, rather than showing abrupt changes in the subsurface resistivity. This approach allows automated imaging without a-priori information about geologic structure. Smooth-model inversion sections may include imaging artifacts if the line crosses or passes adjacent to three-dimensional structure, or the line is not oriented perpendicular to geo-electric strike.

For conciseness, plots showing the apparent resistivity and the smooth-model inversion results are included on the Data CD-ROM.

2-D INVERSION

The MT data for the West Area survey have been inverted for a two-dimensional resistivity structure using the program SCS2D developed by Zonge Engineering. The results are presented as sections of resistivity versus depth.

The smooth-model inversion is a technique for estimating the resistivity variation with depth from the raw Cagniard resistivity and impedance phase data. The depth of penetration of the electromagnetic field is dependent on the ground resistivity and the frequency of the EM signal. By design, the smooth-model inversion produces the smoothest resistivity variation that can fit the data within specified smoothness and error tolerances. Therefore, sharp resistivity boundaries in the subsurface are observed as relatively broad resistivity gradients in the smooth-model sections. Results are presented as colored contour sections of smooth-model resistivity versus depth.

The forward calculations are based on a finite element algorithm of Wannamaker (1987). This program calculates the response of smooth two-dimensional resistivity variations. The program also incorporates and corrects for the distortion of the field caused by the two-dimensional topography along the line.

Results of the 2D inversion for Line 1 are presented as sections of inversion resistivity versus depth. Two results are provided. A cross-section of inversion results using only the Zxy (ExHy) as measured with Ex in the down line (northeast) direction, and assumed to be TM-mode is shown in Figure A29. A second section showing inversion results which utilized both the Zxy and the cross-line Zyx, assumed to reflect TM and TE modes, respectively, are shown in Figure A30.

DATA PRESENTATION

Plots of the observed Cagniard resistivity and impedance phase are provided in Appendix B. These plots show error bars and allow a visual evaluation of the data quality. Also included on these plots are the Tipper magnitude, skew, and impedance ellipticity.

A map showing the locations of MT stations for the East Area is shown in Figure 1 and A5. Also shown on this map are the locations of cross sections of 1D inversion resistivity versus elevation.

Contoured plans of the one-dimensional inversion resistivity are shown for elevations of 1000, 800, 600, 400, 200, 0, -200, -400, -800, -1200, -1600 and -2800 meters in figures A6 through A16. Sections of the one-dimensional inversion results are shown in Figures A17 through A19.

Plan maps of the impedance polar diagrams are shown for frequencies of 4096, 512, 32, 4, 1, 0.125, 0.0625, and .00059 Hertz in figures A21 through A27.

A map showing the location of Line 1 in the West Area is shown in Figure 2 and A28.

Results of two-dimensional smooth-model inversion are shown as sections of inversion resistivity versus depth for the Zxy, (TM mode) in Figure A29 and the combined Zxy and Zyx

(TM and TE modes) in Figure A30. The observed Cagniard resistivity and impedance phase for the Zxy and Zyx, are shown in Figures A32 and A32, respectively.

Digital data files and images are included on the Data CD-ROM. ASCII MT file format is shown in Appendix F.

SAFETY AND ENVIRONMENTAL ISSUES

No health, safety incidents or accidents occurred during the course of this survey. No environmental damage was sustained as a direct result of the survey progress. Vehicle travel was kept to existing roads.

Respectfully submitted,
ZONGE GEOSCIENCES INC.

Gary Oppliger, PhD
Senior Geophysicist

Chester S. Lide
Managing Geophysicist

REFERENCES

Cagniard, L., 1953, Basic theory of the magnetotelluric method of geophysical prospecting, Geophysics, 18, 605-635.

Gamble, T.D., Gaubau, W.M., and Clarke, J., 1985, Magnetotellurics with a remote magnetic reference: Geophysics, 50, 2245-2260.

Pellerin, L. and Hohmann, G.W., 1990, Transient electromagnetic inversion: a remedy for magnetotelluric static shifts, Geophysics, 55, 1242-1250.

Ranganayaki, R.P., 1984, An interpretive analysis of magnetotelluric data, Geophysics, 49, 1730-1748.

Simpson, F., and Bahr, K., 2005, Practical Magnetotellurics, Cambridge University Press, Cambridge, UK.

Sternberg, B.K., Washburne, J.C., and Pellerin, L., 1988, Correction for the static shift in magnetotellurics using transient electromagnetic soundings, Geophysics, 53, 1459-1468.

Vozoff, K., 1987, The magnetotelluric method, in Nabighian, M.N., ed. Electromagnetic methods in applied geophysics, Vol. 2, Society of Exploration Geophysicists, 641-711.

Wannamaker, P.E., Hohmann, G.W., and Ward, S.H., 1984, Magnetotelluric responses of three-dimensional bodies in layered earths, Geophysics, 49, 1517-1533.

APPENDIX A: Data Plots

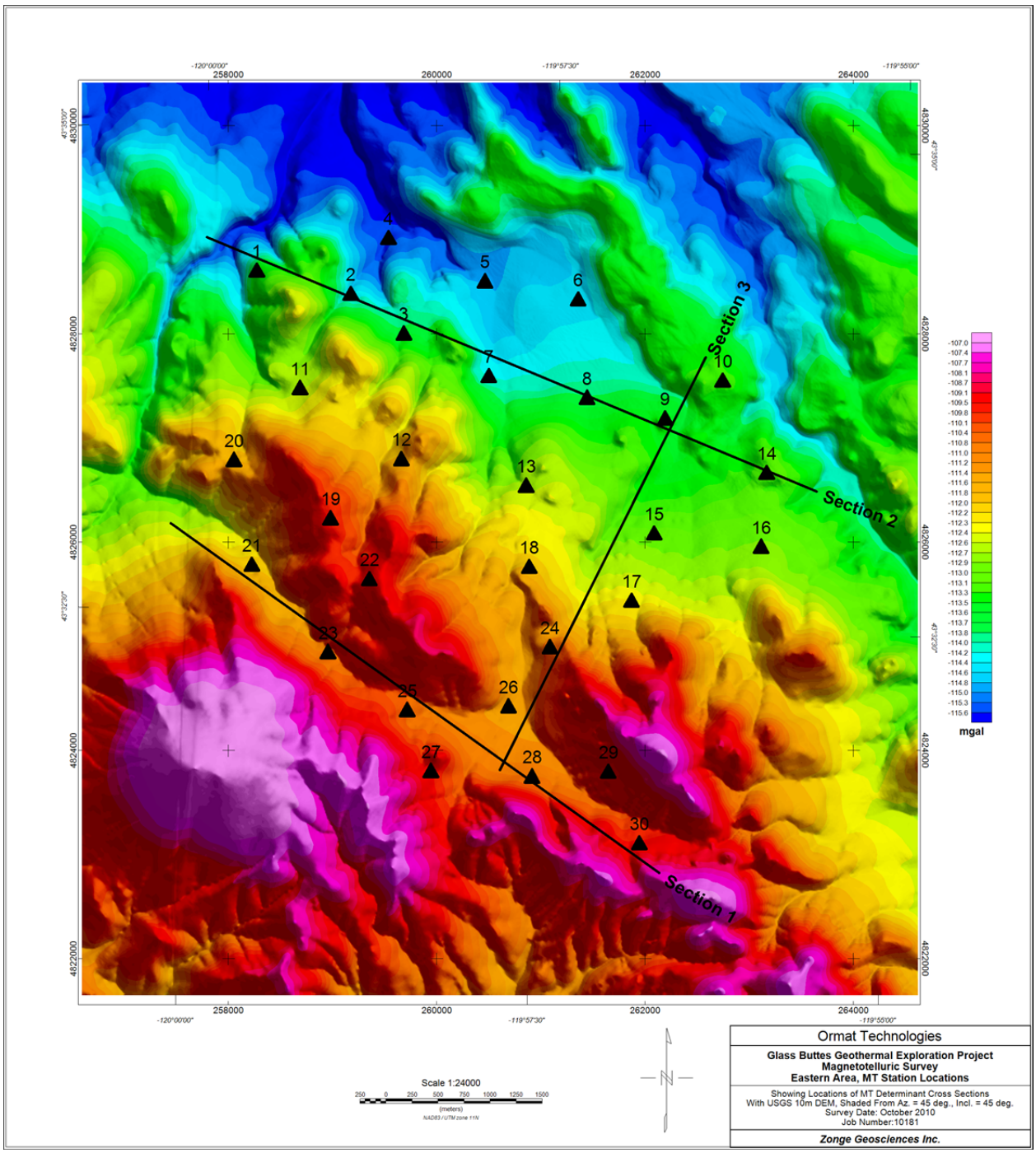

Figure A5: East Area, MT Station Locations.

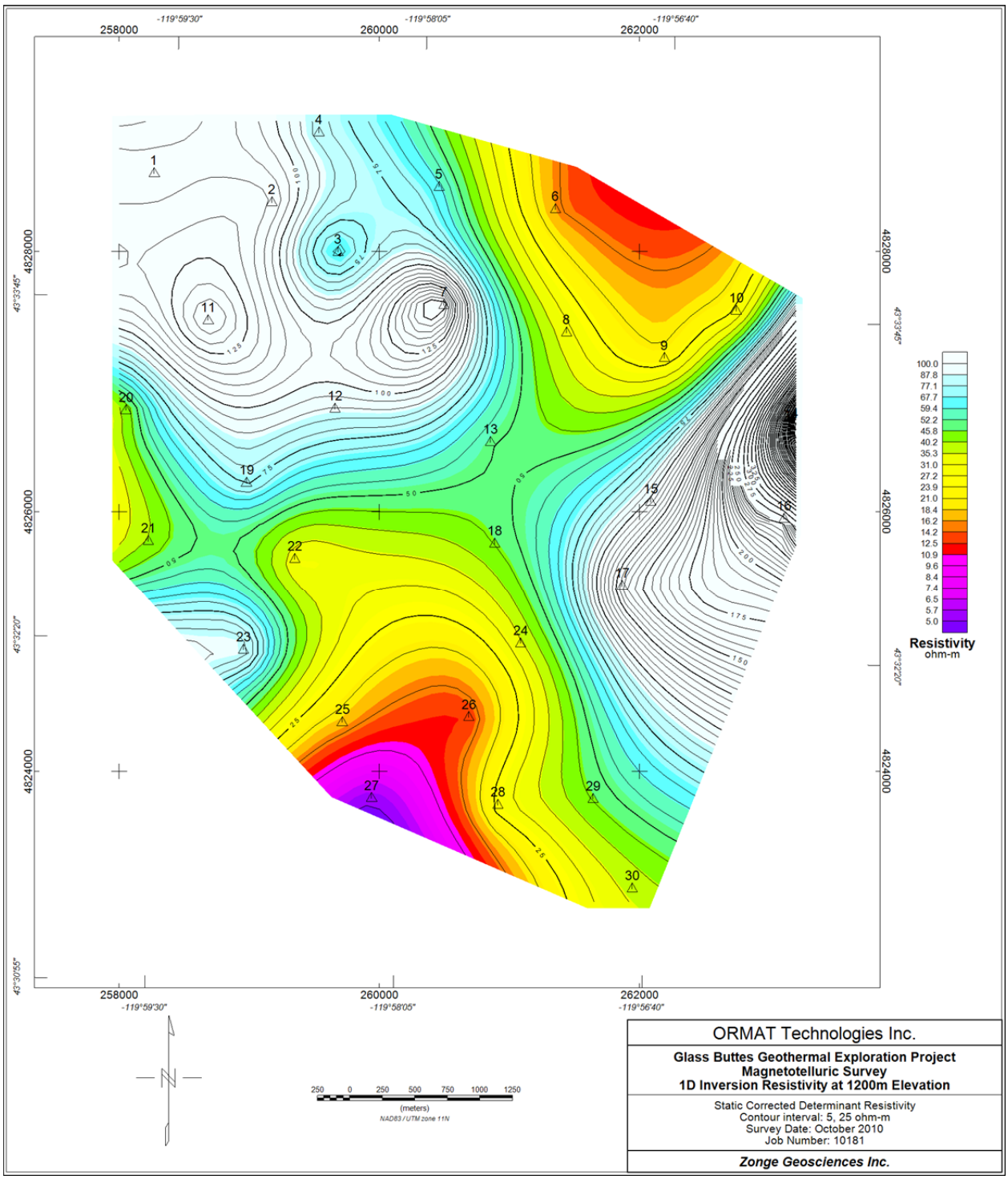

Figure A6: 1D inversion resistivity at 1200m elevation.

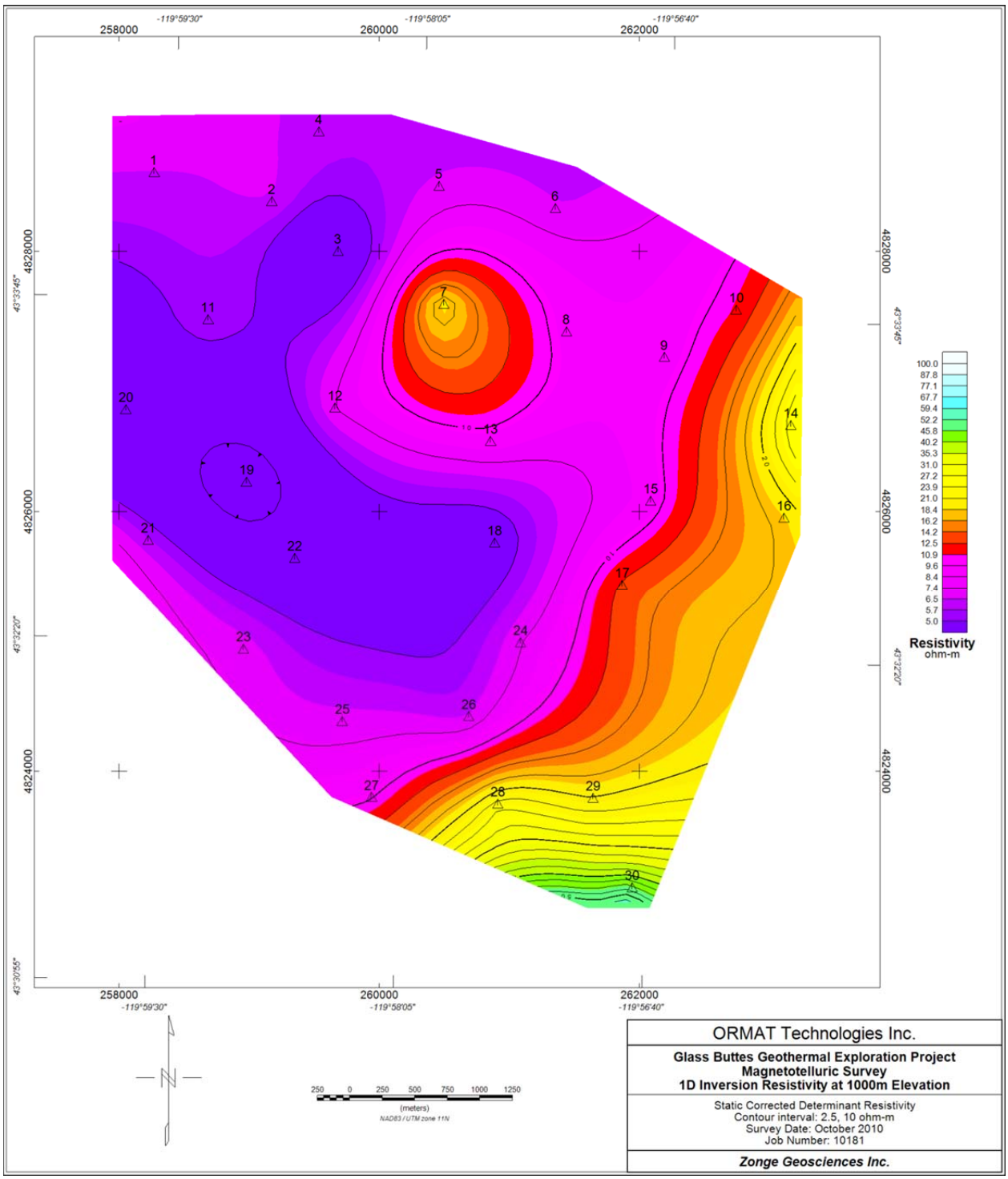

Figure A7: 1D inversion resistivity at 1000m elevation.

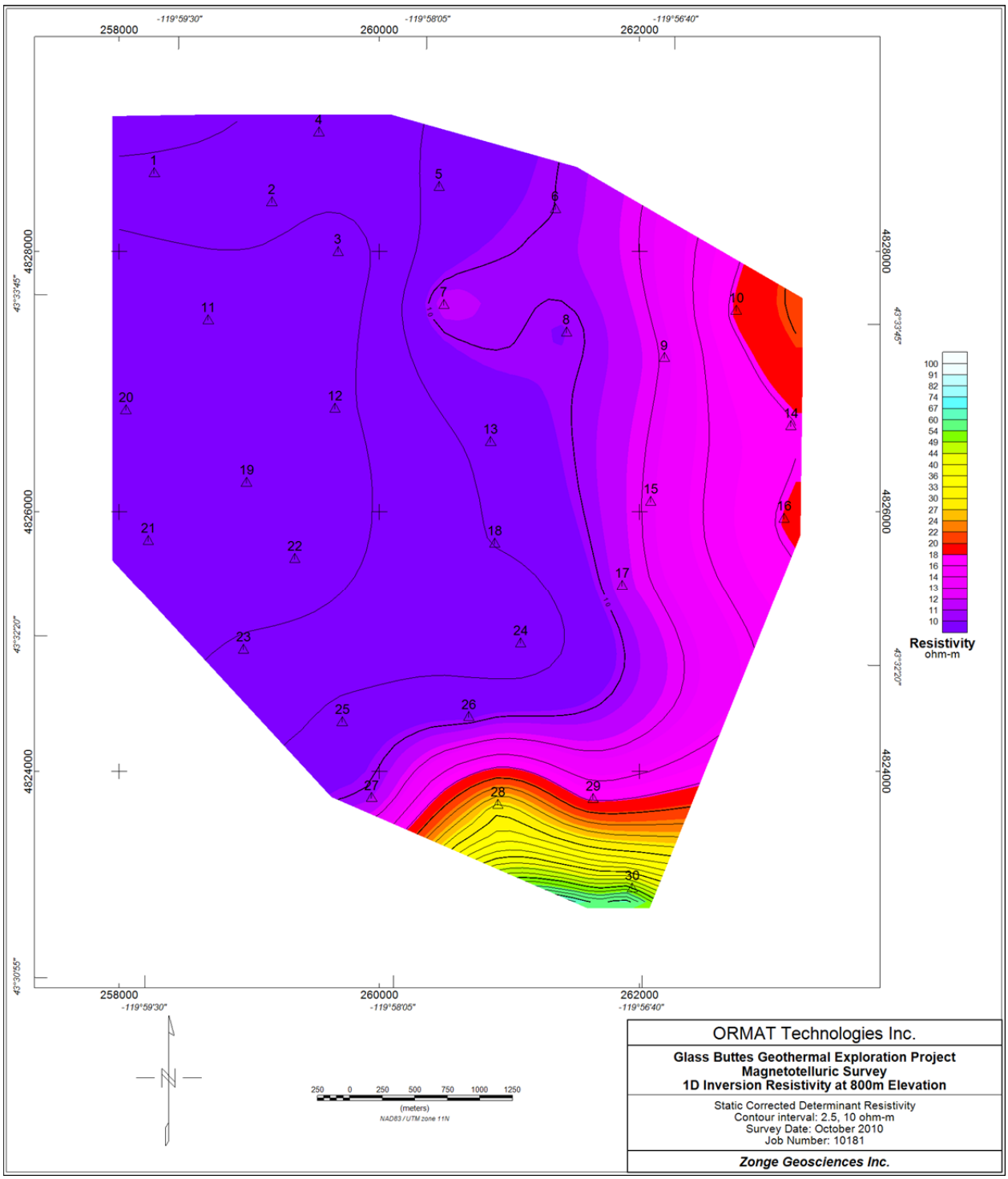

Figure A8: 1D inversion resistivity at 800m elevation.

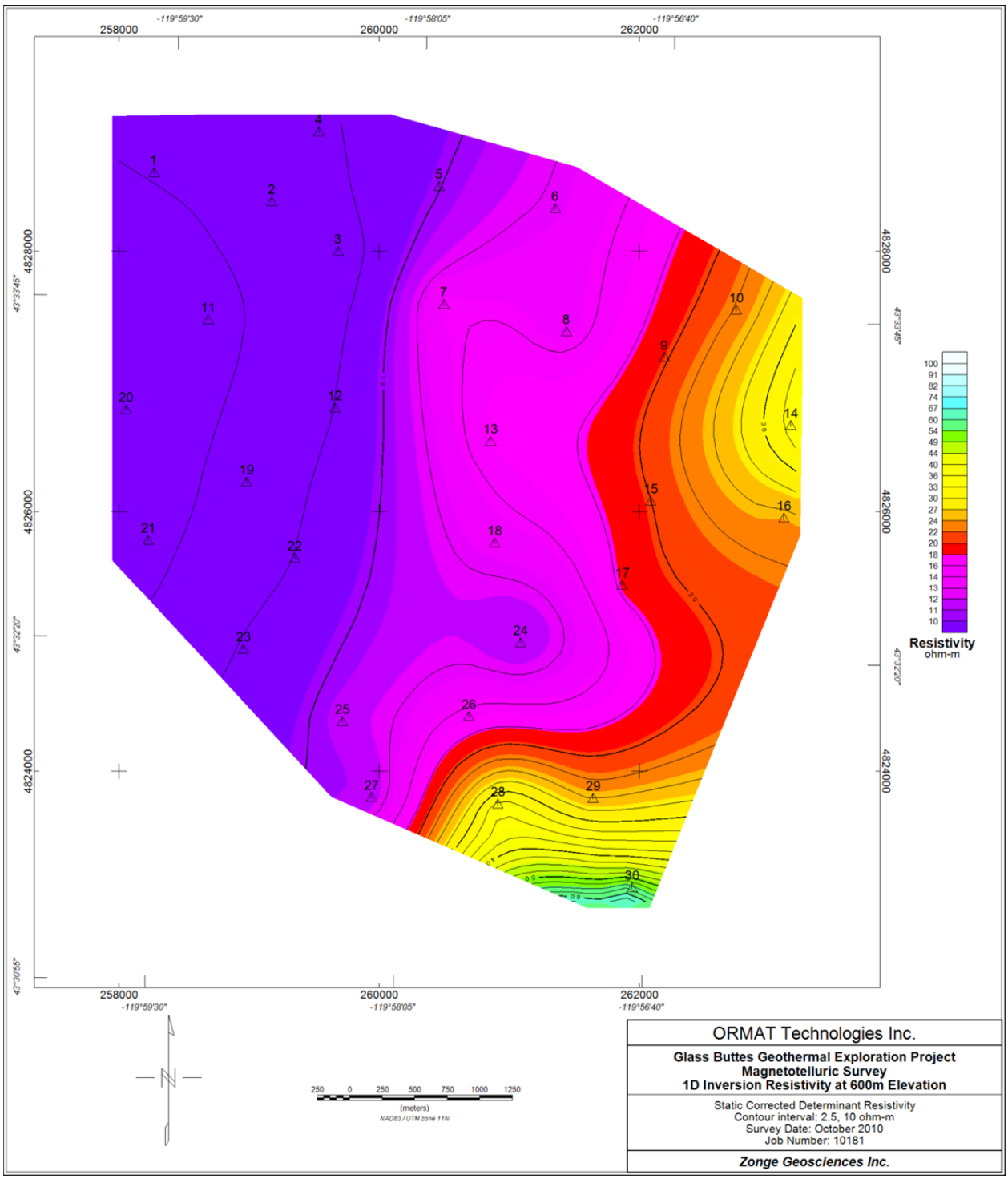

Figure A9: 1D inversion resistivity at 600m elevation.

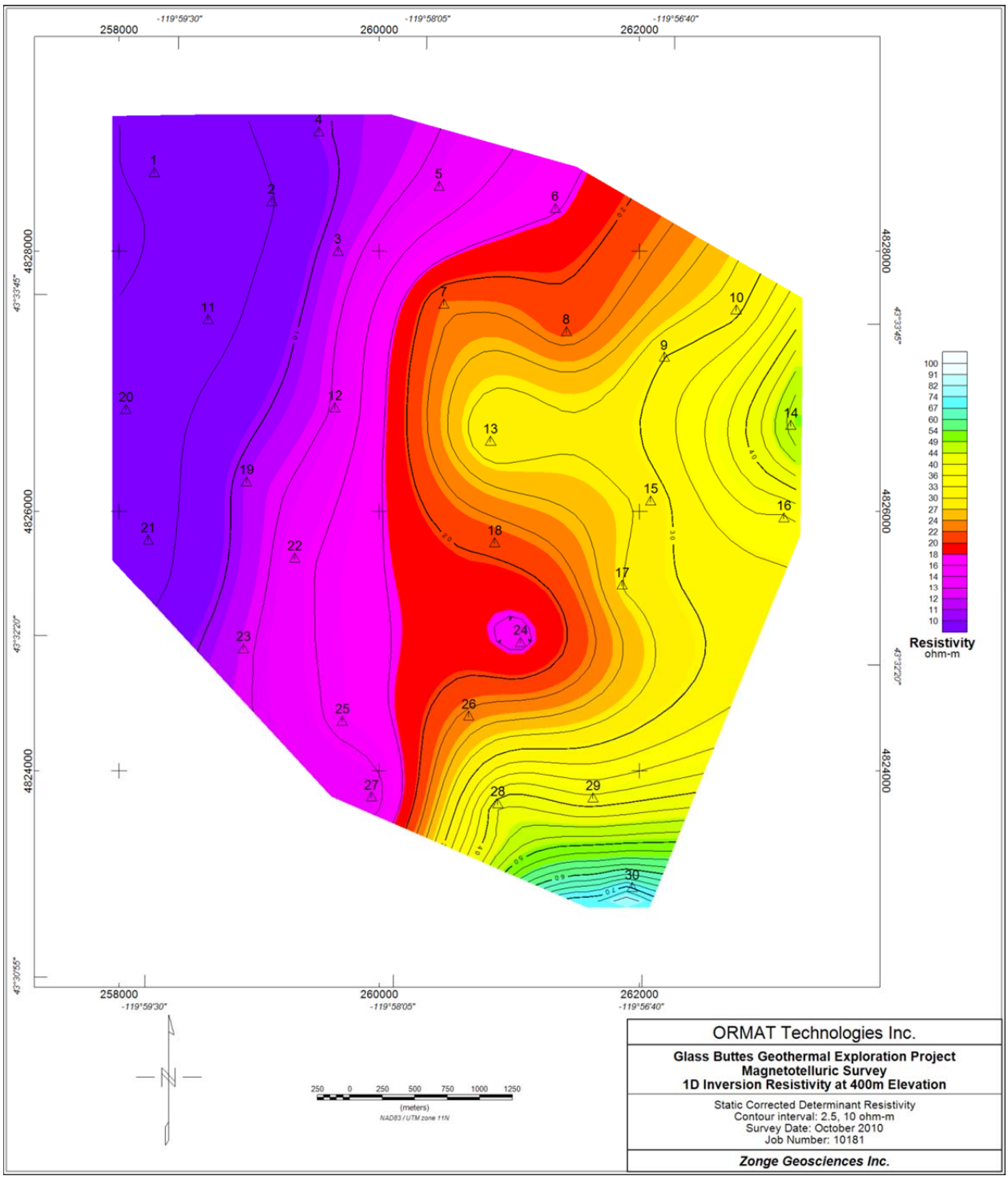

Figure A10: 1D inversion resistivity at 400m elevation.

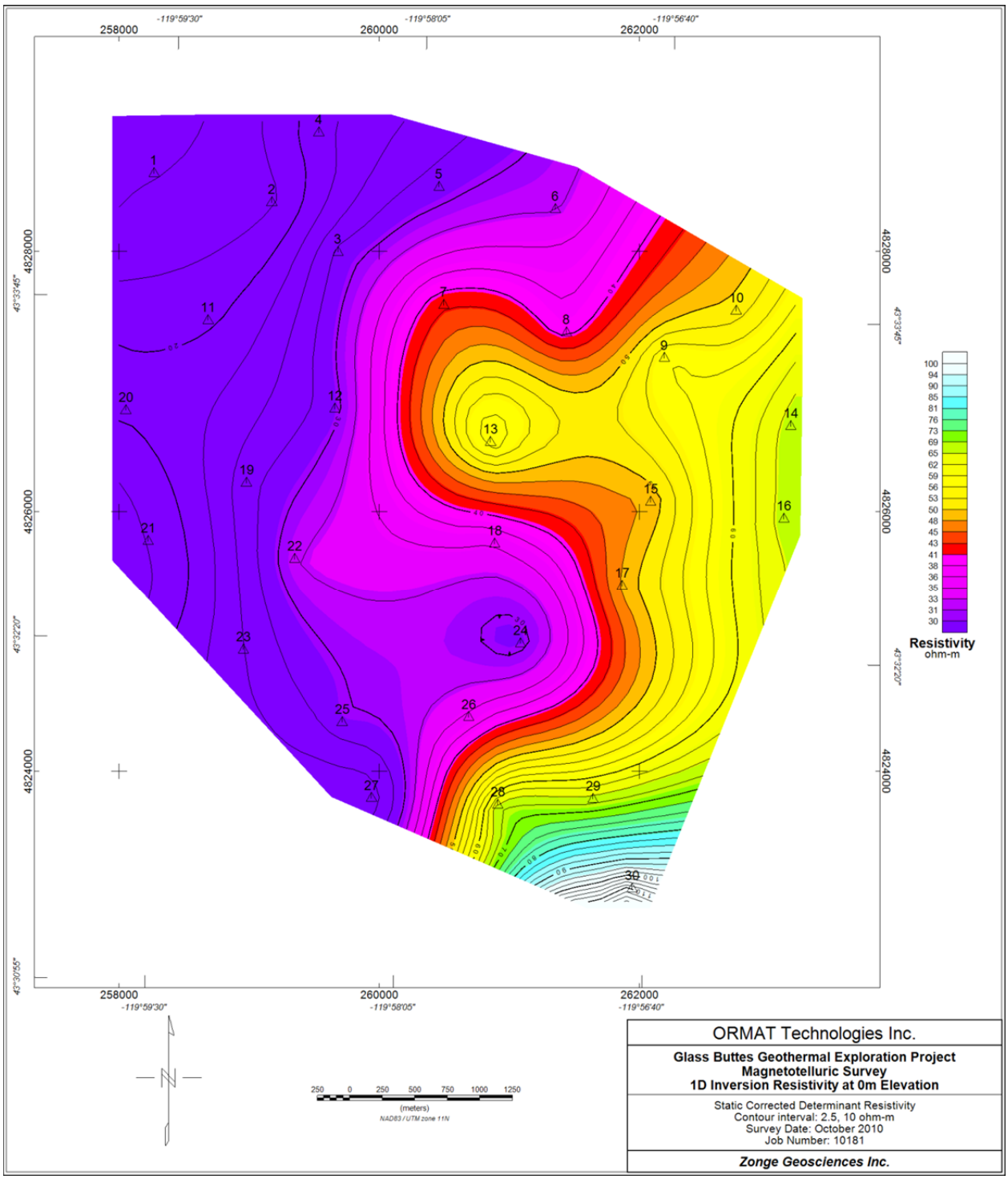

Figure A11: 1D inversion resistivity at 0m elevation.

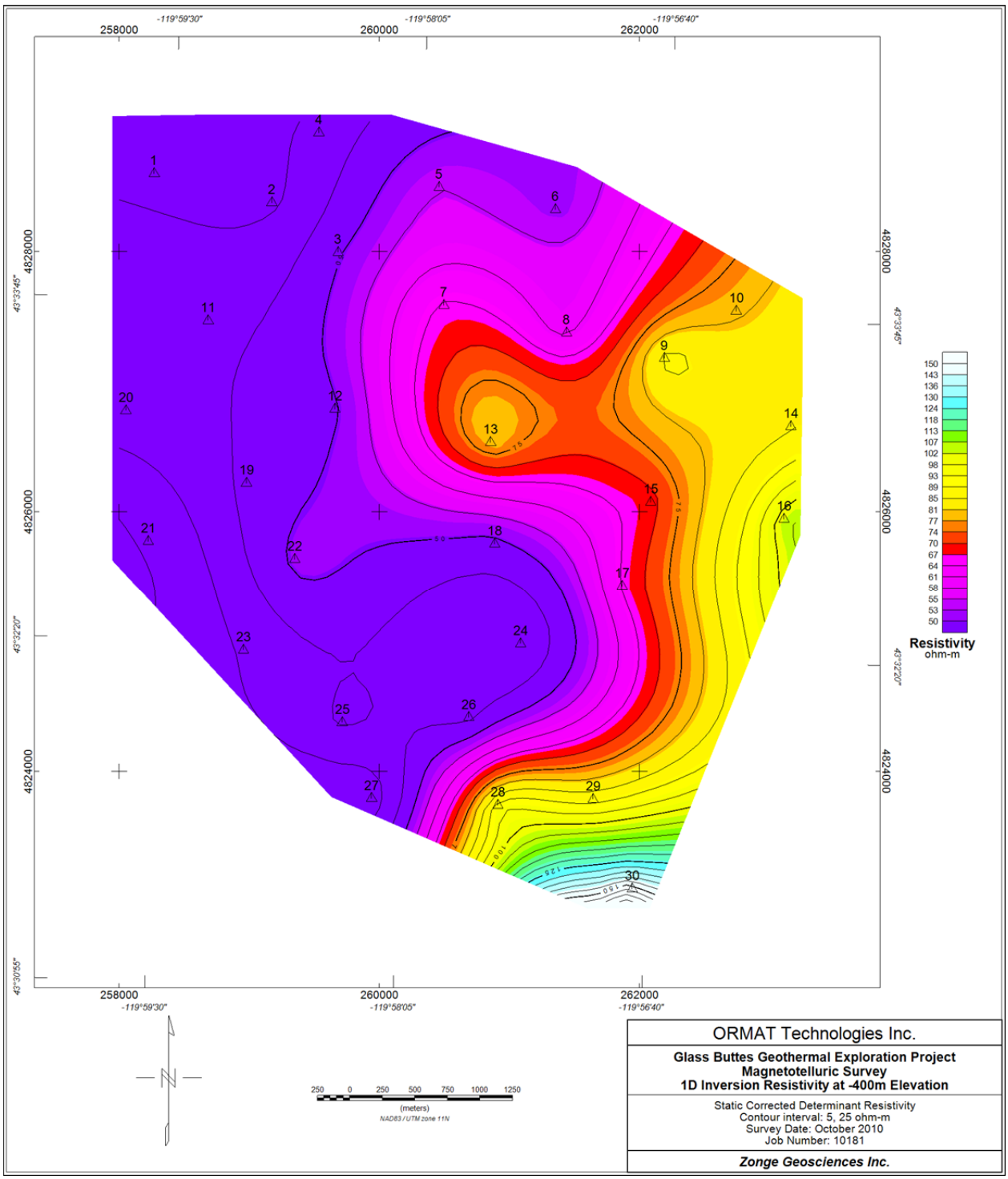

Figure A12: 1D inversion resistivity at -400m elevation.

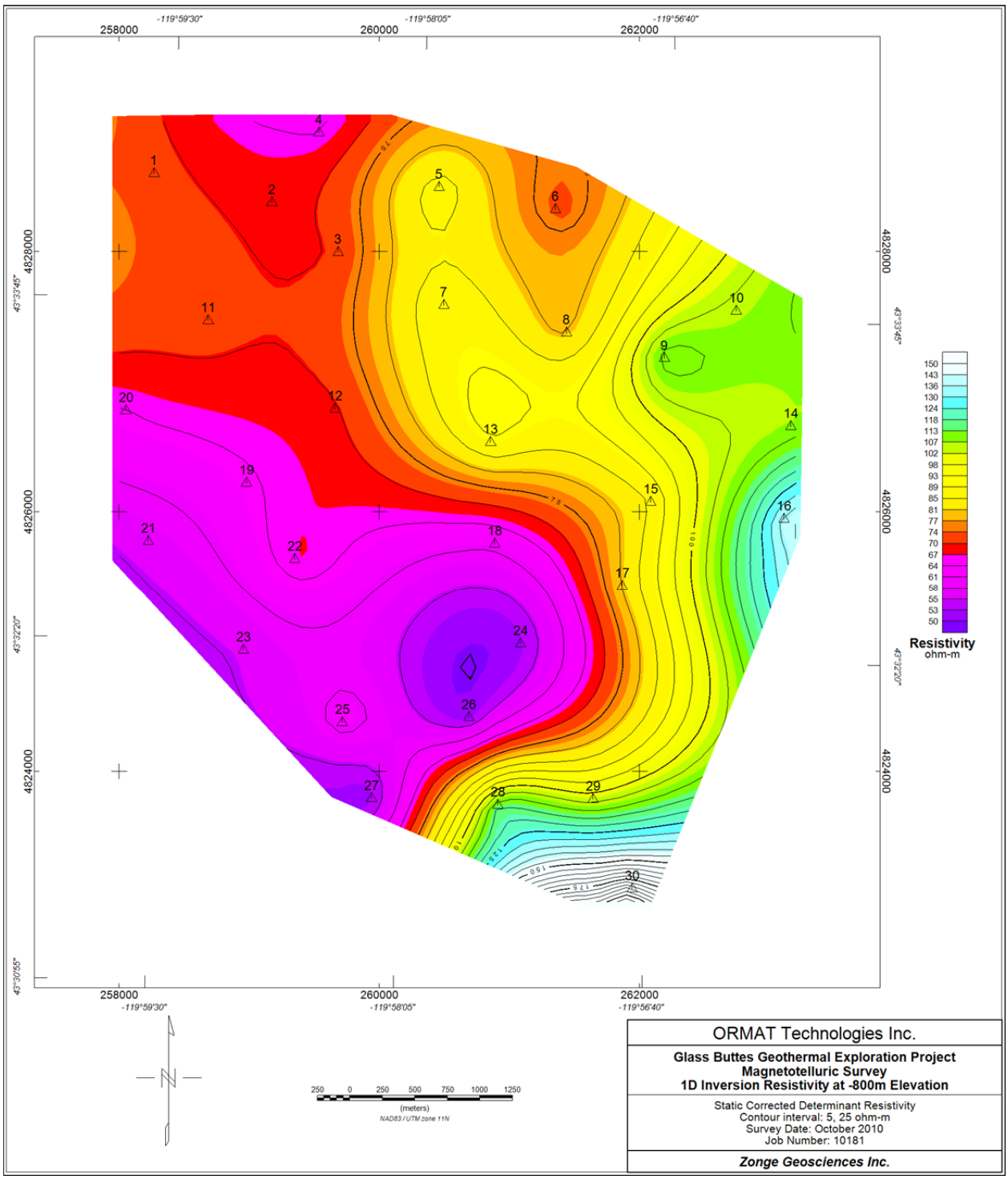

Figure A13: 1D inversion resistivity at -800m elevation.

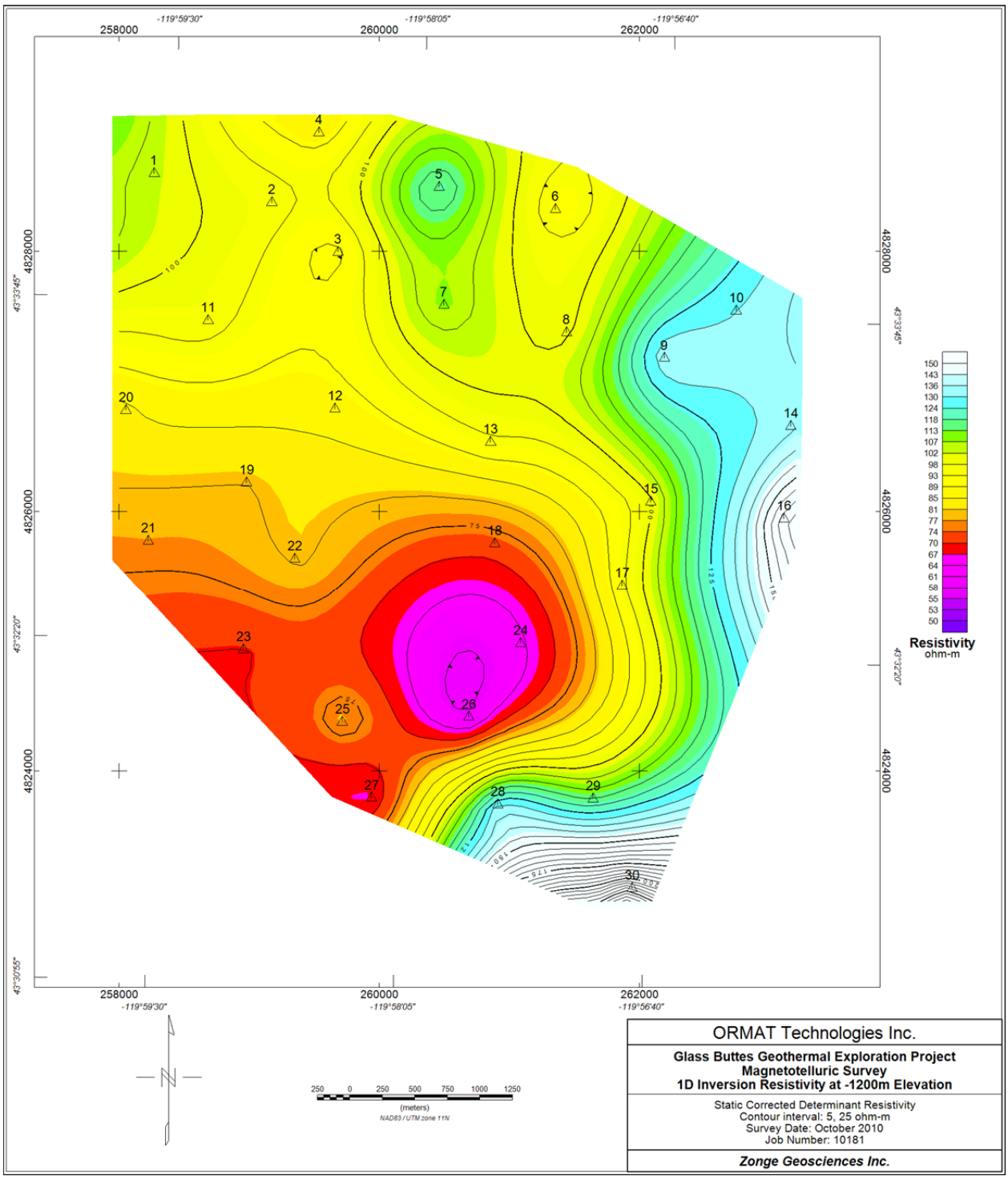

Figure A14: 1D inversion resistivity at -1200m elevation.

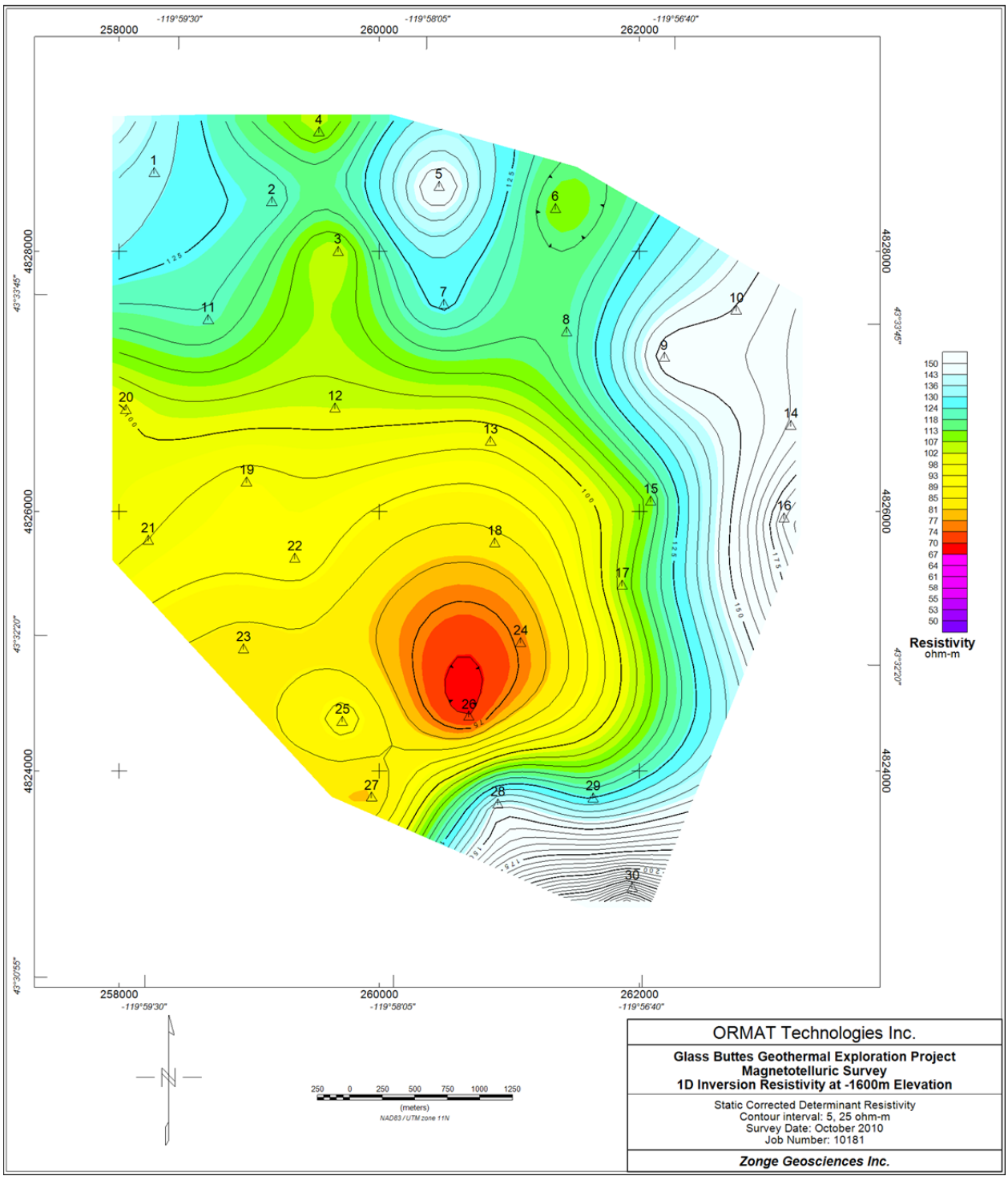

Figure A15:1D inversion resistivity at -1600m elevation.

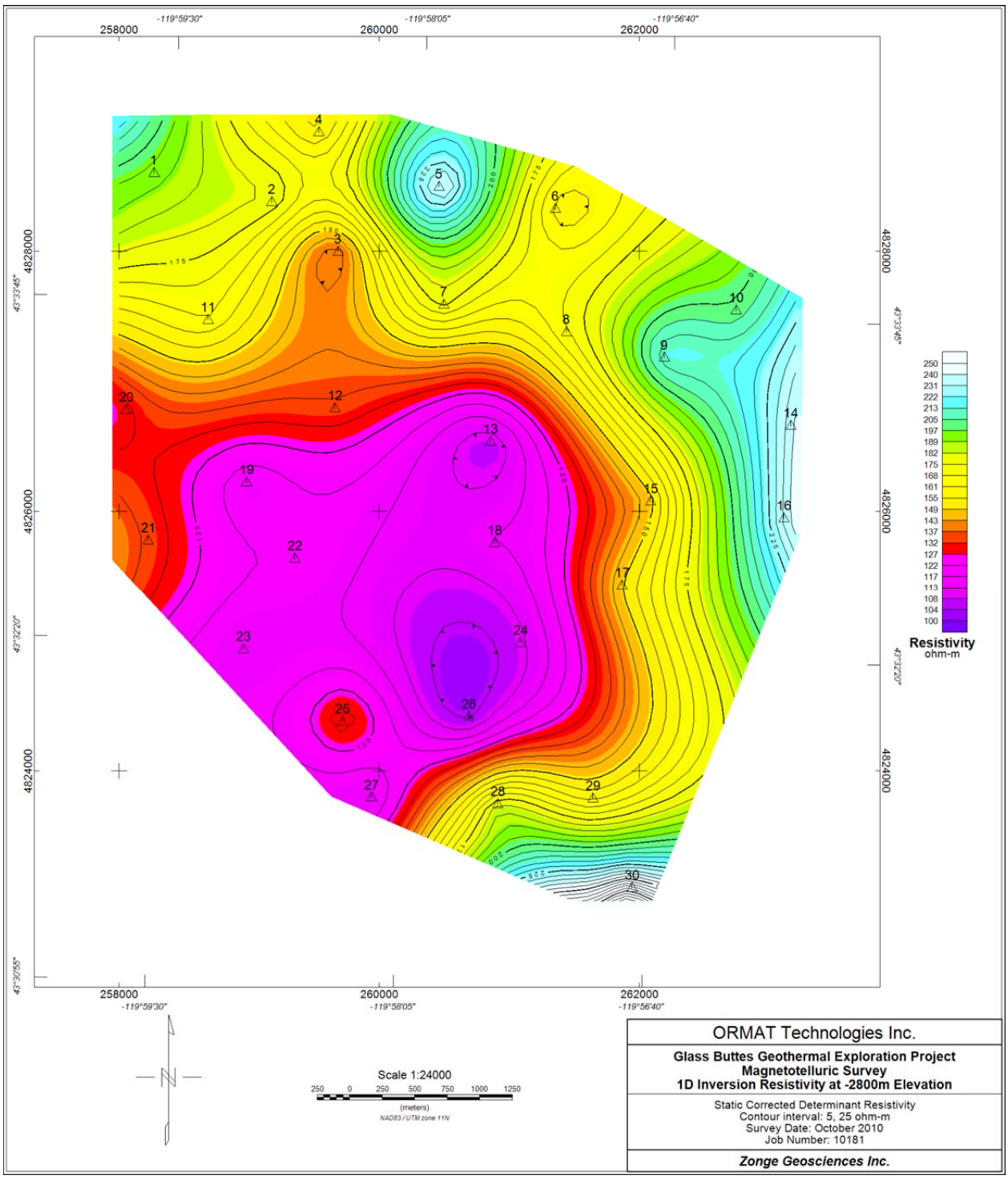

Figure A16: 1D inversion resistivity at -2800m elevation.

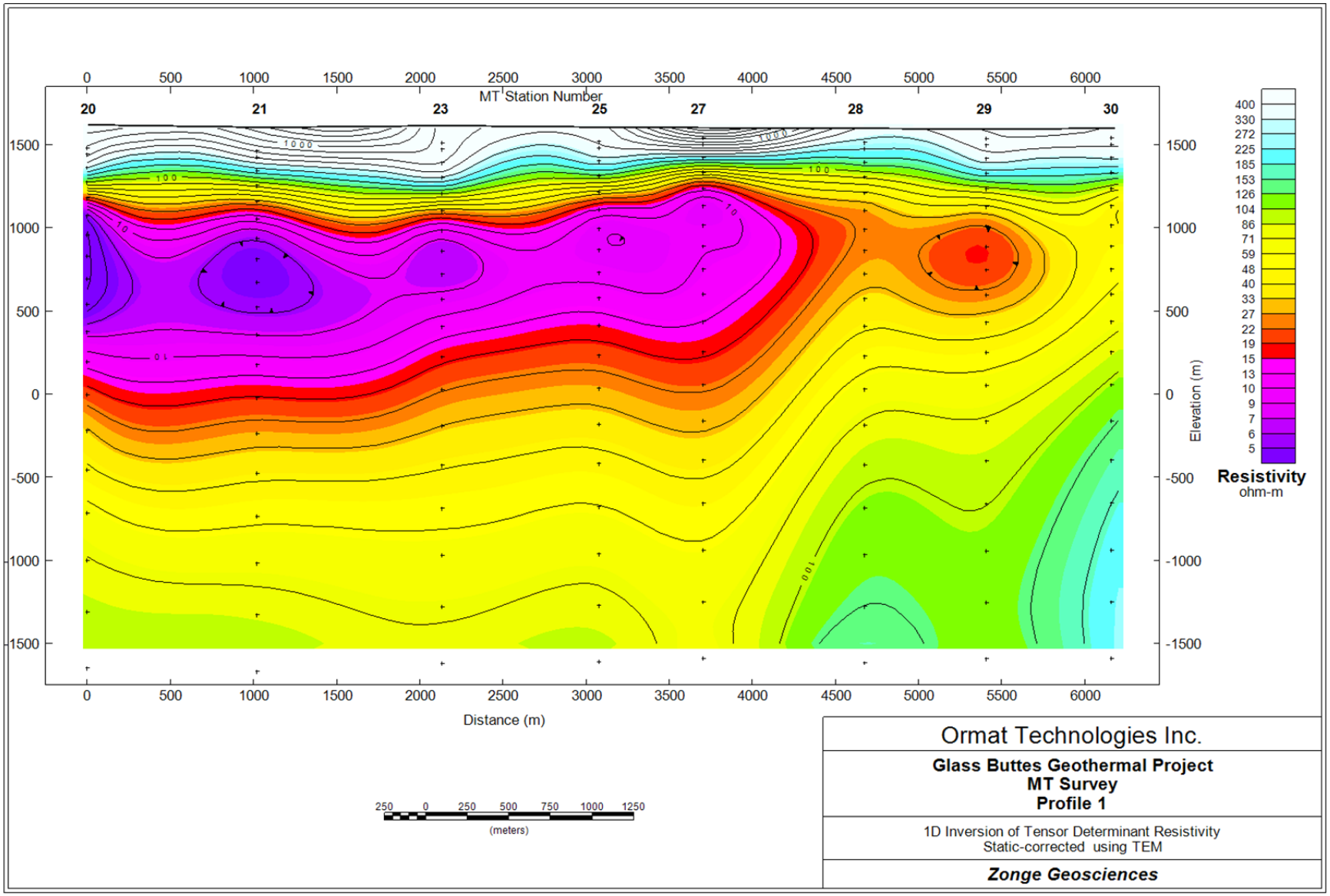

Figure A17: 1D inversion resistivity-depth section, Profile 1.

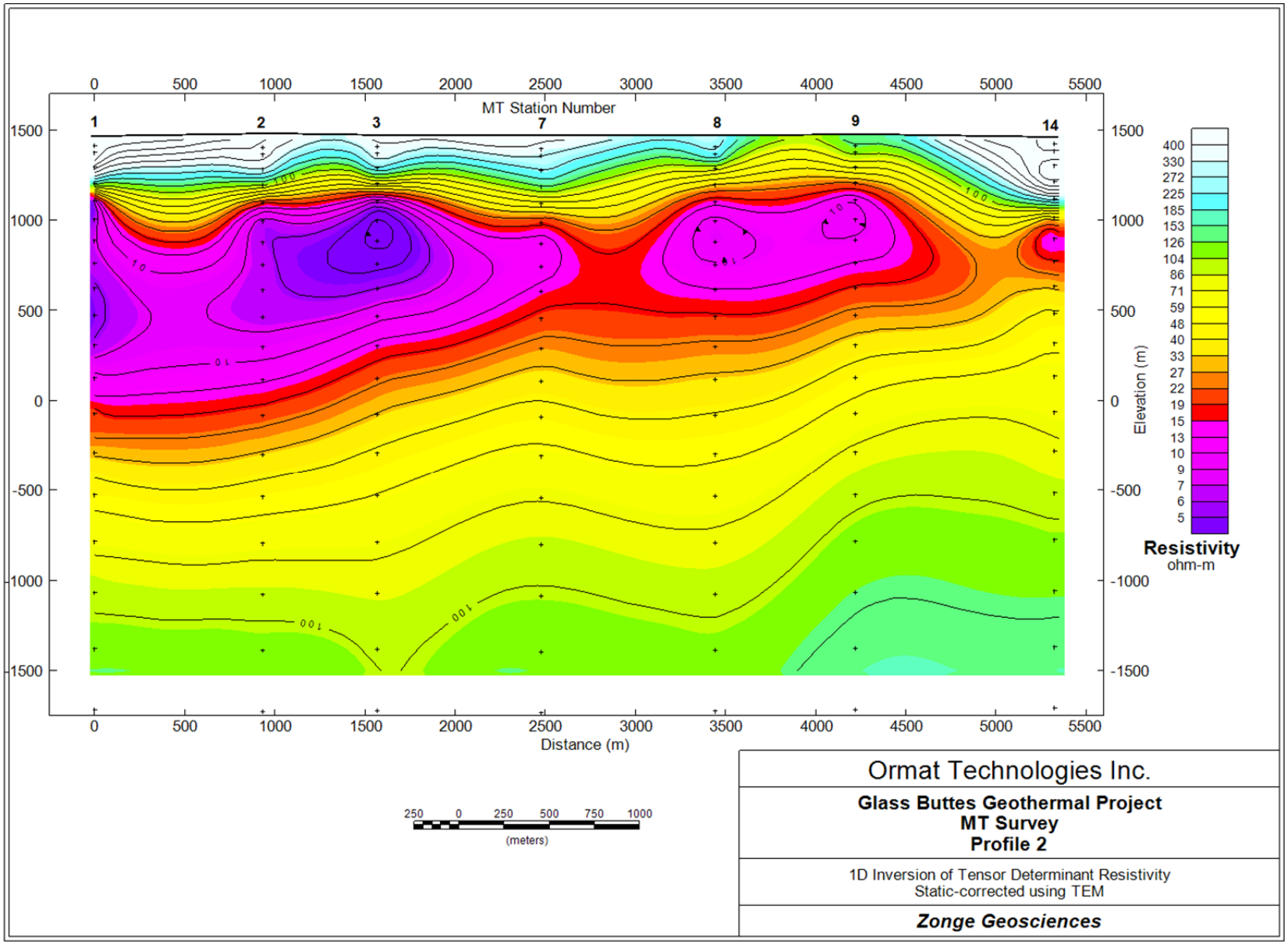

Figure A18: 1D inversion resistivity-depth section, Profile 2.

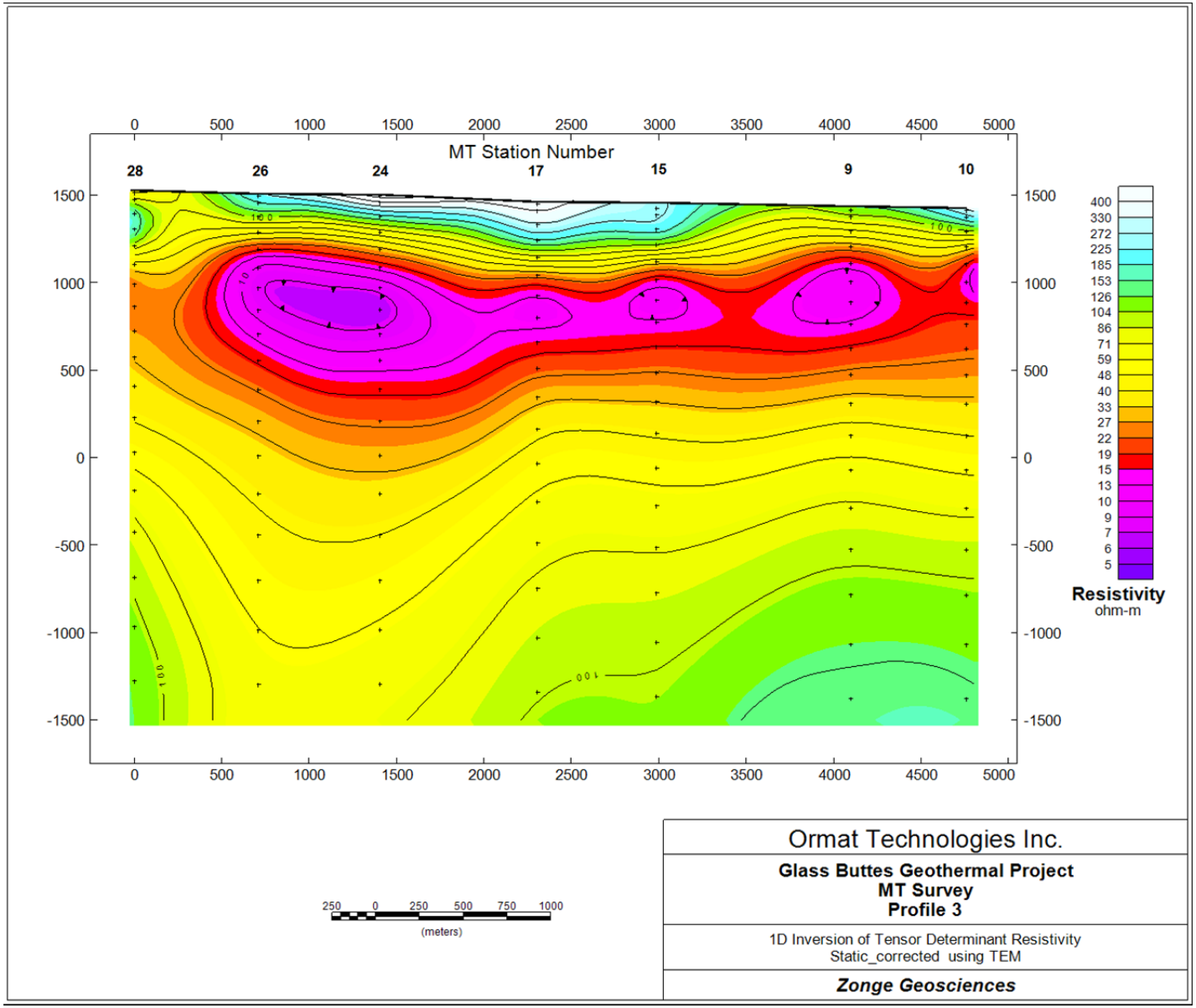

Figure A19: 1D inversion resistivity-depth section, Profile 3.

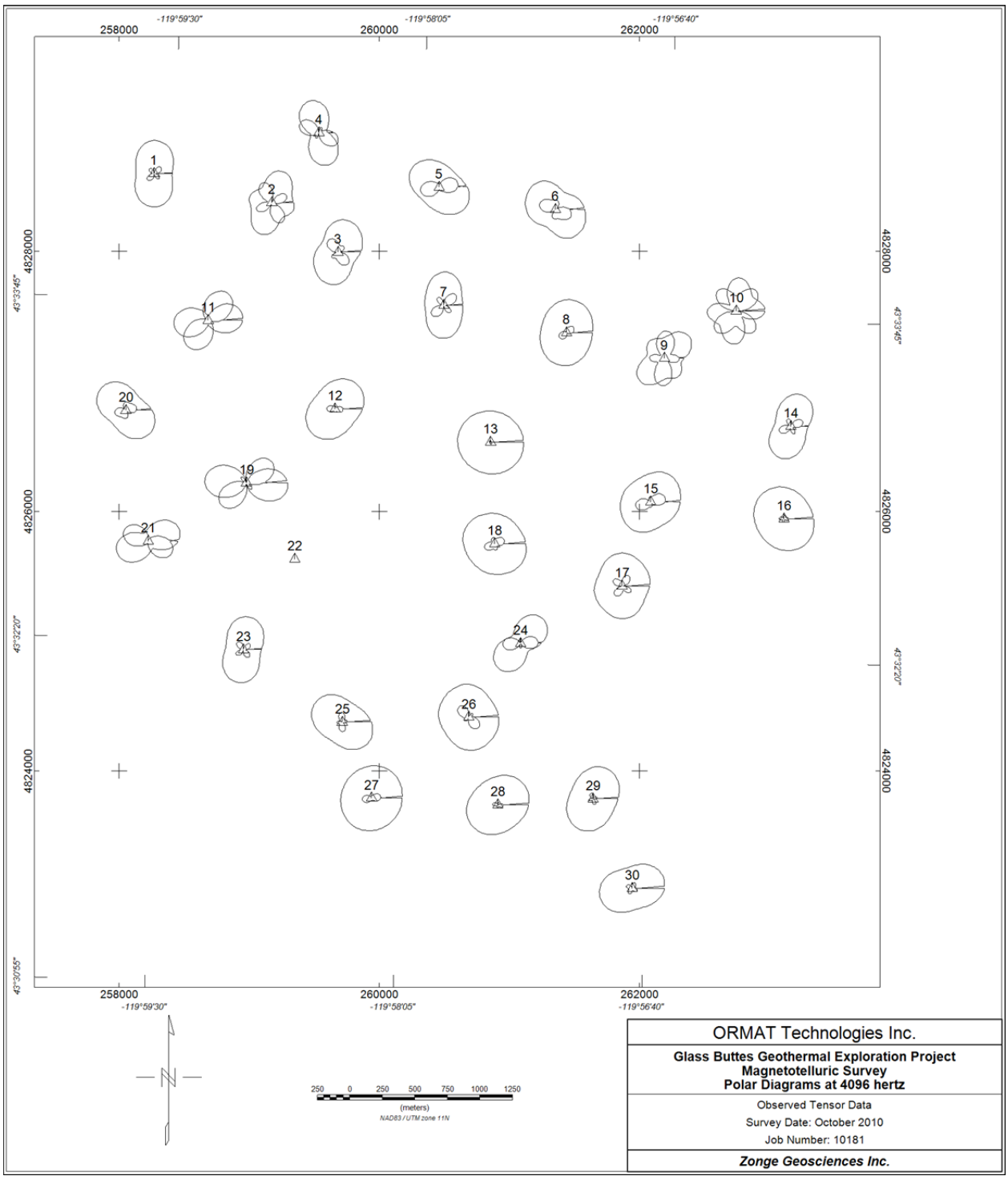

Figure A20: Impedance polar diagrams at 4096 hz.

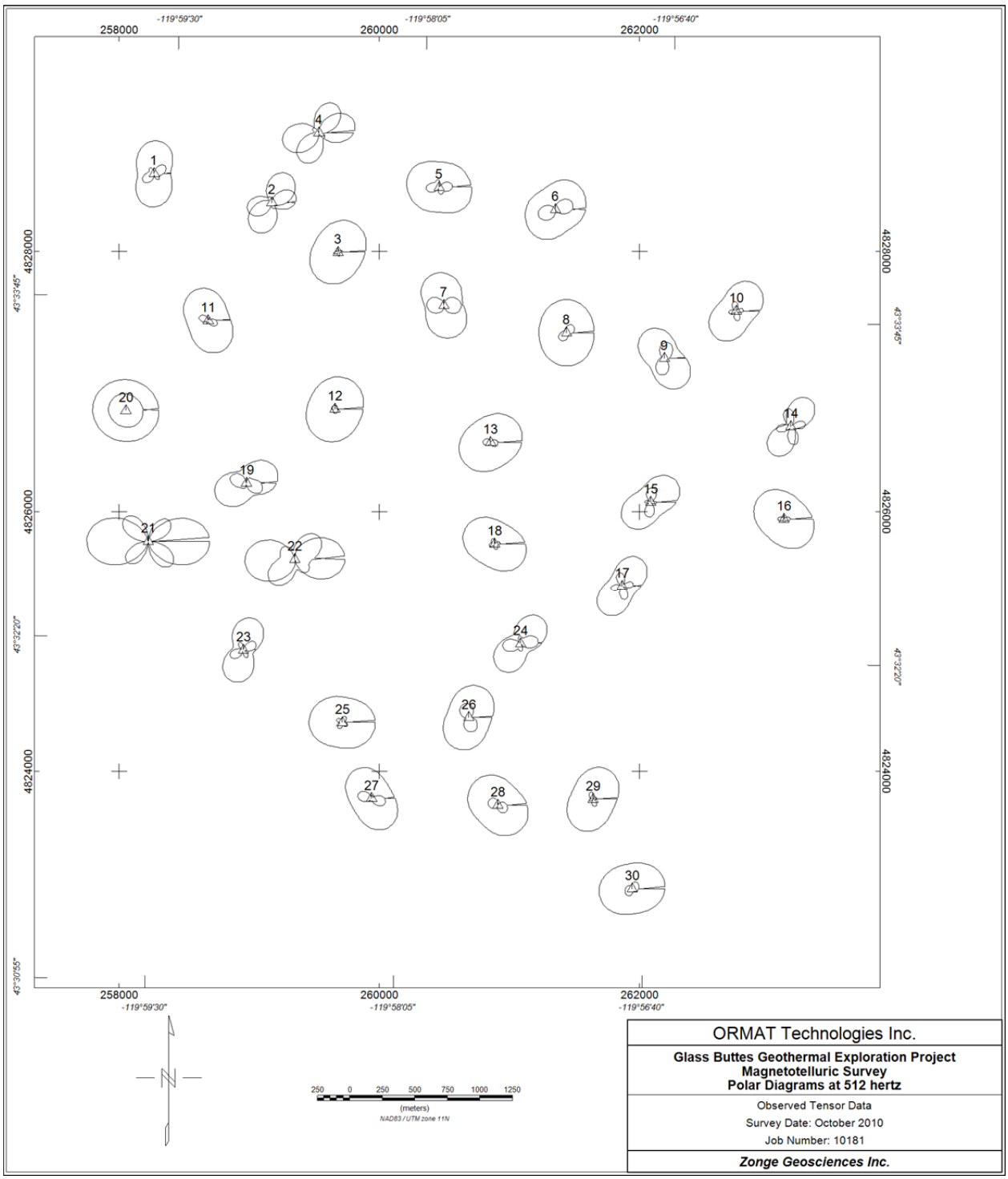

Figure A21: Impedance polar diagrams at 512 hz.

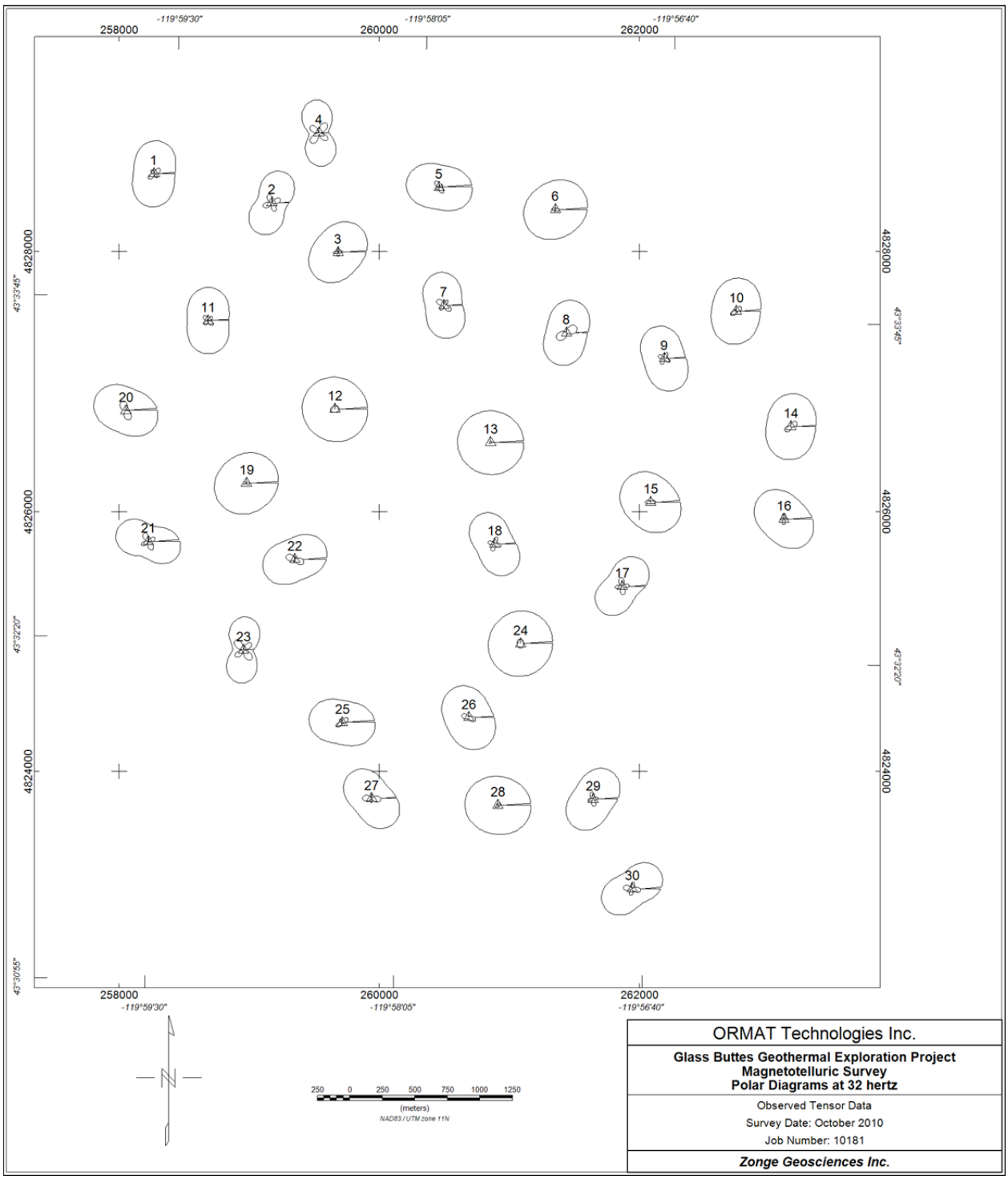

Figure A22: Impedance polar diagrams at 32 hz.

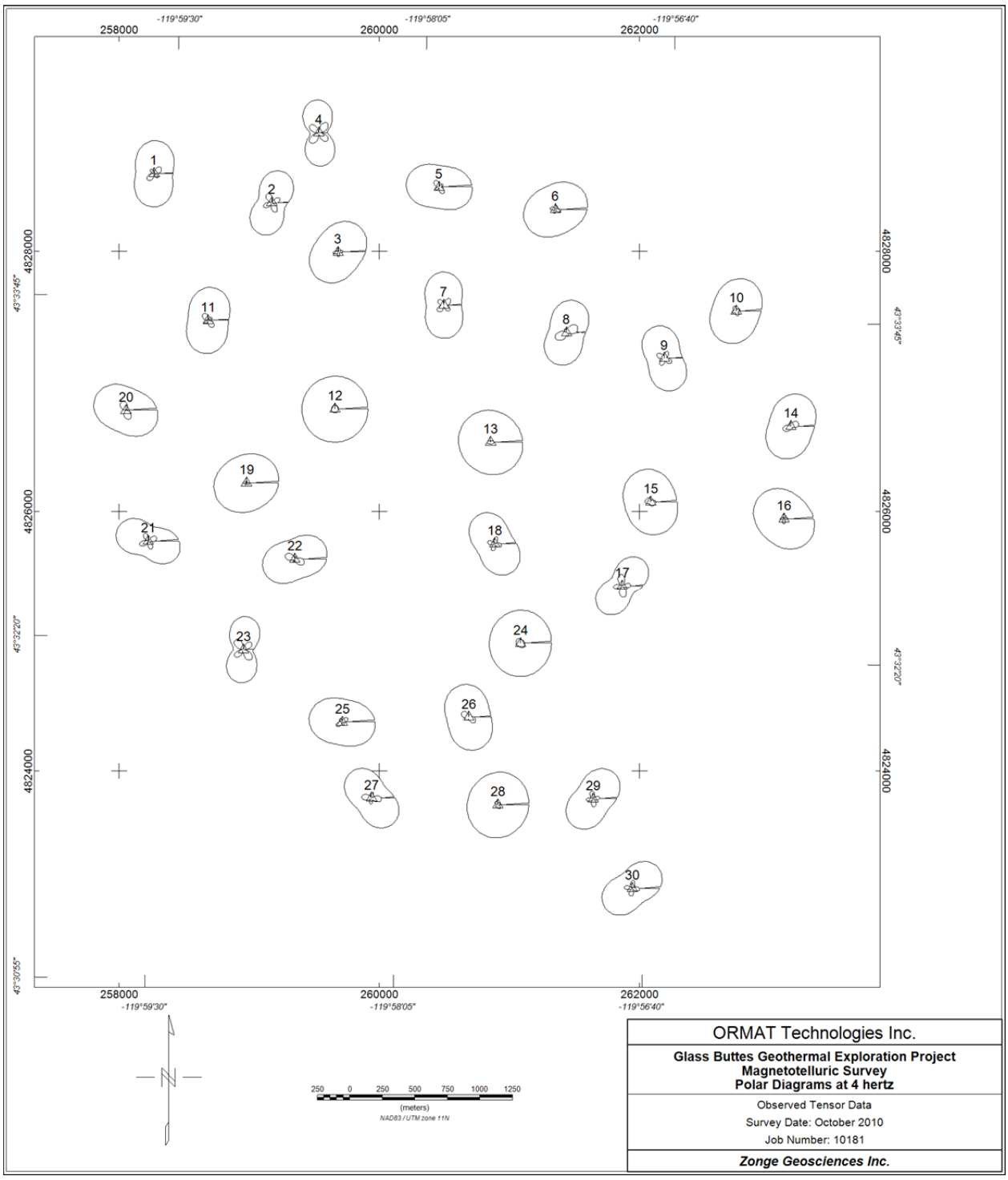

Figure A23: Impedance polar diagrams at 4 hz.

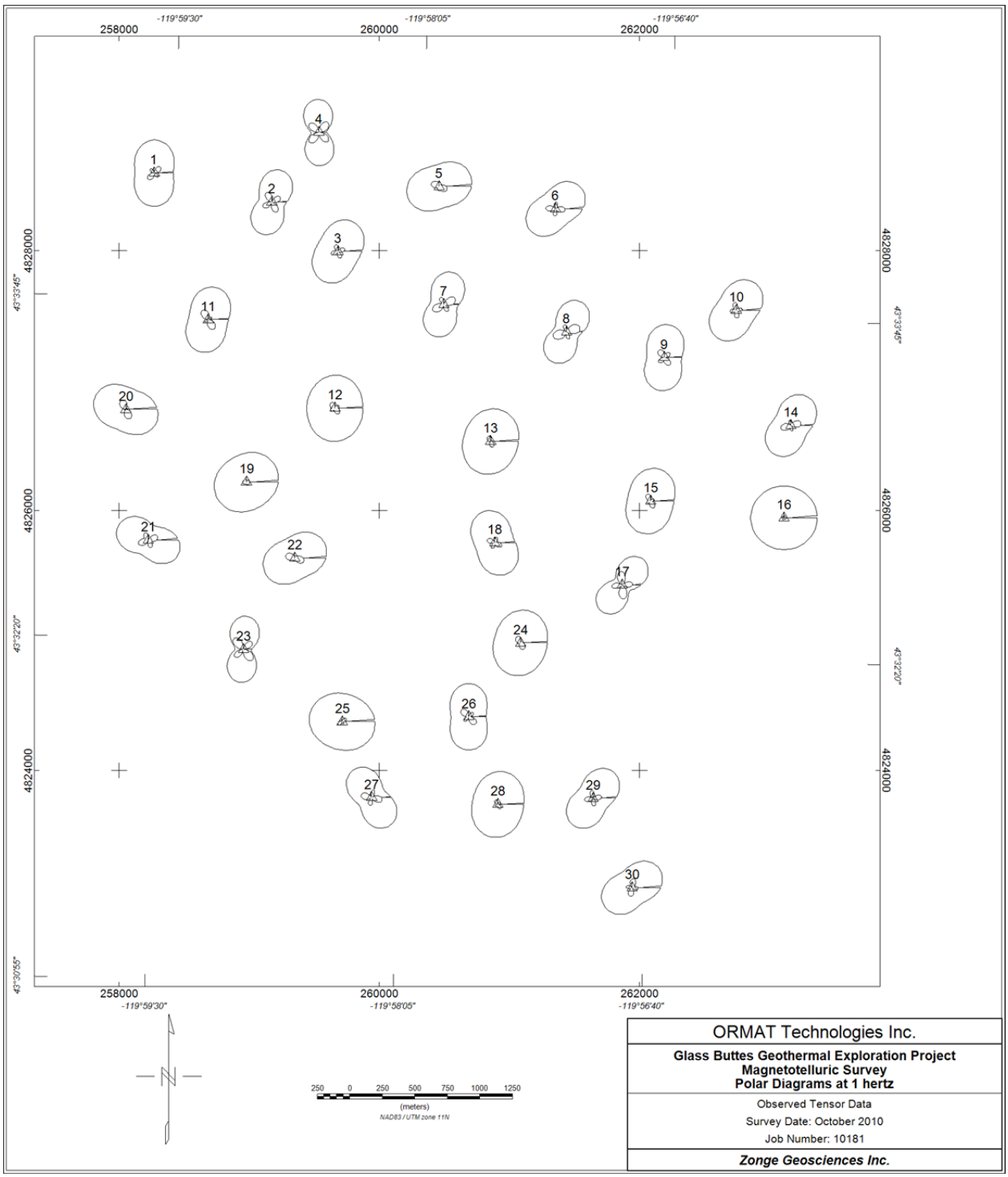

Figure A24: Impedance polar diagrams at hz.

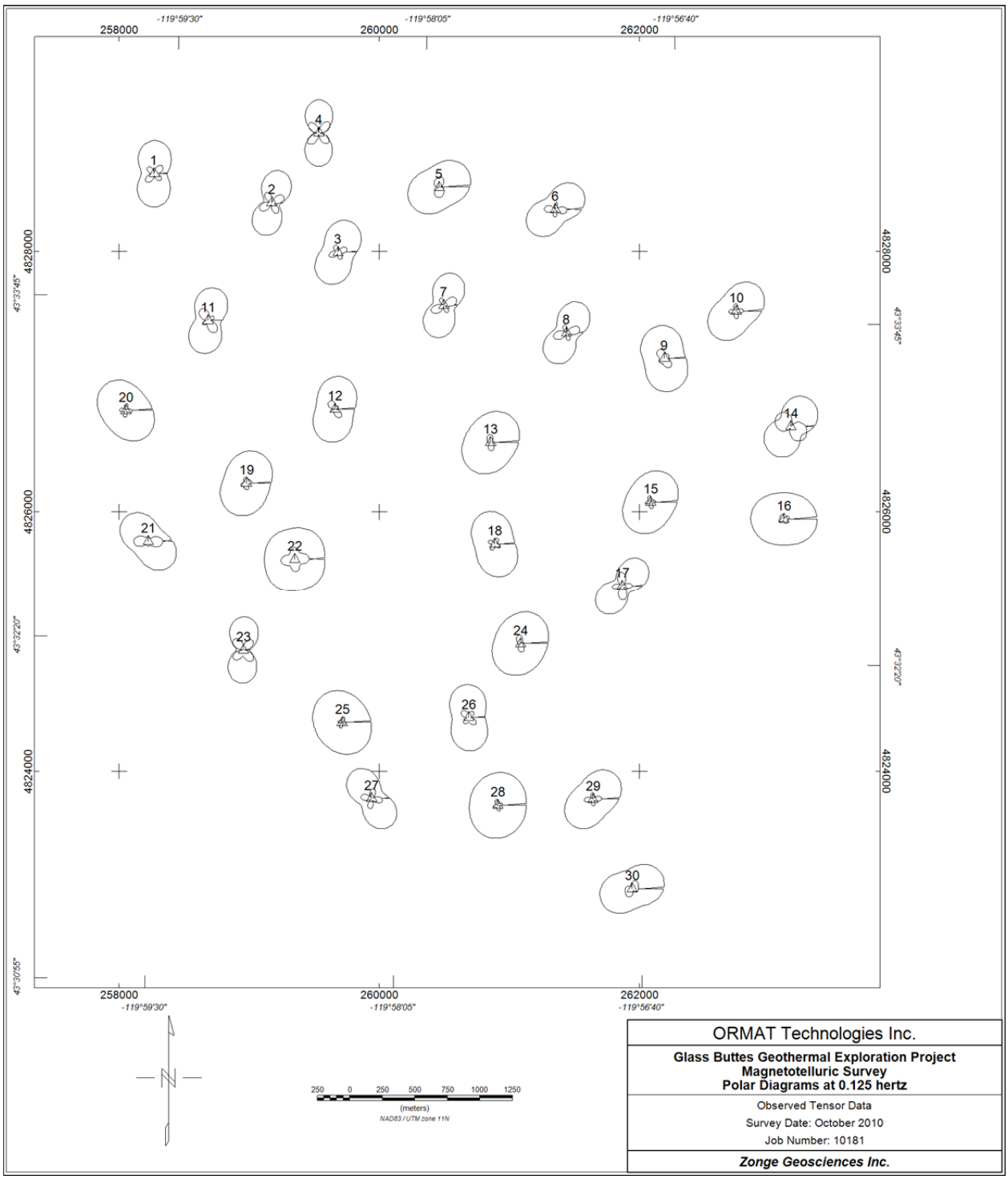

Figure A25: Impedance polar diagrams at 0.125 hz.

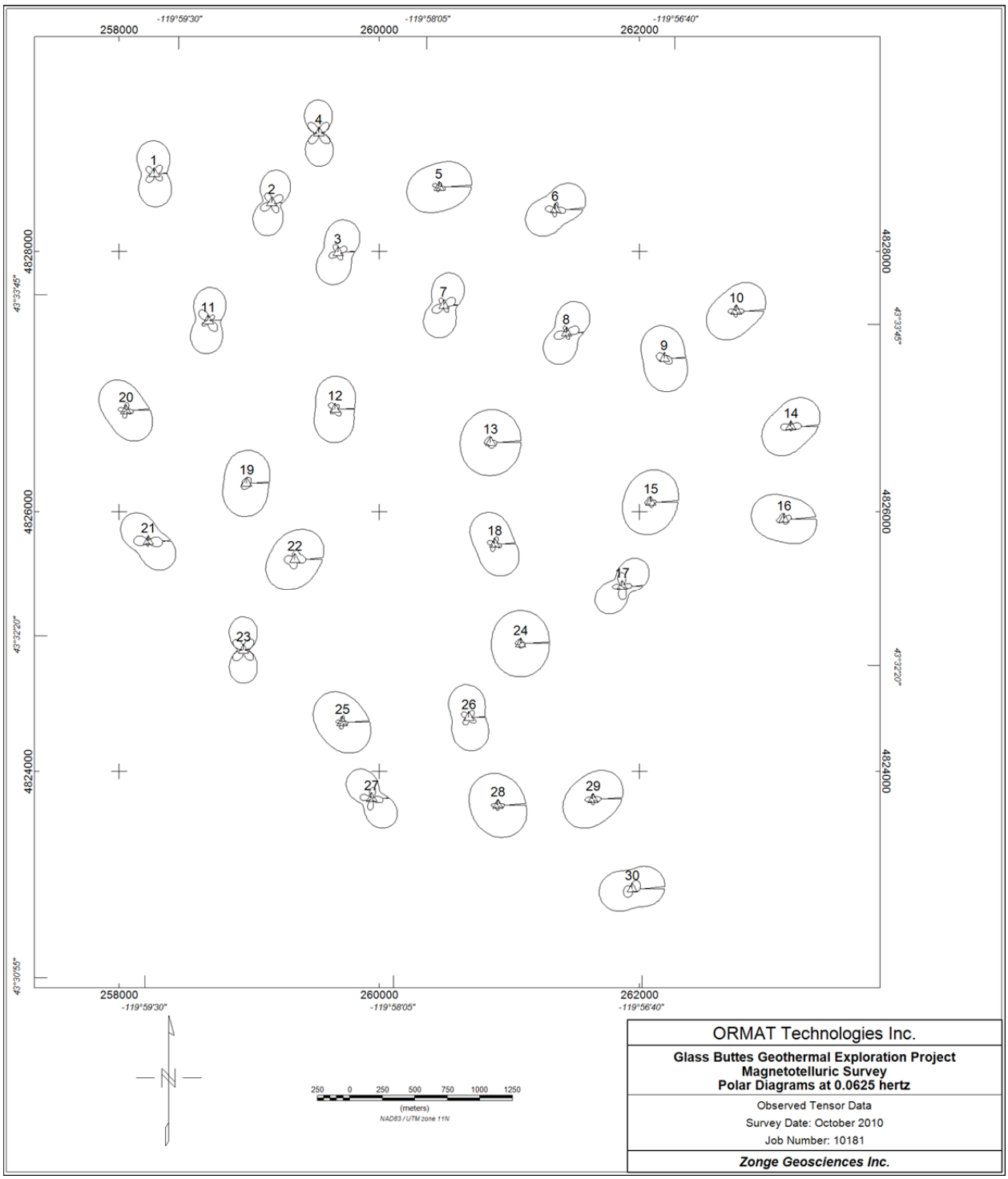

Figure A26: Impedance polar diagrams at 0.0625 hz.

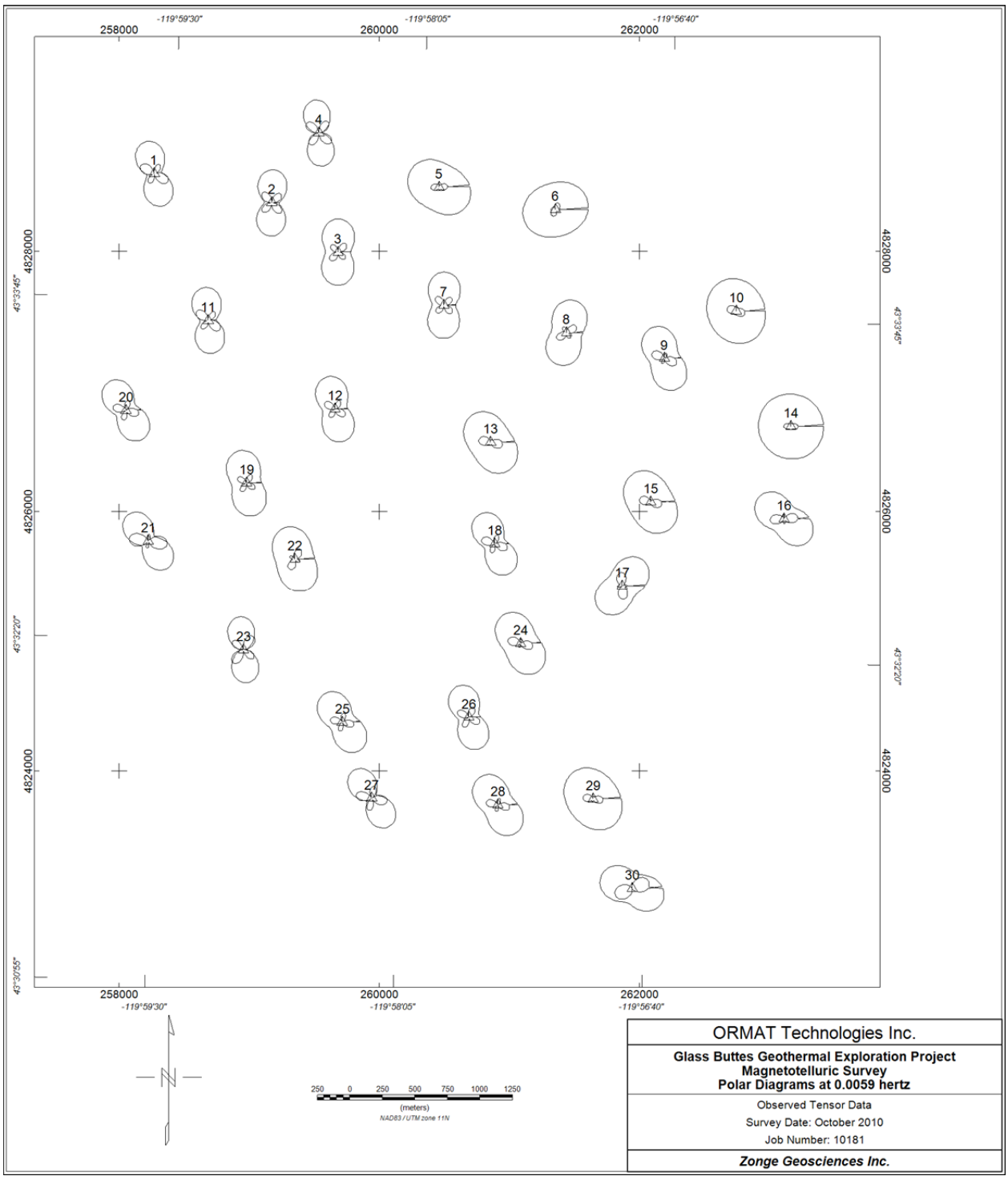

Figure A27: Impedance polar diagrams at 0.0059 hz.

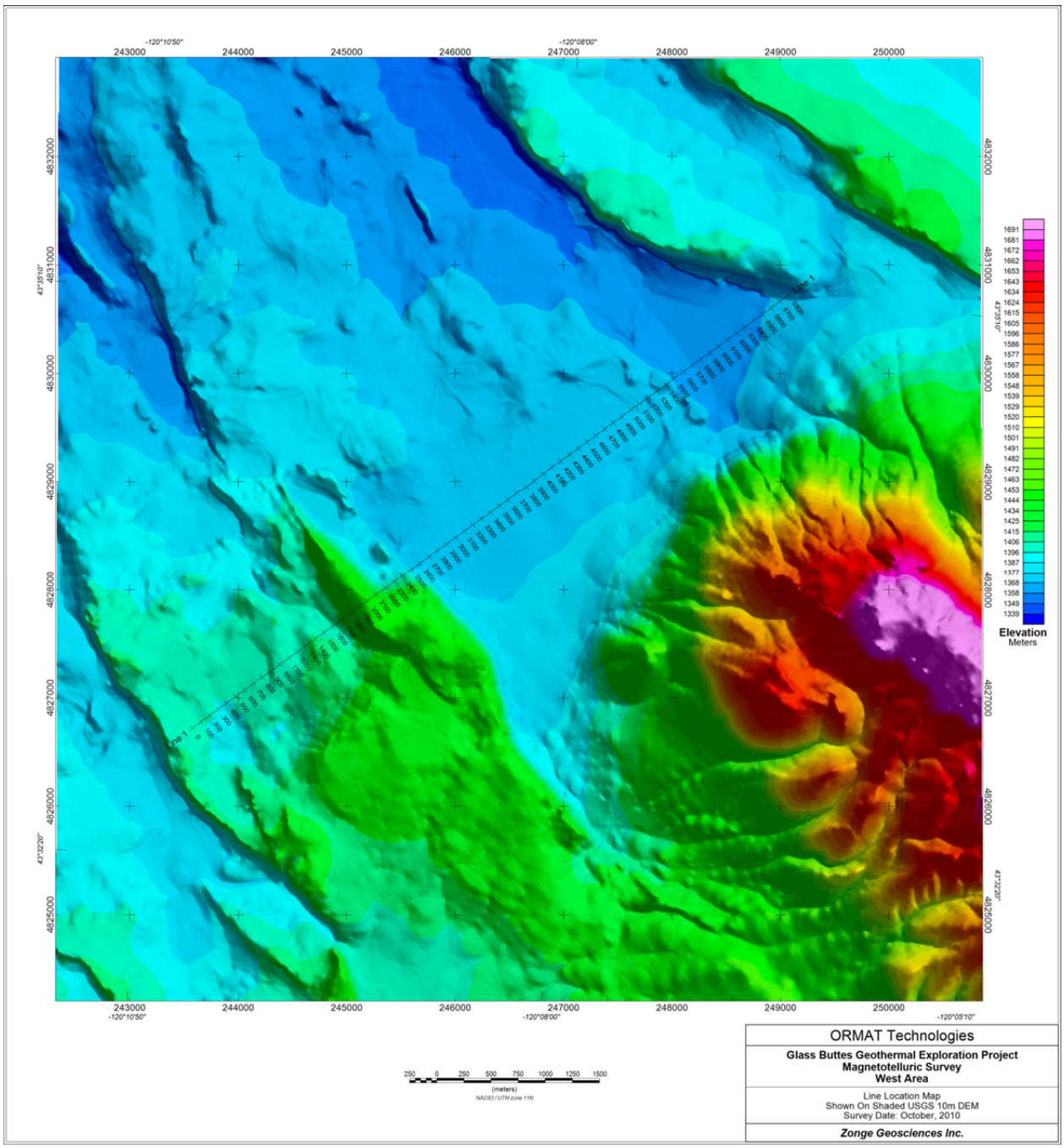

Figure A28: West Area, MT line 1 location on USGS DEM.

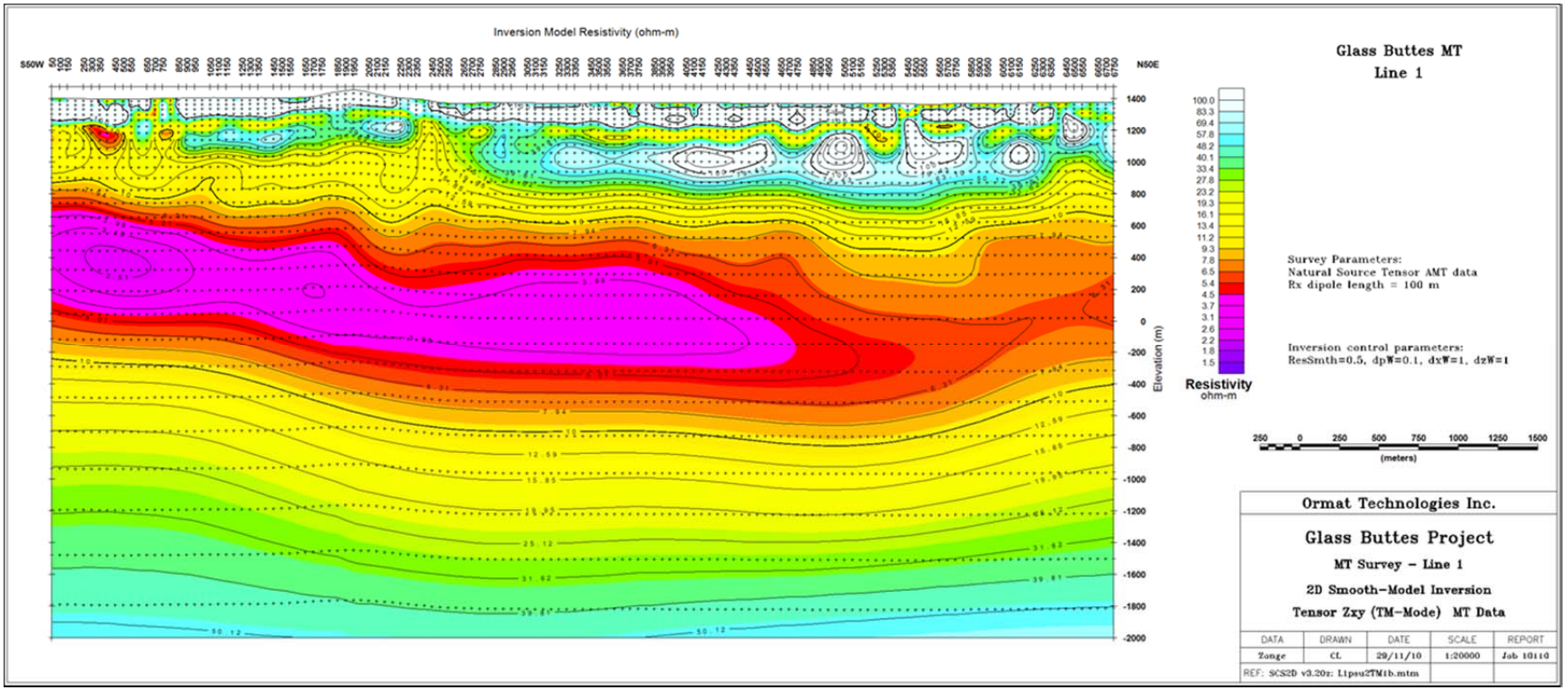

Figure A29: Line 1, Section of 2D smooth-model inversion of Zxy (TM) data.

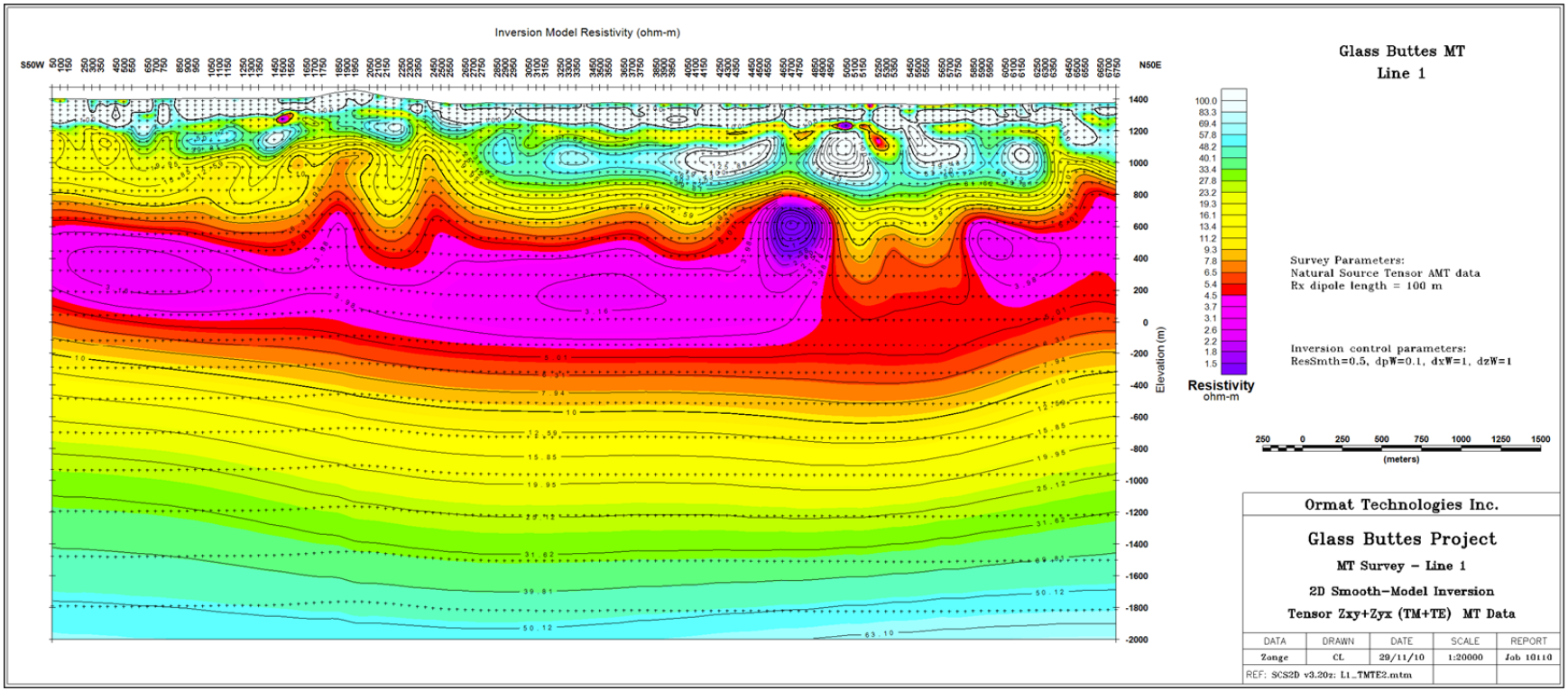

Figure A30:Line 1, Section of 2D smooth-model inversion of Zyx+Zyx (TM+TE) data.

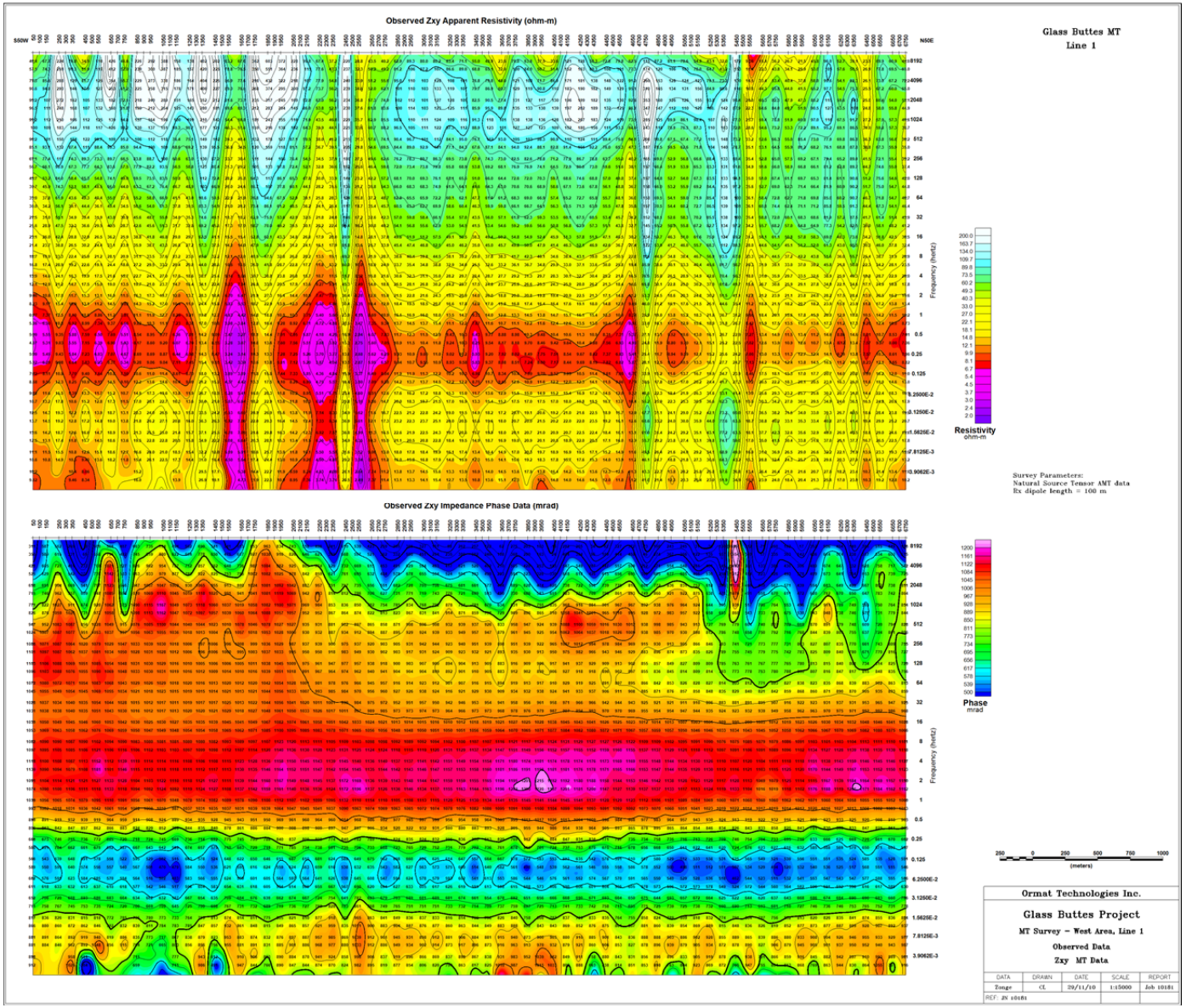

Figure A31: Line 1, Observed Cagniard resistivity and Impedance Phase for Zxy.

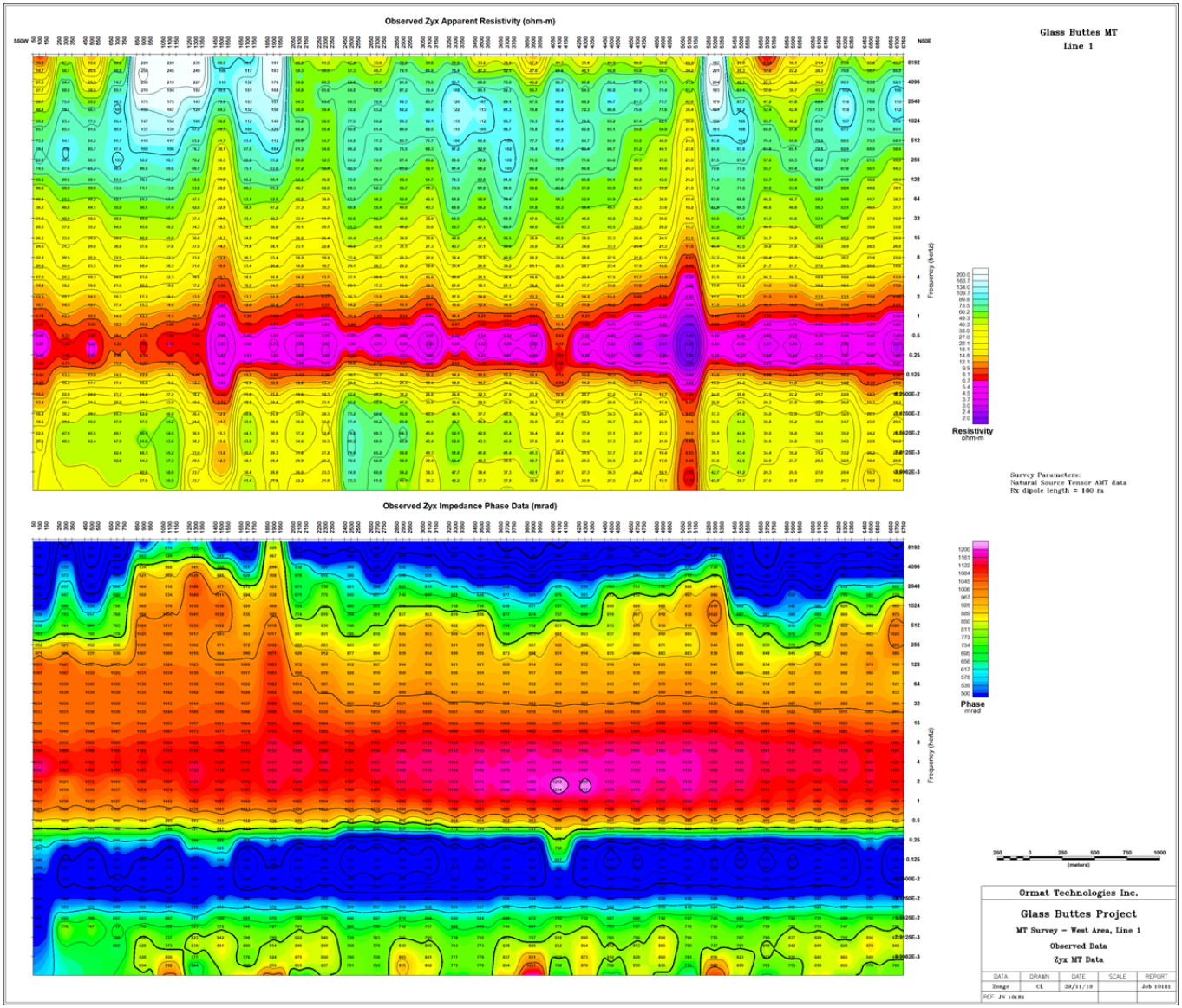

Figure A32: Line 1, Observed Cagniard resistivity and impedance phase for Zyx.

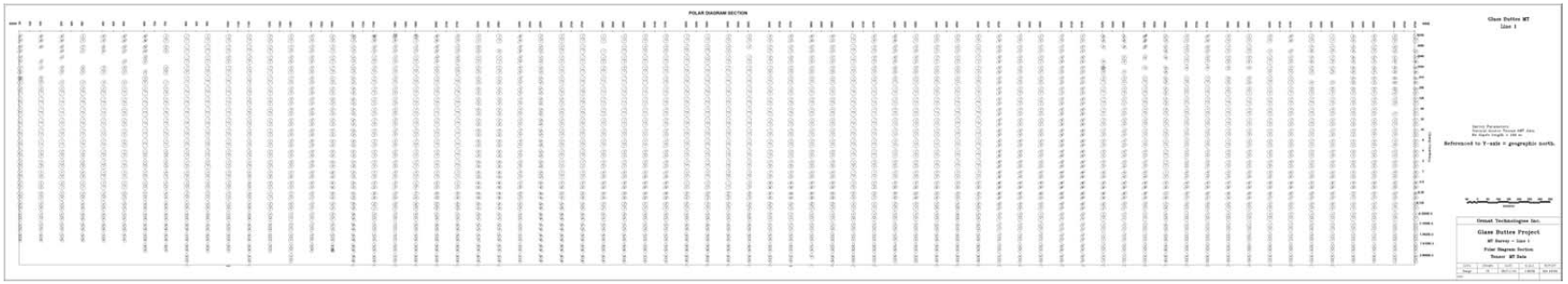

Figure A33: Line 1, Section showing polar diagrams.

APPENDIX B: East Area, Data Plots

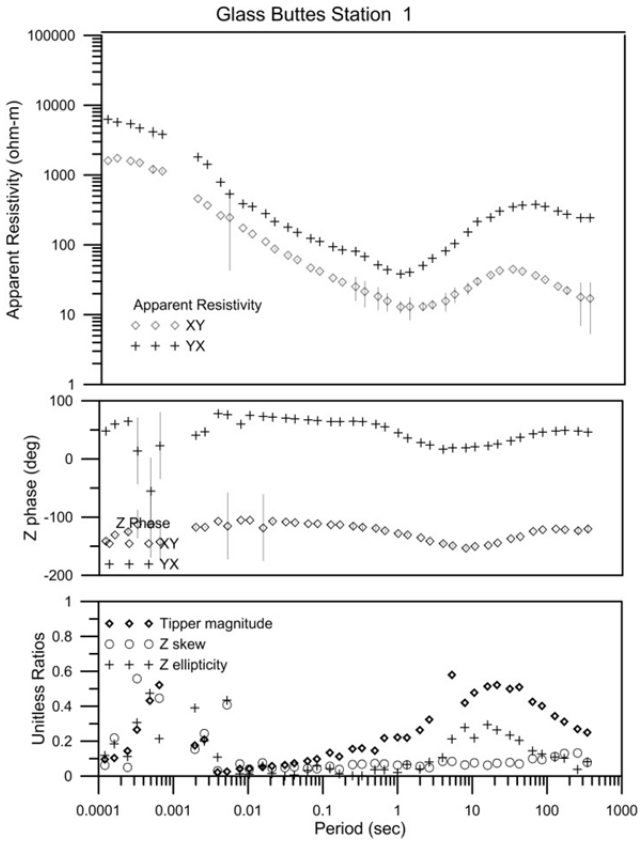
Glass Buttes Station 1
Apparent Resistivity (ohm-m)
Apparent Resistivity
XY
YX
Z phase (deg)
Z Phase
XY
YX
Unitless Ratios
Tipper magnitude
Z skew
Z ellipticity
Period (sec)

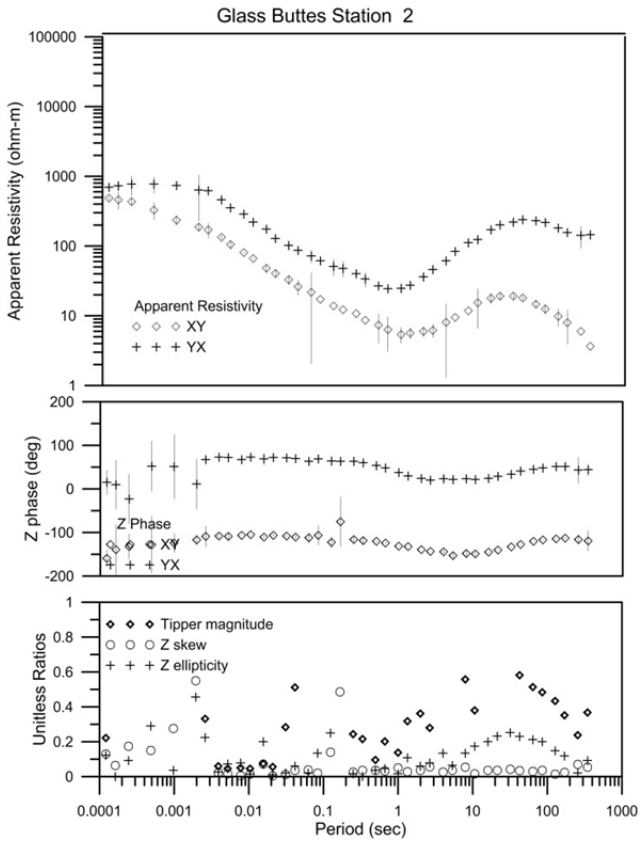
Glass Buttes Station 2
Apparent Resistivity (ohm-m)
Apparent Resistivity
XY
YX
Z phase (deg)
Z Phase
XY
YX
Unitless Ratios
Tipper magnitude
Z skew
Z ellipticity
Period (sec)

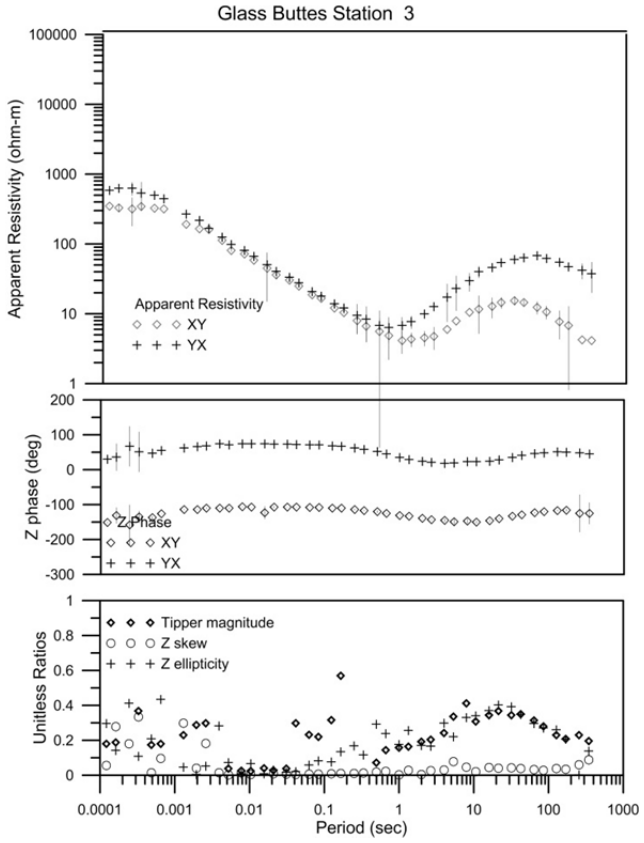
Glass Buttes Station 3
Apparent Resistivity (ohm-m)
Apparent Resistivity
XY
YX
Z phase (deg)
Z Phase
XY
YX
Unitless Ratios
Tipper magnitude
Z skew
Z ellipticity
Period (sec)

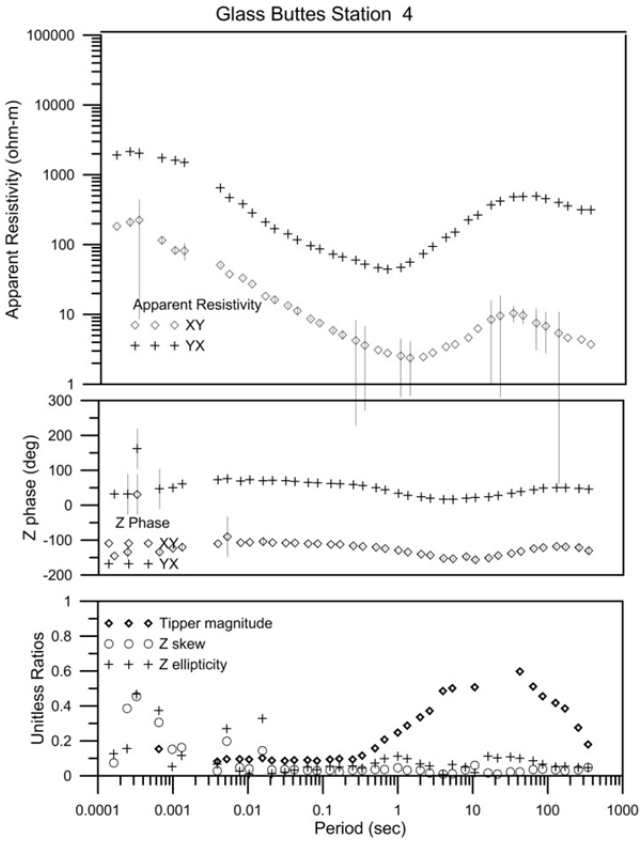
Glass Buttes Station 4
Apparent Resistivity (ohm-m)
Apparent Resistivity
XY
YX
Z phase (deg)
Z Phase
XY
YX
Unitless Ratios
Tipper magnitude
Z skew
Z ellipticity
Period (sec)

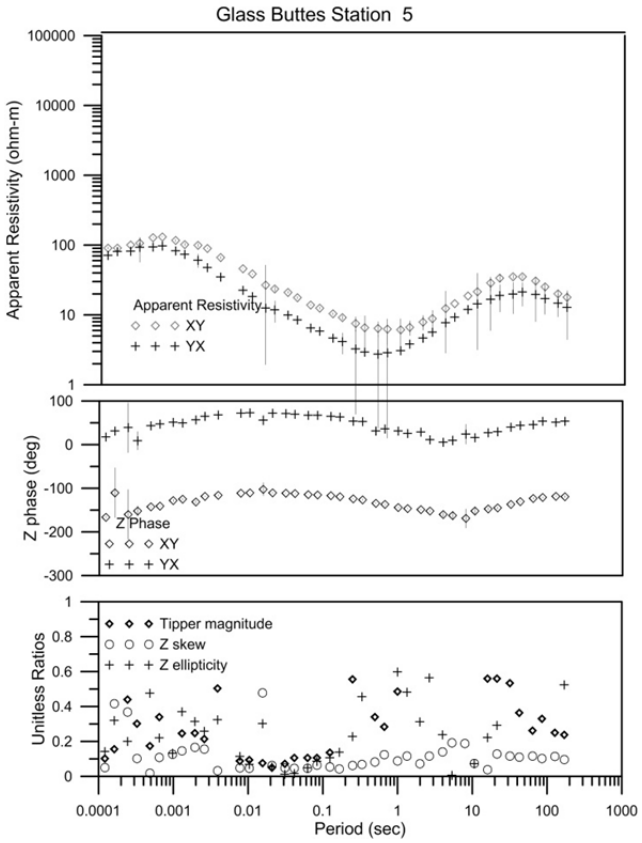
Glass Buttes Station 5
Apparent Resistivity (ohm-m)
Apparent Resistivity
XY
YX
Z phase (deg)
Z Phase
XY
YX
Unitless Ratios
Tipper magnitude
Z skew
Z ellipticity
Period (sec)

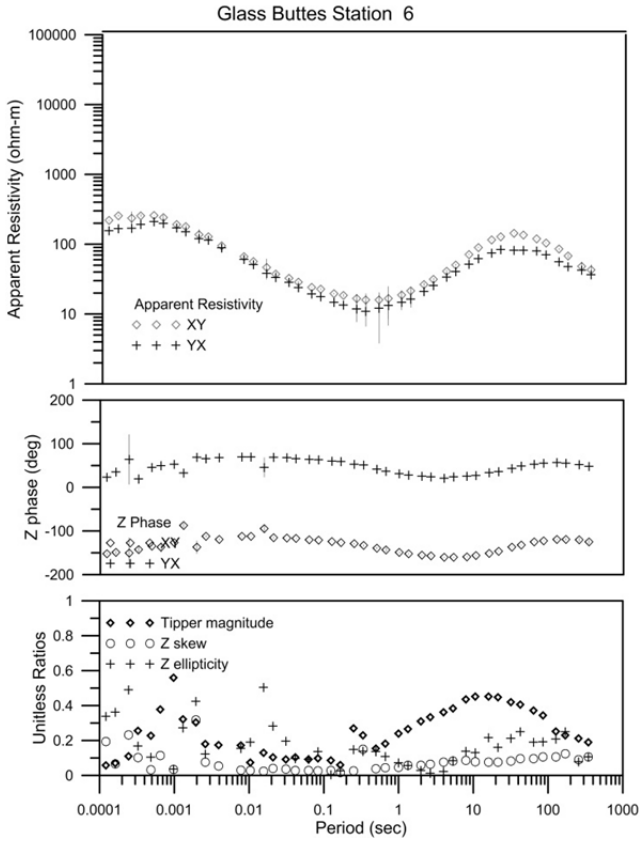
Glass Buttes Station 6
Apparent Resistivity (ohm-m)
Apparent Resistivity
XY
YX
Z phase (deg)
Z Phase
XY
YX
Unitless Ratios
Tipper magnitude
Z skew
Z ellipticity
Period (sec)

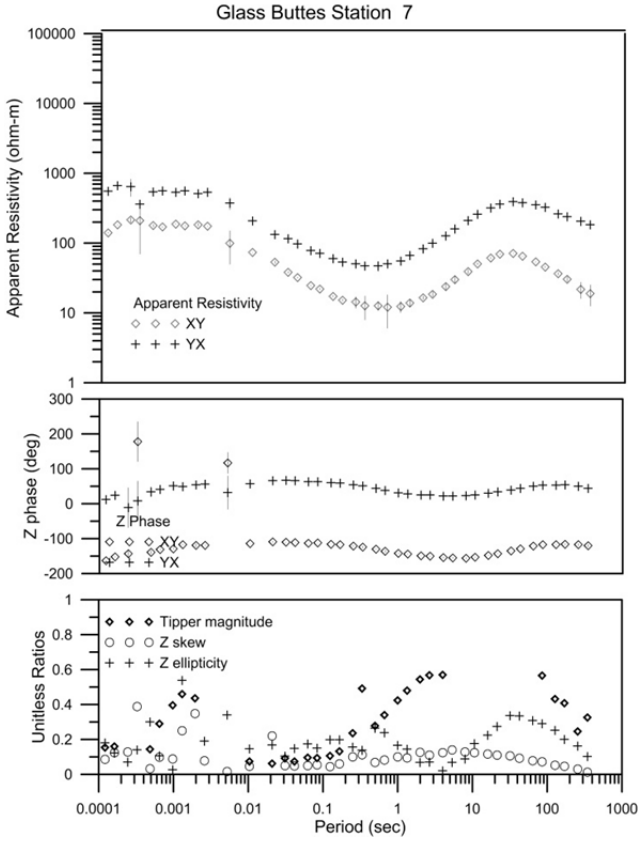
Glass Buttes Station 7
Apparent Resistivity (ohm-m)
Apparent Resistivity
XY
YX
Z phase (deg)
Z Phase
XY
YX
Unitless Ratios
Tipper magnitude
Z skew
Z ellipticity
Period (sec)

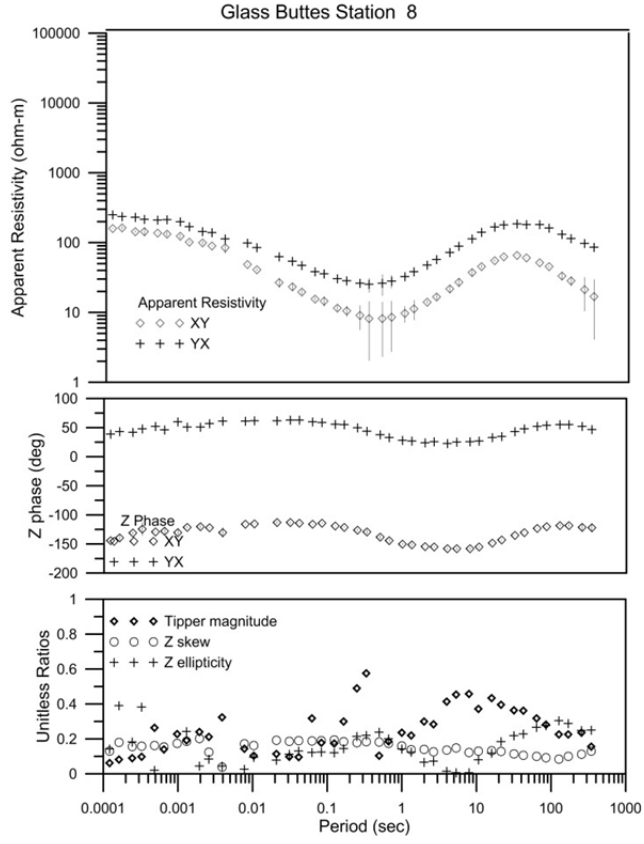
Glass Buttes Station 8
Apparent Resistivity (ohm-m)
Apparent Resistivity
XY
YX
Z phase (deg)
Z Phase
XY
YX
Unitless Ratios
Tipper magnitude
Z skew
Z ellipticity
Period (sec)

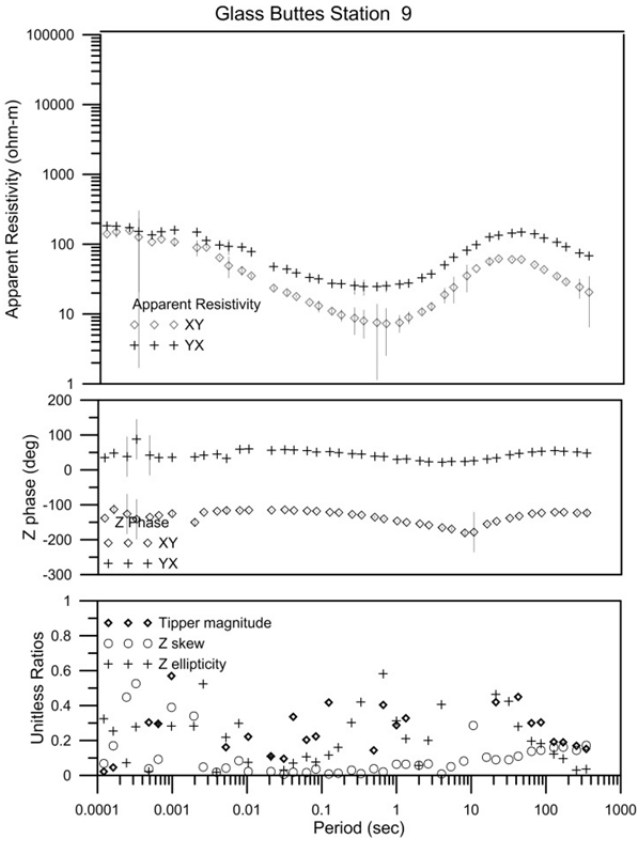
Glass Buttes Station 9
Apparent Resistivity (ohm-m)
Apparent Resistivity
XY
YX
Z phase (deg)
Z Phase
XY
YX
Unitless Ratios
Tipper magnitude
Z skew
Z ellipticity
Period (sec)

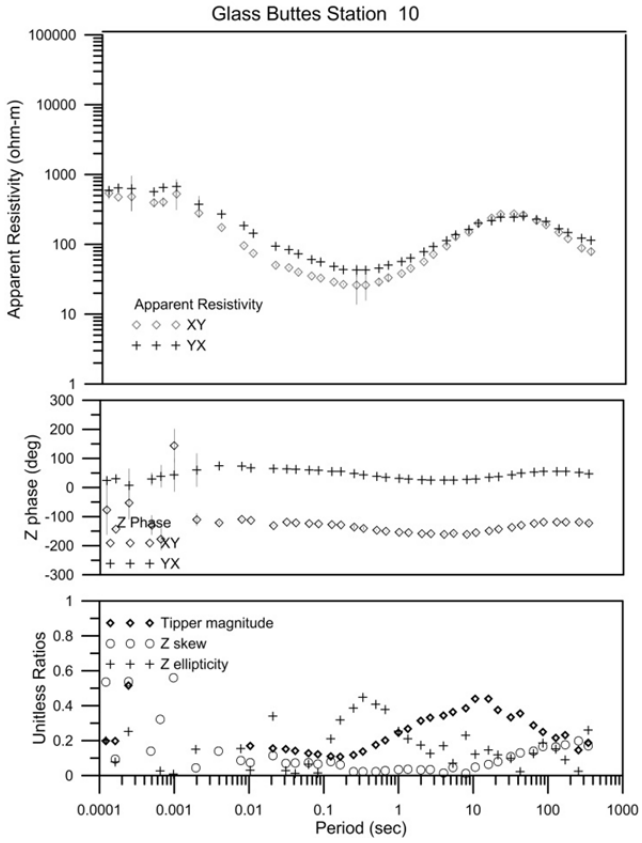
Glass Buttes Station 10
Apparent Resistivity (ohm-m)
Apparent Resistivity
XY
YX
Z phase (deg)
Z Phase
XY
YX
Unitless Ratios
Tipper magnitude
Z skew
Z ellipticity
Period (sec)

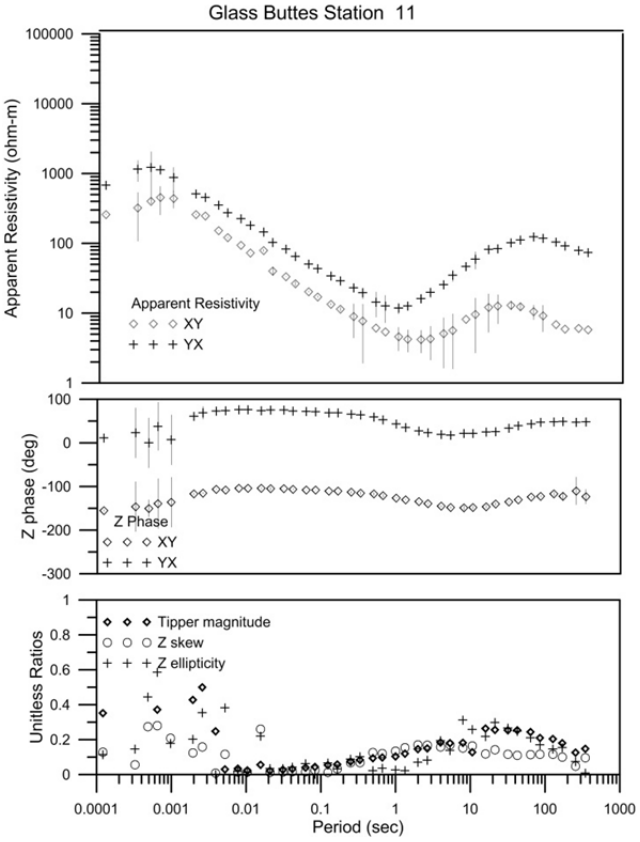
Glass Buttes Station 11
Apparent Resistivity (ohm-m)
Apparent Resistivity
XY
YX
Z phase (deg)
Z Phase
XY
YX
Unitless Ratios
Tipper magnitude
Z skew
Z ellipticity
Period (sec)

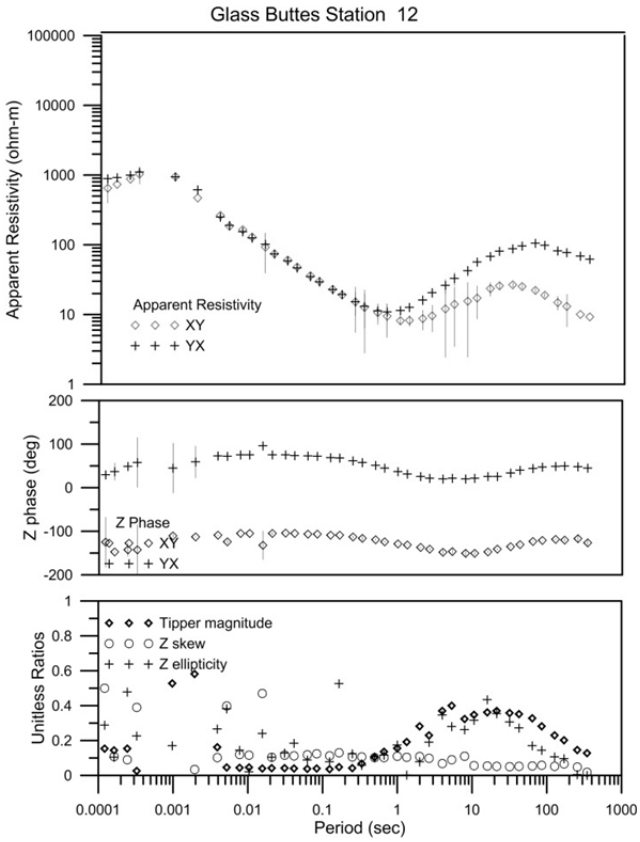
Glass Buttes Station 12
Apparent Resistivity (ohm-m)
Apparent Resistivity
XY
YX
Z phase (deg)
Z Phase
XY
YX
Unitless Ratios
Tipper magnitude
Z skew
Z ellipticity
Period (sec)

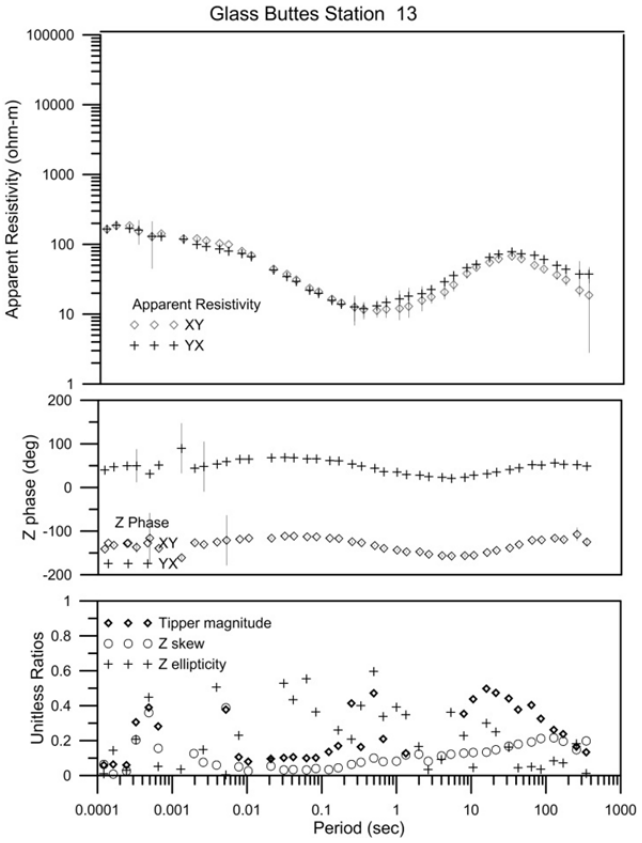
Glass Buttes Station 13
Apparent Resistivity (ohm-m)
Apparent Resistivity
XY
YX
Z phase (deg)
Z Phase
XY
YX
Unitless Ratios
Tipper magnitude
Z skew
Z ellipticity
Period (sec)

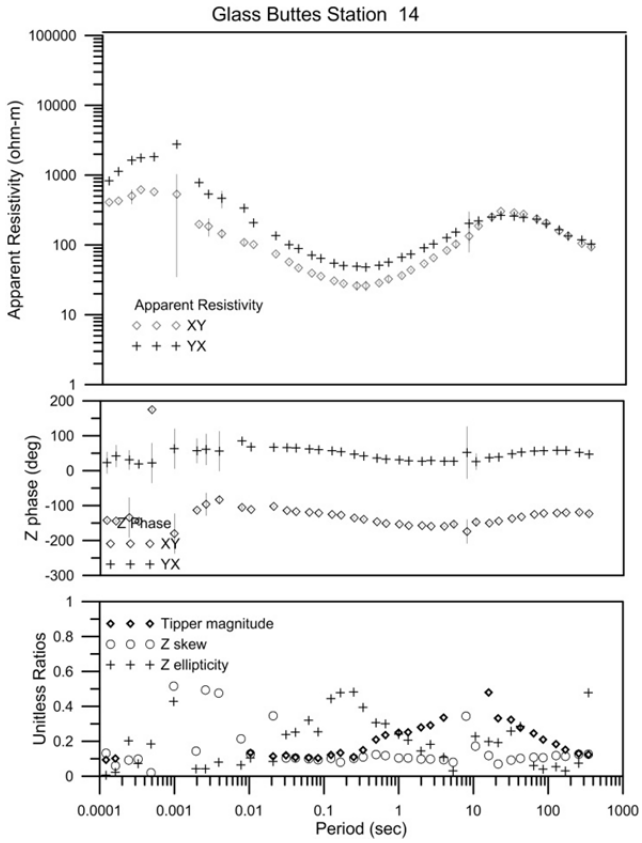
Glass Buttes Station 14
Apparent Resistivity (ohm-m)
Apparent Resistivity
XY
YX
Z phase (deg)
Z Phase
XY
YX
Unitless Ratios
Tipper magnitude
Z skew
Z ellipticity
Period (sec)

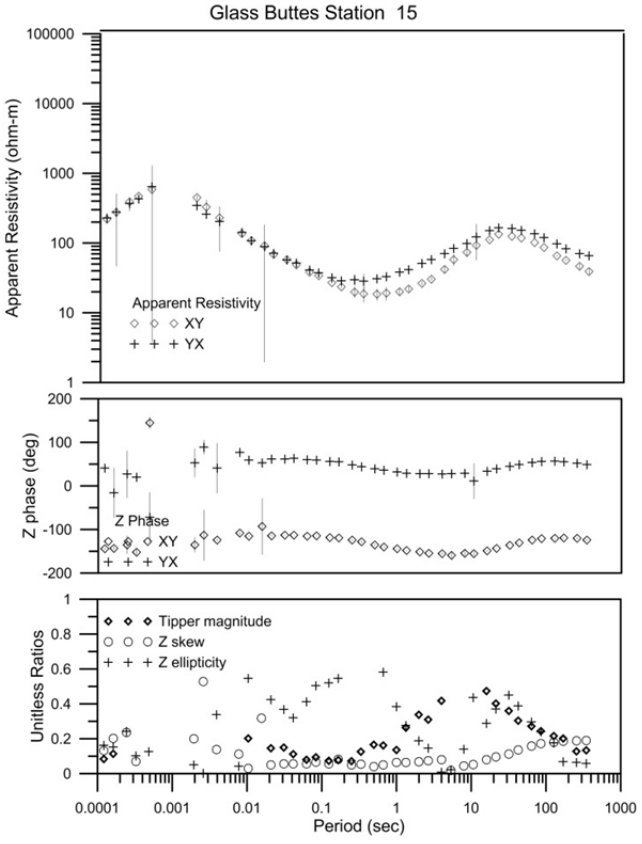
Glass Buttes Station 15
Apparent Resistivity (ohm-m)
Apparent Resistivity
XY
YX
Z phase (deg)
Z Phase
XY
YX
Unitless Ratios
Tipper magnitude
Z skew
Z ellipticity
Period (sec)

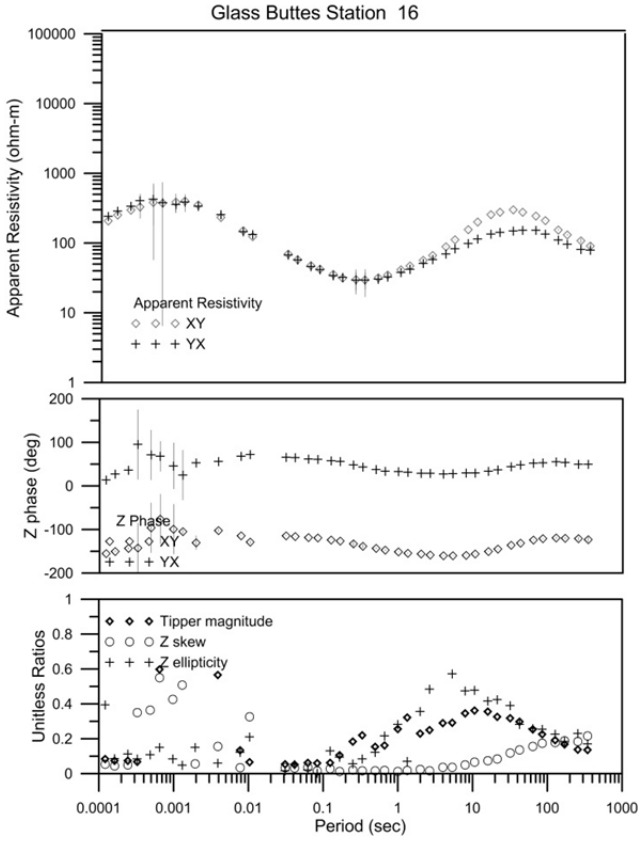
Glass Buttes Station 16
Apparent Resistivity (ohm-m)
Apparent Resistivity
XY
YX
Z phase (deg)
Z Phase
XY
YX
Unitless Ratios
Tipper magnitude
Z skew
Z ellipticity
Period (sec)

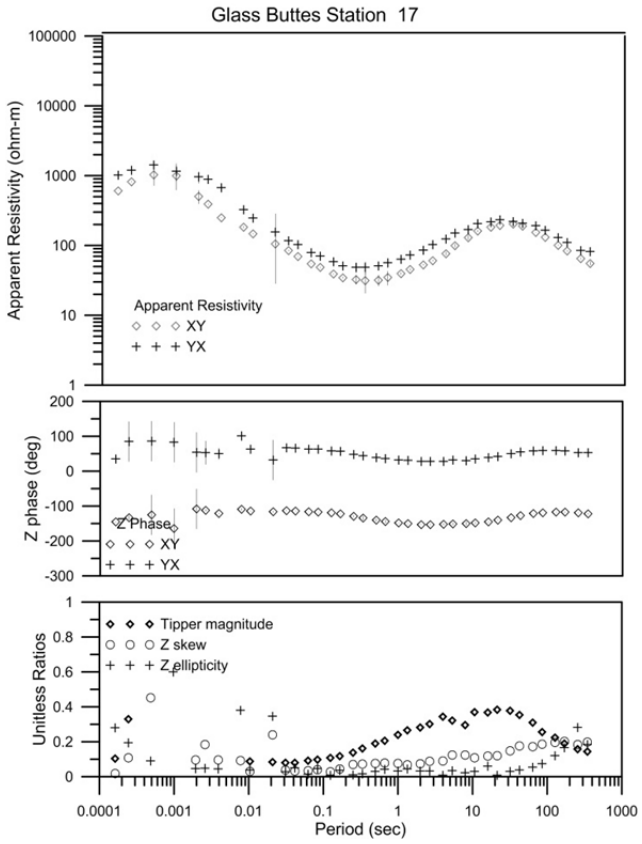
Glass Buttes Station 17
Apparent Resistivity (ohm-m)
Apparent Resistivity
XY
YX
Z phase (deg)
Z Phase
XY
YX
Unitless Ratios
Tipper magnitude
Z skew
Z ellipticity
Period (sec)

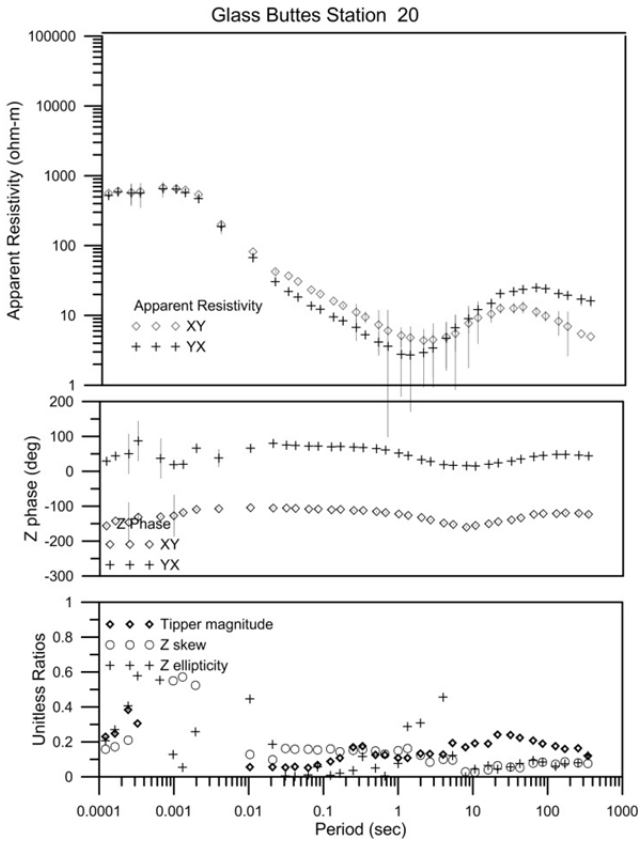
Glass Buttes Station 20
Apparent Resistivity (ohm-m)
Apparent Resistivity
XY
YX
Z phase (deg)
Z Phase
XY
YX
Unitless Ratios
Tipper magnitude
Z skew
Z ellipticity
Period (sec)

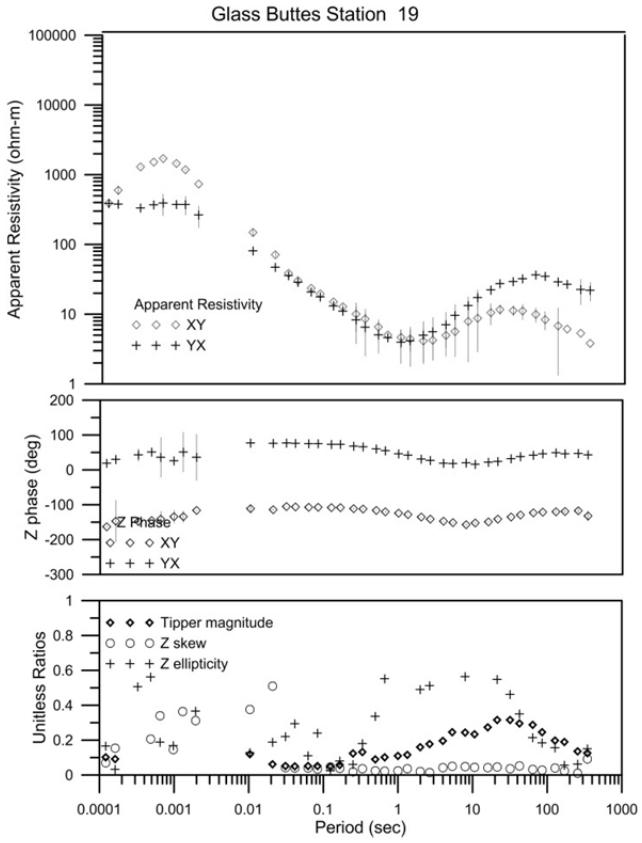
Glass Buttes Station 19
Apparent Resistivity (ohm-m)
Apparent Resistivity
XY
YX
Z phase (deg)
Z Phase
XY
YX
Unitless Ratios
Tipper magnitude
Z skew
Z ellipticity
Period (sec)

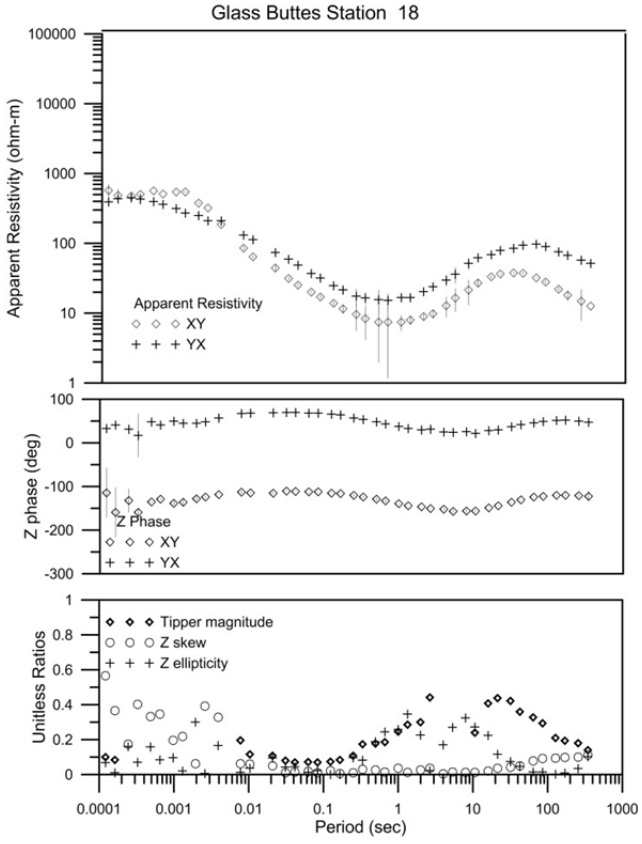
Glass Buttes Station 18
Apparent Resistivity (ohm-m)
Apparent Resistivity
XY
YX
Z phase (deg)
Z Phase
XY
YX
Unitless Ratios
Tipper magnitude
Z skew
Z ellipticity
Period (sec)

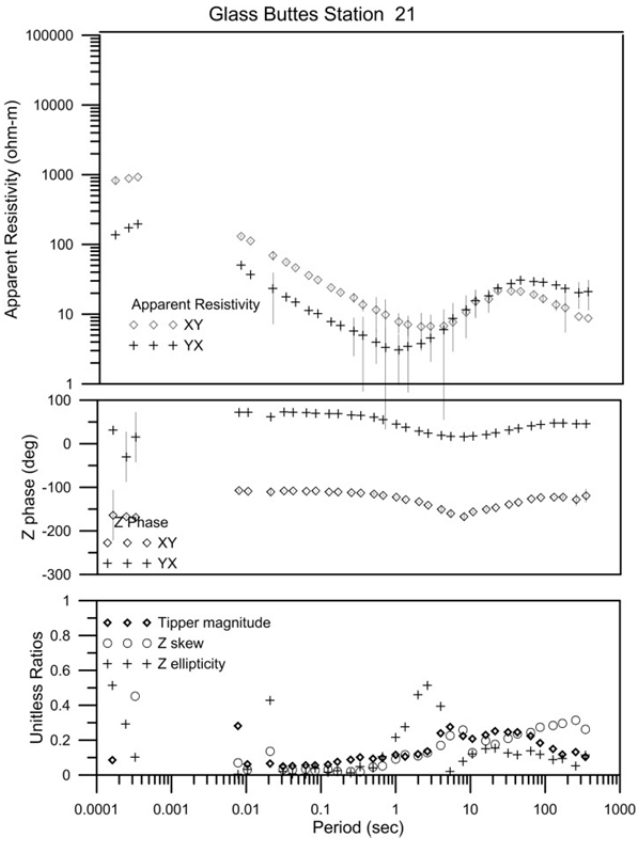
Glass Buttes Station 21
Apparent Resistivity (ohm-m)
Apparent Resistivity
XY
YX
Z phase (deg)
Z Phase
XY
YX
Unitless Ratios
Tipper magnitude
Z skew
Z ellipticity
Period (sec)

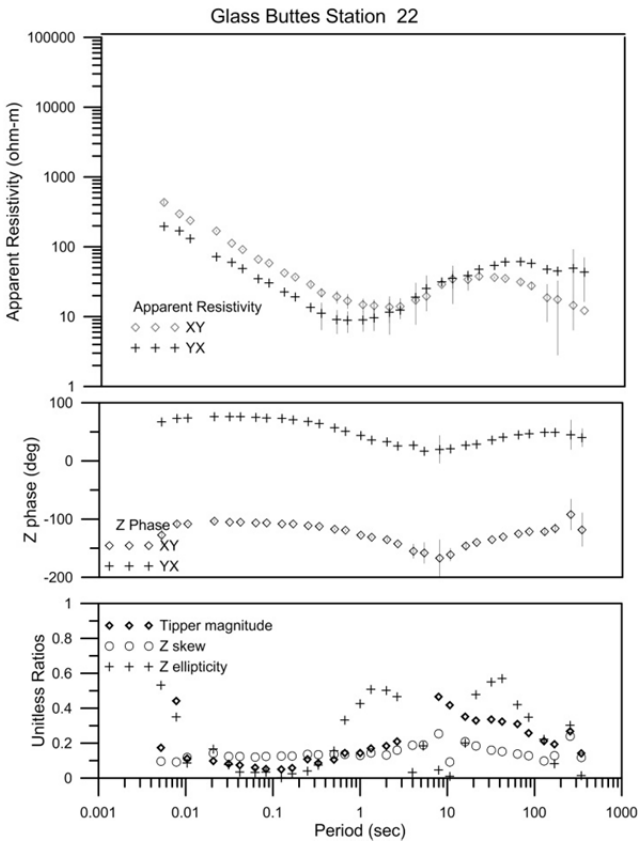
Glass Buttes Station 22
Apparent Resistivity (ohm-m)
Apparent Resistivity
XY
YX
Z phase (deg)
Z Phase
XY
YX
Unitless Ratios
Tipper magnitude
Z skew
Z ellipticity
Period (sec)

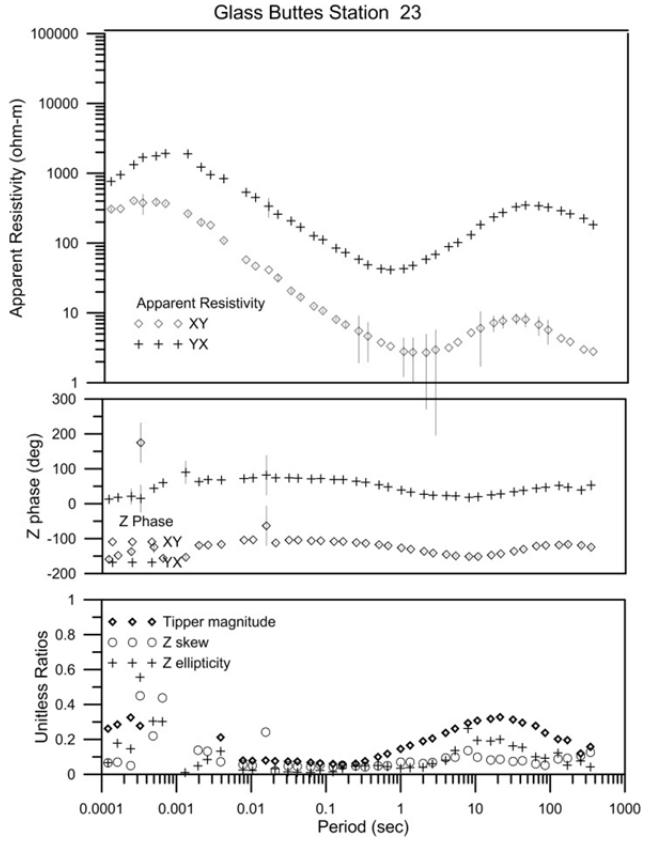
Glass Buttes Station 23
Apparent Resistivity (ohm-m)
Apparent Resistivity
XY
YX
Z phase (deg)
Z Phase
XY
YX
Unitless Ratios
Tipper magnitude
Z skew
Z ellipticity
Period (sec)

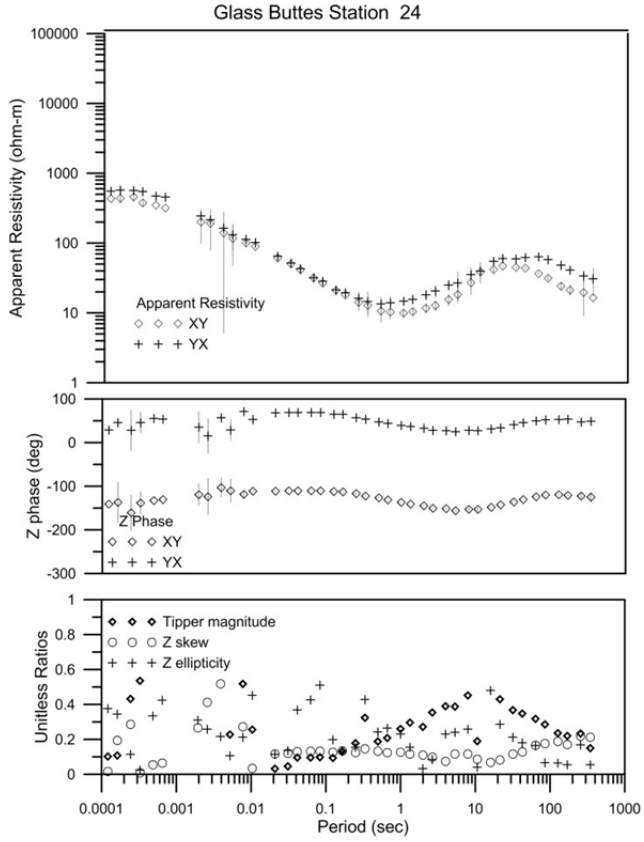
Glass Buttes Station 24
Apparent Resistivity (ohm-m)
Apparent Resistivity
XY
YX
Z phase (deg)
Z Phase
XY
YX
Unitless Ratios
Tipper magnitude
Z skew
Z ellipticity
Period (sec)

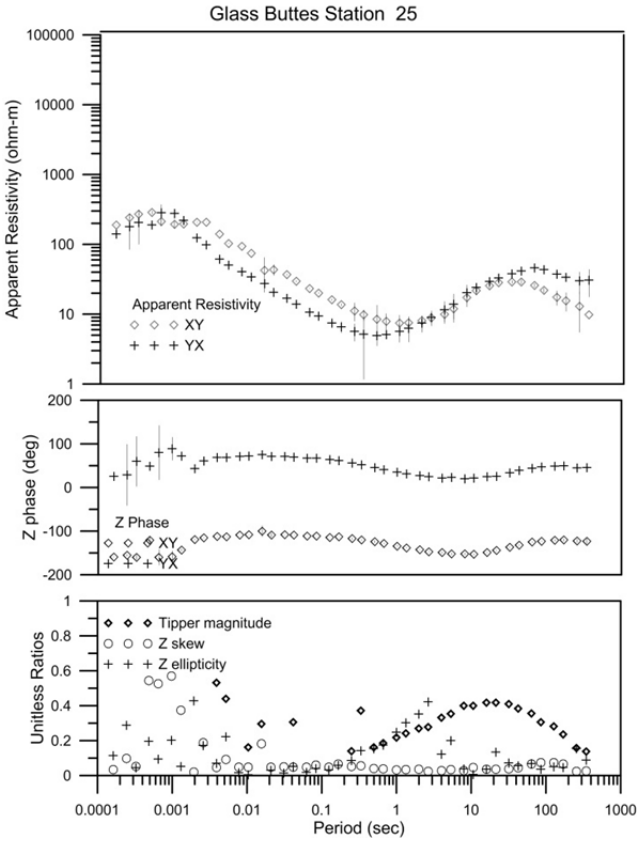
Glass Buttes Station 25
Apparent Resistivity (ohm-m)
Apparent Resistivity
XY
YX
Z phase (deg)
Z Phase
XY
YX
Unitless Ratios
Tipper magnitude
Z skew
Z ellipticity
Period (sec)

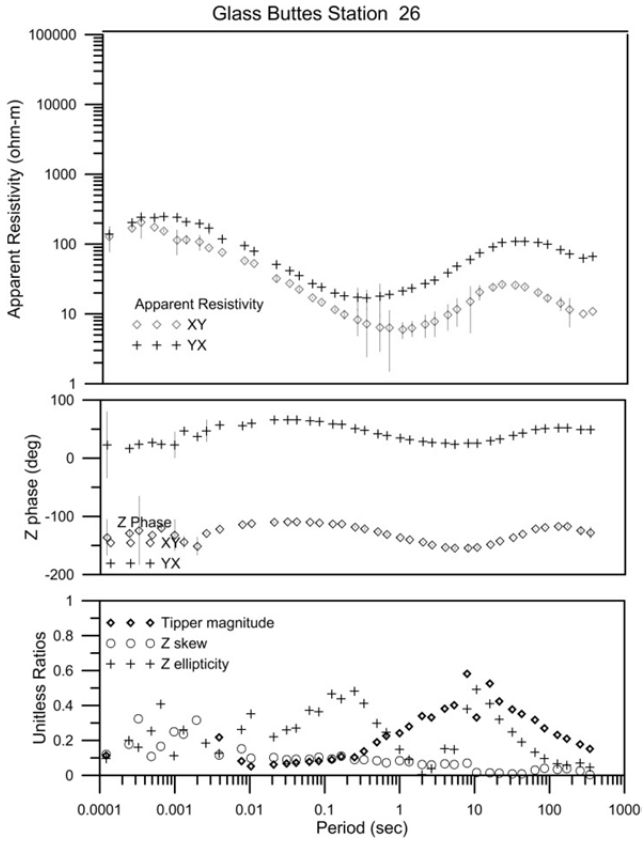
Glass Buttes Station 26
Apparent Resistivity (ohm-m)
Apparent Resistivity
XY
YX
Z phase (deg)
Z Phase
XY
YX
Unitless Ratios
Tipper magnitude
Z skew
Z ellipticity
Period (sec)

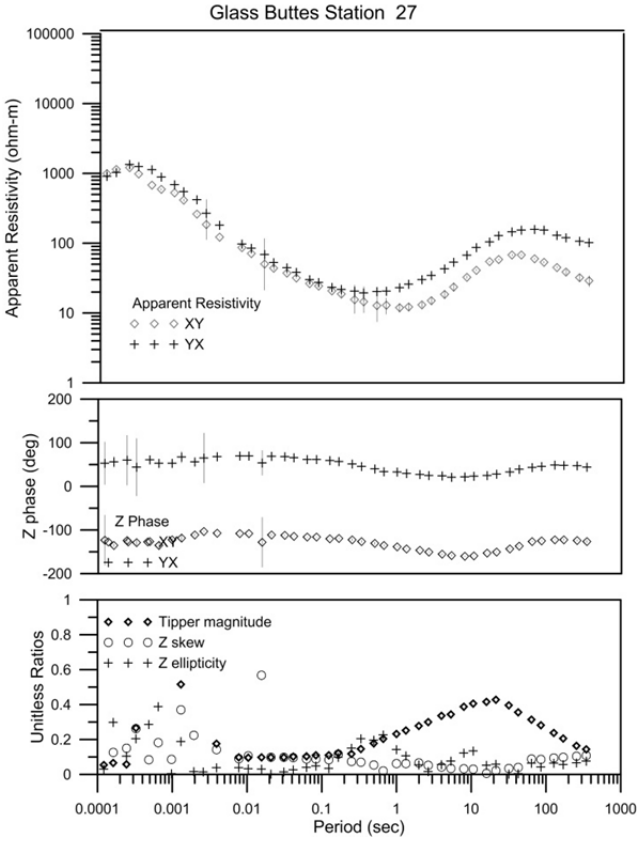
Glass Buttes Station 27
Apparent Resistivity (ohm-m)
Apparent Resistivity
XY
YX
Z phase (deg)
Z Phase
XY
YX
Unitless Ratios
Tipper magnitude
Z skew
Z ellipticity
Period (sec)

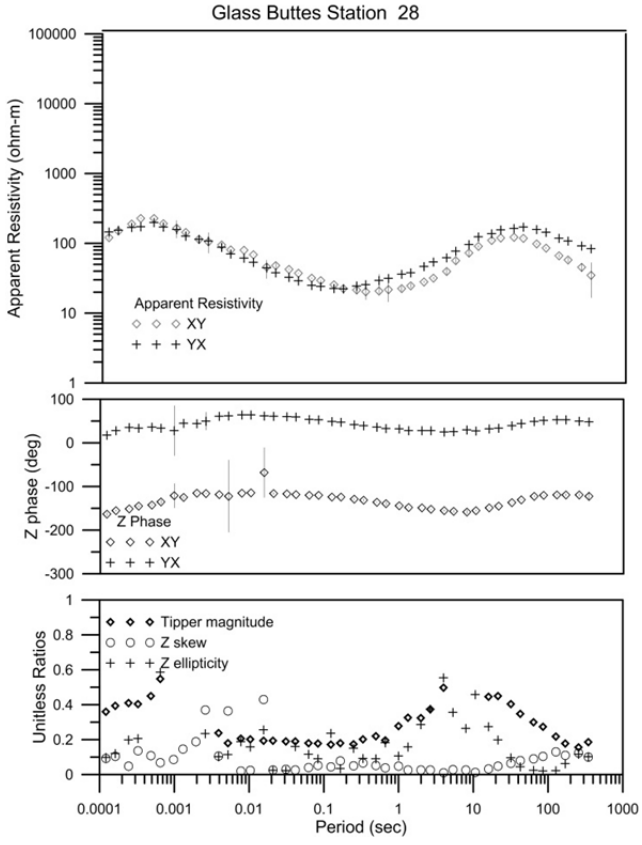
Glass Buttes Station 28
Apparent Resistivity (ohm-m)
Apparent Resistivity
XY
YX
Z phase (deg)
Z Phase
XY
YX
Unitless Ratios
Tipper magnitude
Z skew
Z ellipticity
Period (sec)

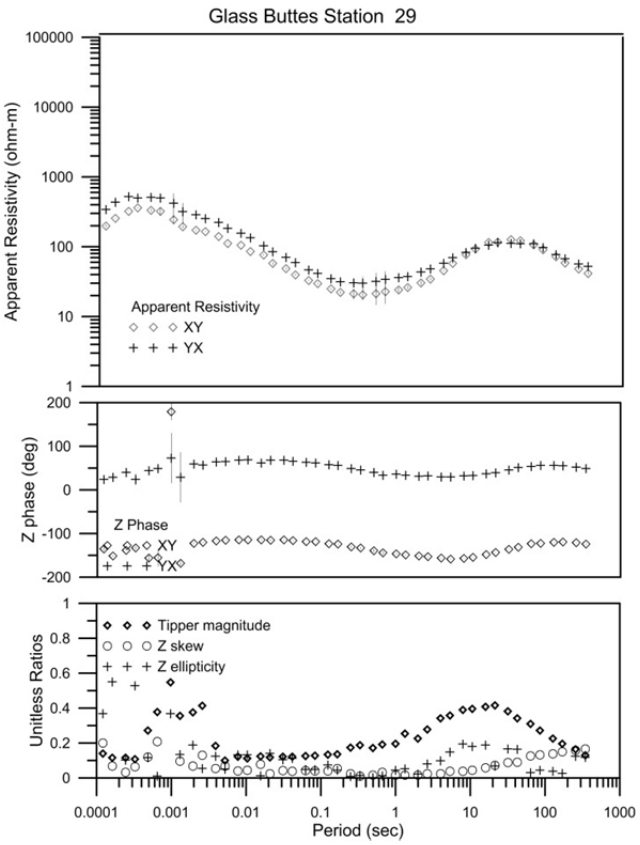
Glass Buttes Station 29
Apparent Resistivity (ohm-m)
Apparent Resistivity
XY
YX
Z phase (deg)
Z Phase
XY
YX
Unitless Ratios
Tipper magnitude
Z skew
Z ellipticity
Period (sec)

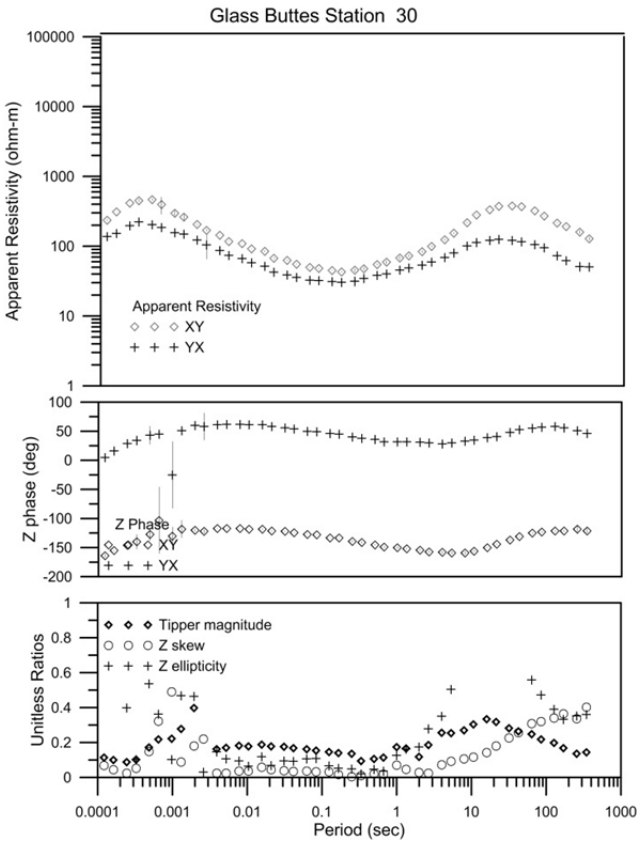
Glass Buttes Station 30
Apparent Resistivity (ohm-m)
Apparent Resistivity
XY
YX
Z phase (deg)
Z Phase
XY
YX
Unitless Ratios
Tipper magnitude
Z skew
Z ellipticity
Period (sec)

APPENDIX C: Production Log

This appendix contains a daily log of field logistics and production.

DATE	NOTES AMT/MT
7-Oct	Mobilization from Reno, NV to Bend, OR.
8-Oct	Built remote station 1. Read Low (L) band station 10, station 14.
9-Oct	Read Medium (M), High (H), Very High (VH) bands station 10, station 14. Read TEM stations 10, 14. Read TEM stations 15, 17. Began L band data data acquisition stations 15, 17.
10-Oct	Read M, H, VH bands stations 15, 17. TEM stations 9, 16. Read M, H, VH bands stations 9, 16. Began L band data acquisition.
11-Oct	TEM stations 5, 6. Read M, H, VH bands and began L band data acquisition stations 5, 6.
12-Oct	TEM stations 7, 8. Read M, H, VH bands and began L band data acquisition stations 7, 8.
13-Oct	TEM stations 2, 3. Read M, H, VH bands and began L band data acquisition stations 2, 3.
14-Oct	TEM stations 1, 12. Began L band data acquisition stations 1, 12.
15-Oct	Built remote station 2. Read M, H, VH bands stations 1, 12. TEM stations 4, 11. Began L band data acquisition stations 4, 11.
16-Oct	Read M, H, VH bands stations 4, 11. TEM stations 19, 20. Began L band data acquisition stations 19, 20.
17-Oct	Read M, H, VH bands stations 19, 20. TEM stations 21, 22. Began L band data acquisition stations 21, 22.
18-Oct	Read M, H, VH bands stations 21, 22. TEM stations 23, 25. Began L band data acquisition stations 23, 25.
19-Oct	Read M, H, VH bands stations 23, 25. TEM stations 24, 26. Began L band data acquisition stations 24, 26.
20-Oct	Read M, H, VH bands stations 24, 26. TEM stations 18, 27. Began L band data acquisition stations 18, 27.
21-Oct	Read M, H, VH bands stations 18, 27. TEM station 28. Began L band data acquisition stations 18 (repeat), 28.
22-Oct	Read M, H, VH bands stations 28, 29. TEM stations 28, 29. Began L band data acquisition stations 28, 29.
23-Oct	Read M, H, VH bands stations 13, 30. TEM stations 13, 30. Began L band data acquisition stations 13, 30.
24-Oct	Retrieved all electronics from field due to heavy rain.
25-Oct	Weather day
26-Oct	Read M, H, VH bands stations 14 (repeat), 15 (repeat). Began L band data acquisition stations 14 (repeat), 15 (repeat).
27-Oct	Built remote station 3. Line 1 Rx=3400: Began L band data acquisition.
28-Oct	Line 1: Rx=3400: Read M, H, VH bands. Line 1 Rx=3000, Rx=2600: Read M, H, VH bands. Began L band data acquisition.
29-Oct	Line 1: Rx=1800, Rx=2200: Read M, H, VH bands. Began L band data acquisition.
30-Oct	Line 1: Rx=1000, Rx=1400: Read M, H, VH bands. Began L band data acquisition.
31-Oct	Line 1: Rx=200, Rx=600: Read M, H, VH bands. Began L band data acquisition.
1-Nov	Line 1: Rx=3800, Rx=4200: Read M, H, VH bands. Began L band data acquisition.
2-Nov	Line 1: Rx=4600, Rx=5000: Read M, H, VH bands. Began L band data acquisition.
3-Nov	Line 1: Rx=5400, Rx=5800: Read M, H, VH bands. Began L band data acquisition.
4-Nov	Line 1: Rx=6200, Rx=6600: Read M, H, VH bands. Began L band data acquisition.
5-Nov	TEM station 12 (repeat). Read M, H, VH bands stations 2 (repeat), 5 (repeat), 4 (repeat), 9 (repeat)
6-Nov	Read M, H, VH bands stations 8 (repeat), 3 (repeat)
7-Nov	Read M, H, VH bands stations 6 (repeat), 7 (repeat)
8-Nov	Demobilized from Bend, OR to Reno, NV.

APPENDIX D: MT Station Locations

This appendix contains information on MT station locations for East and West areas, and notes on cultural features that could influence data.

East Area MT Station Locations

	NAD 83 UTM Zone 10	NAD 83 UTM Zone 10	
Station	East (m)	North (m)	Elevation (m)
1	742777	4828635	1413
2	743694	4828477	1403
3	744230	4828135	1409
4	744017	4829038	1378
5	744970	4828690	1392
6	745874	4828582	1401
7	745072	4827787	1395
8	746027	4827645	1405
9	746791	4827501	1414
10	747315	4827904	1412
11	743273	4827540	1439
12	744293	4826930	1480
13	745506	4826761	1435
14	747800	4827050	1423
15	746765	4826393	1425
16	747797	4826338	1425
17	746594	4825731	1450
18	745592	4825985	1468
19	743655	4826313	1536
20	742690	4826805	1482
21	742934	4825814	1463
22	744069	4825756	1547
23	743724	4825029	1511
24	745846	4825231	1496
25	744522	4824528	1520
26	745490	4824635	1495
27	744791	4823961	1541
28	745763	4823979	1514
29	746489	4824079	1537
30	746838	4823414	1541

West Area Line 1 end-point Locations

	NAD 83 UTM Zone 10	NAD 83 UTM Zone 10	
Station	**East (m)**	**North (m)**	**Elevation (m)**
0	728257	4825705	1405
6800	733453	4830092	1380

Cultural Feature Locations

	NAD 83 UTM Zone 10	NAD 83 UTM Zone 10	
Feature	**East (m)**	**North (m)**	**Elevation (m)**
Fence	733417	4830063	1378
Fence-1	730847	4827885	1366
Fence-1E	730878	4827886	1366
Fence-1W	730818	4827886	1366
Fence-E	733459	4830064	1378
Fence-NW	730525	4827665	1365
Fence-SE	730525	4827596	1365
Fence-W	733386	4830065	1376
Fence	729848	4827005	1455
Optic Cable	733425	4830069	1377

APPENDIX E: Instrument Specifications

GDP-32 Receiver GDP-32 Receivers

- 1 to 16 channels, large case, user expandable
- 1 to 6 channels, small case, user expandable
- Alphanumeric keypad
- 386SX MPU, 387SL math coprocessor
- All programs resident in memory:
  Resistivity, Time/Frequency Domain IP, CR, CSAMT/MT, Harmonic Analysis CSAMT/MT (HACSAMT/MT), AMT, MT, TEM & NanoTEM®
- Screen graphics: plots of time-domain decay, resistivity and phase, complex plane plots, etc., on a 256 x 128 pixel LCD
- Internal humidity and temperature sensors
- Automatic time-schedule program for remote operation with the XMT-32 transmitter controller.
- Use as a data logger for analog data, borehole data, etc.
- 0.015625 Hz to 8 kHz frequency range standard, 0.0007 Hz minimum for MT
- One 16 bit A/D per channel for maximum speed and phase accuracy
- 1.5 MB ROM, up to 15 MB RAM for program execution
- 1 MB SRAM for data storage standard, stores several days' worth of data, expansion up to 4 MB SRAM plus optional hard disk
- Real-time data and statistics display
- Anti-alias, power line notch and telluric filtering
- Automatic SP buck out, gain setting and calibration
- Rugged, portable and environmentally sealed
- Modular design for upgrades and board replacement

ANT/6 CSAMT/MT Antenna

- Power: 2 internal 9 volt alkaline batteries.
- Battery Life at 12 hours per day:
  - Alkaline: 10 days
  - Lithium: 20 days
  - Carbon Zinc: 4 days (temporary use only)
- Sensitivity in Passband: 250 millivolts/gamma (250 mV/nT)

- Frequency Range: 0.1 to 10,000 Hz
- Noise Level:
  - 200 microgamma (200 fT) per squareroot_Hz at 1 Hz
  - 1 microgamma (1 fT) per squareroot_Hz nominal > 200 Hz

- Tube diameter: 4.8 cm (1.875 in)
- Length: 91 cm (36.0 in)
- Weight: 3.2 kg (7.0 lb)

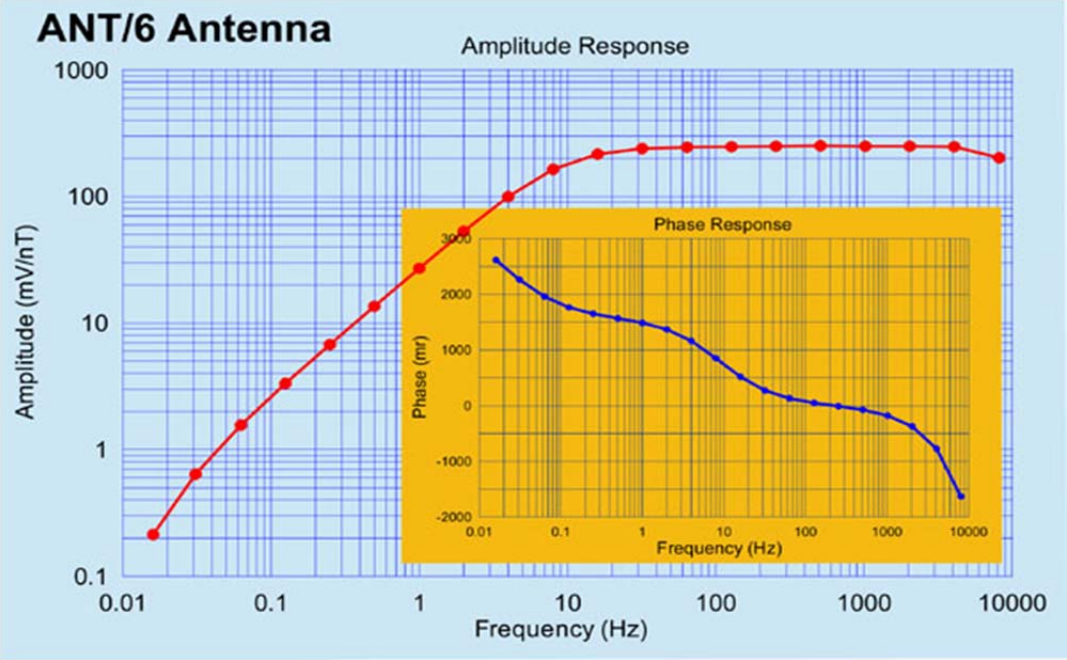

ANT/4 MT Antenna

- Power: 2 internal 9 volt alkaline batteries.
- Battery Life at 12 hours per day:
  - Alkaline: 10 days
  - Lithium: 20 days
  - Carbon Zinc: 4 days (temporary use only)
- Sensitivity in Passband: 100 millivolts/gamma (100 mV/nT)
- Frequency Range: 0.0005 to 1000 Hz
- Noise Level:
  - 100 microgamma (100 fT) per squareroot_Hz at 1 Hz
  - 20 microgamma (20 fT) per squareroot_Hz nominal > 1 Hz

- Tube diameter: 4.8 cm (1.875 in)
- Length: 138 cm (54.0 in)
- Weight: 6.2 kg (13.5 lb)

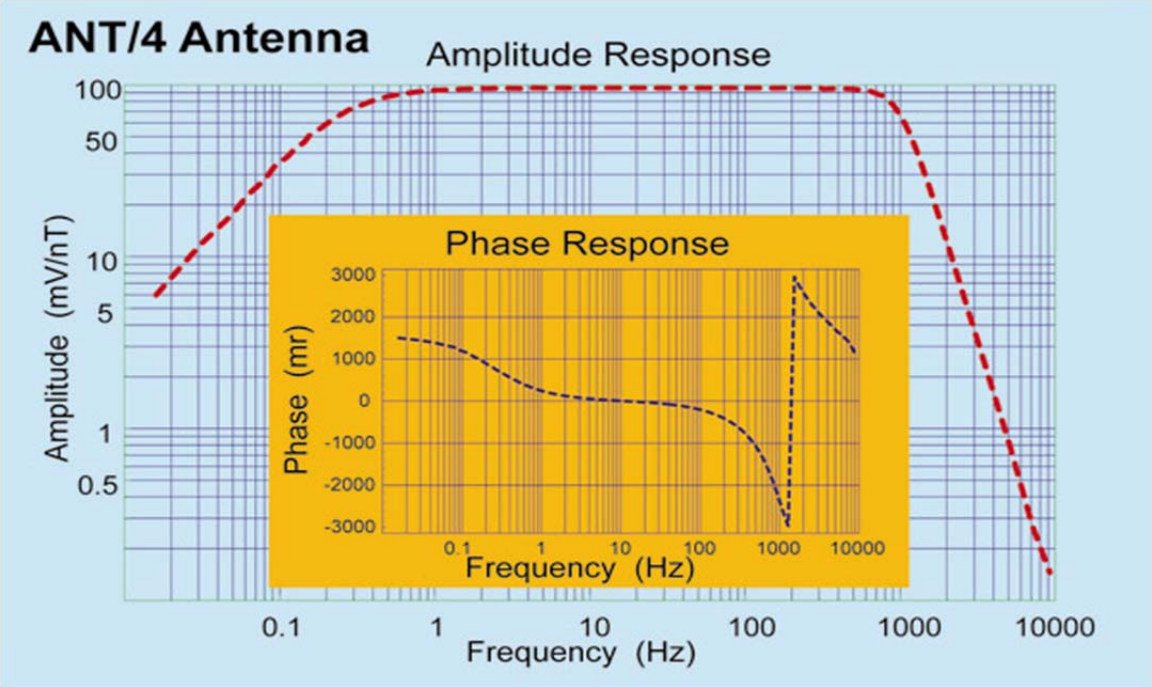

Signal conditioning preamplifier for MT/AMT measurements

The SC-8 Signal Conditioning Box is used to amplify and filter electric and magnetic telluric signals prior to entering the GDP receiver system. Use of this device is recommended to provide low-noise amplification, radio-noise filtering, and limiting of low-frequency tellurics. The SC-9 can also be used as a radio signal filter for CSAMT and IP surveys.

Electrical Specifications
Analog channels: 8
Gain settings: x1, x8, x32, x128
High pass filters 1, .1, .01, .001 Hz
Low pass filter: 10 Hz
Saturation detector: +/- 4.5 volts
Noise: Less than 50 nV per squareroot-Hz at 1 Hz
Batteries: One set of 12-volt batteries

Mechanical Specifications
Analog input: 5-way Pomona connectors, 8 pairs red and black. BNC inputs for channels 6, 7, 8 for capacitor (ac) coupling.
Analog output: 26-pin connector (same as GDP input connector)
Analog common for input: black 5-way Pomona connector.
LCD Display: 8-character, for gain, high-pass/low-pass filter settings, serial port ON/OFF, analog meter ON/OFF, and time schedule information.
Analog Meter: +/- 5-volt analog output and battery level monitor.
LED: +/- saturation indicator, red positive, green negative.
Switches: **On / Off** (on side panel).

Manual / Time Schedule operation
Filter / Gain selection.
Analog Meter Function, selects +/- battery voltage monitor and analog signal monitor for each channel.
Push button Functions:
When the **Filter / Gain** switch is in the **Filter** position:
- Pressing **Select** will change the high pass filters in sequence: 1. .1, .01, .001 Hz
- Pressing **Function** will set the 10 Hz low-pass filter in/out and turn the analog meter on/off.
When the **Filter / Gain** switch is in the **Gain** position:
- Pressing **Function** will select a channel (1 - 8).
- Pressing **Select** will set the gain for the displayed channel (x1, x8, x32, x128), and turn the channel on/off (if channel 4, 5, 6, 7, or 8).
Battery charge: 24 volt, 4-pin port, on side panel. This port also serves as an external battery connection.
Serial input: 10-pin port for time schedule input.

Input Connections for the SC-8

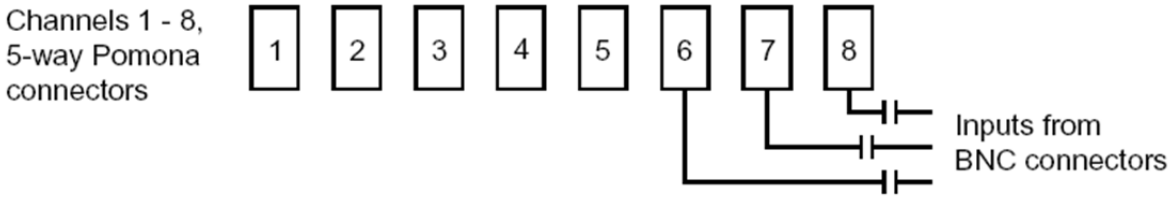

NOTICE: All channels have a 9.5 MΩ resistor installed in parallel with the input.
Signals connected through the BNC connector inputs to channels 6, 7 and 8, pass through a 10-microfarad capacitor on the positive (red) inputs, and are connected directly to the negative (black) inputs. This capacitor is installed to remove the strong DC offsets obtained with the EMI antennas. The capacitor along with the 9.4 MΩ resistors provides a high-pass filter with a corner frequency of .0017 Hz. If connection is made directly to the 5-way Pomona connectors, the 10-microfarad capacitor is bypassed.

Block Diagram of the SC-8

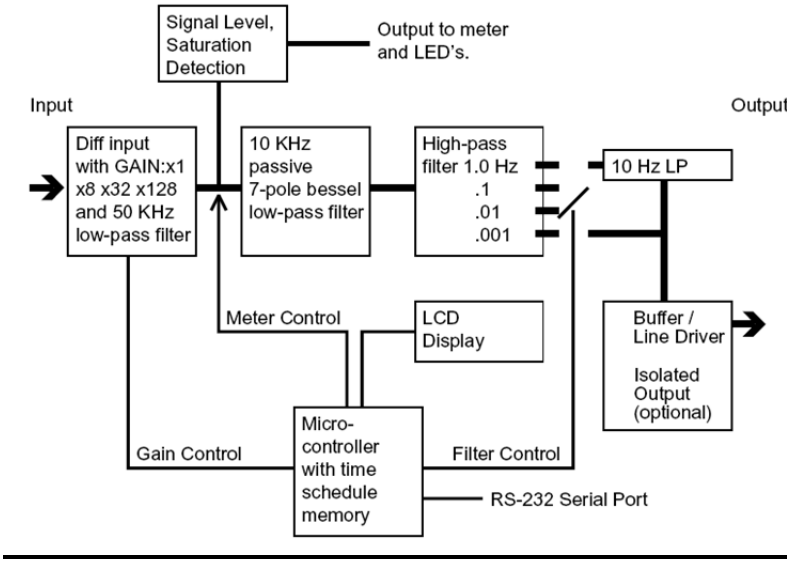

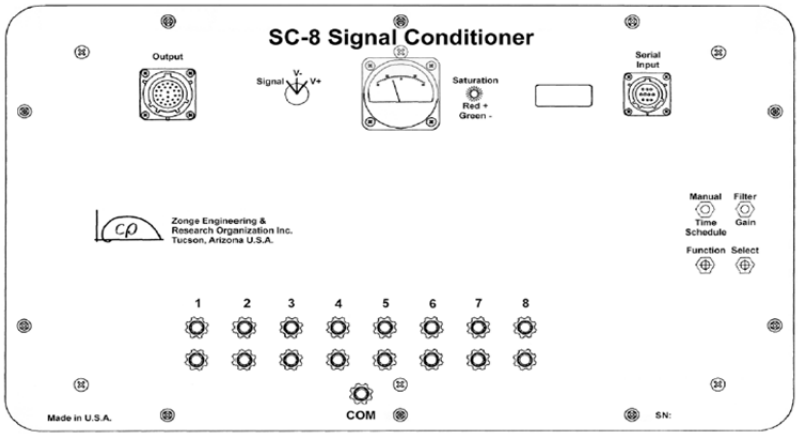
SC-8 Signal Conditioner
Output
Signal
V-
V+
Saturation
Red +
Green -
Serial Input
Zonge Engineering & Research Organization Inc. Tucson, Arizona U.S.A.
Manual Time Schedule
Filter Gain
Function Select
1 2 3 4 5 6 7 8
COM
Made in U.S.A.
SN:

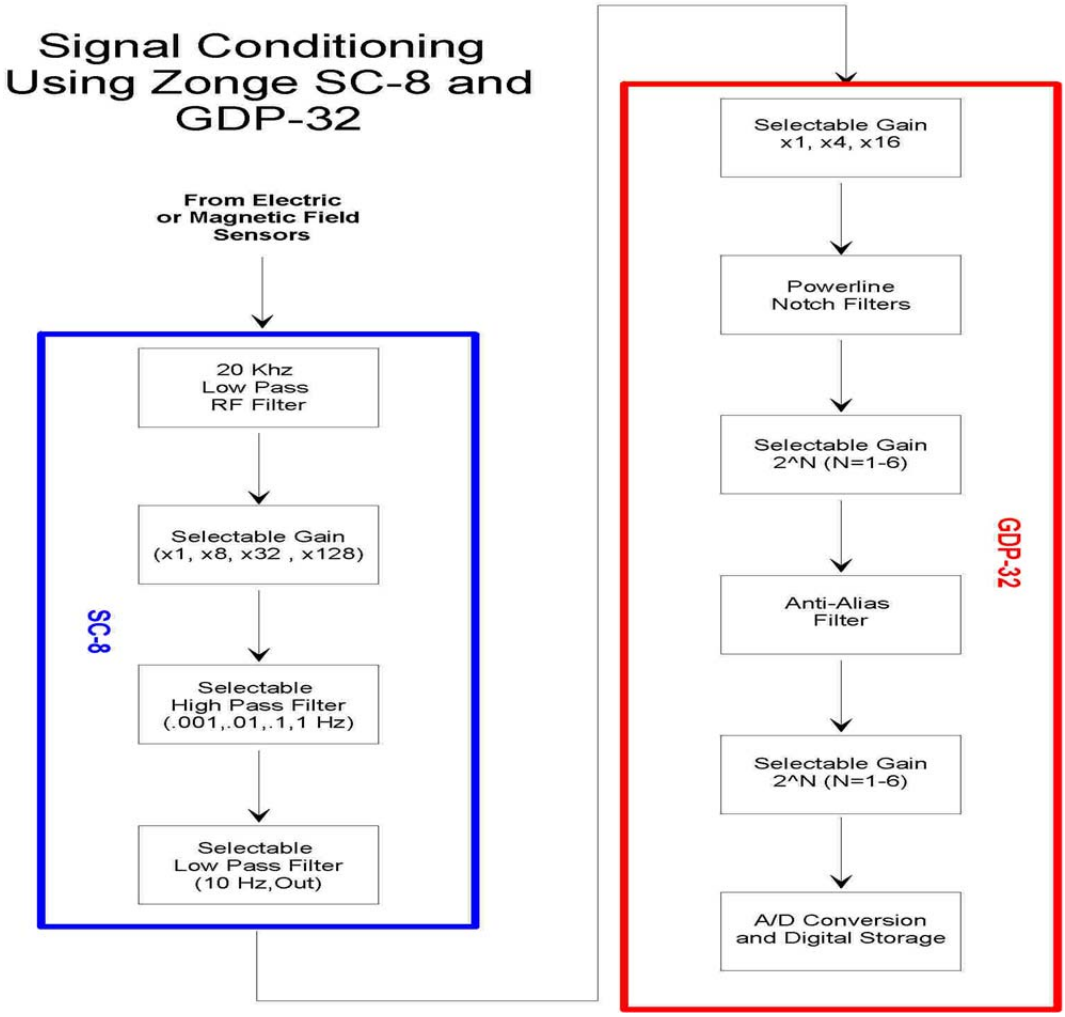
Signal Conditioning Using Zonge SC-8 and GDP-32
From Electric or Magnetic Field Sensors
20 Khz Low Pass RF Filter
Selectable Gain (x1, x8, x32 , x128)
Selectable High Pass Filter (.001,.01,.1,1 Hz)
Selectable Low Pass Filter (10 Hz,Out)
SC-8
Selectable Gain x1, x4, x16
Powerline Notch Filters
Selectable Gain 2^N (N=1-6)
Anti-Alias Filter
Selectable Gain 2^N (N=1-6)
A/D Conversion and Digital Storage
GDP-32

APPENDIX F: Overview of magnetotellurics

Electric currents within the earth produce the magnetotelluric signals that are measured by the Zonge AMT/MT System. The earth currents are induced by two types of natural electromagnetic activity above the earth's surface. Atmospheric electrical discharge, i.e., lighting from distant continents and nearby are the primary sources electromagnetic fields at frequencies above 3 Hz. These signals are channeled globally in the "waveguide" between the earth's surface and ionosphere. Below 3 Hz the electromagnetic sources are associated with the interaction between the earth's magnetosphere (several thousand kilometers above the earth's ionosphere) and the solar wind plasma. These magnetic fluctuations, in turn, induce horizontal electrical current circulation in the ionosphere and in the earth's crust and oceans.

These natural sources produce unpredictable daily variation in the magnitude of the source field used for magnetotelluric (MT) and audiomagnetotelluric (AMT) measurements, which occasionally make it desirable to re-occupy or extend the recording time at a station. For most areas and applications, a single over-night observation period is sufficient. (MT refers to measurements below approximately 300 Hz, AMT to measurements at frequencies from 10 to 10,000 Hz.)

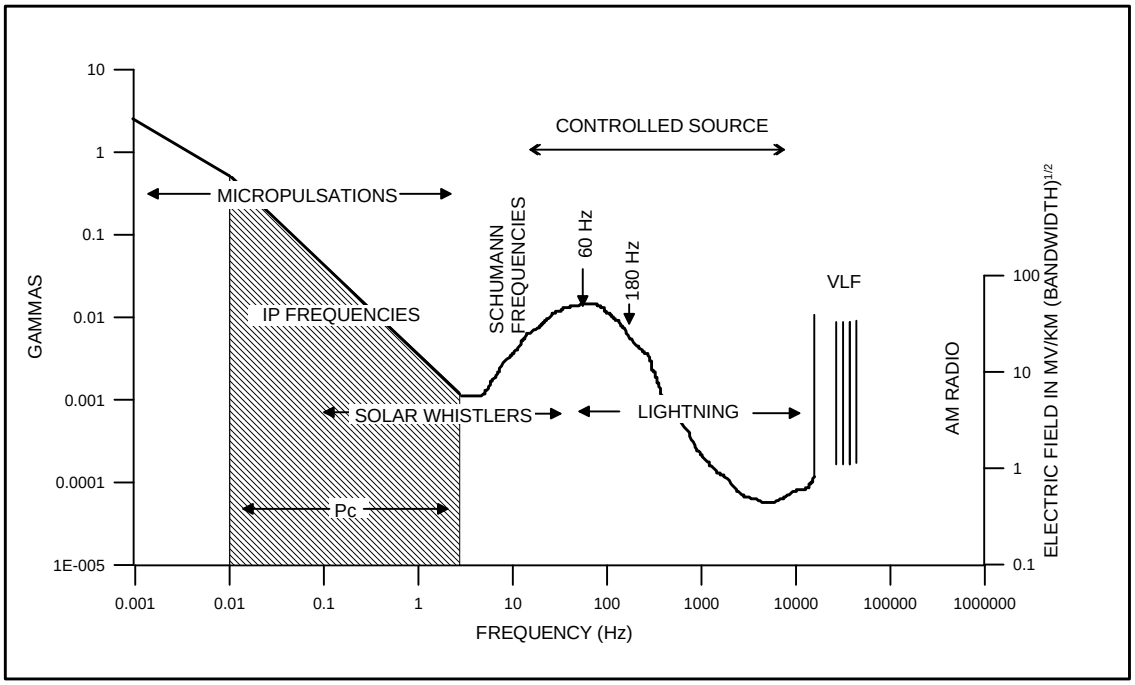

Figure D1: Natural Source AMT and MT, power spectra.

The theoretical foundations the MT/AMT methods and the practical interpretation of the field observation rest securely on several assumptions about the geometry of the electromagnetic source fields and the earth materials electrical properties over the range of frequencies employed.

- The natural EM (electromagnetic) fields are generated by large-scale current systems in the ionosphere or electrical discharges in the ionosphere-earth wave guide. These sources are typically far enough away from the Earth's surface that the observed fields can be treated as uniform, EM plane waves which are refracted into vertically propagating, horizontally uniform, electric and magnetic fields in the earth. Any locally uniform magnetic field variations originating above the surface will meet the plane wave assumption. This includes any natural or artificial electrical or magnetic source located at least six to eight horizontal earth skin-depths distance for the frequencies of interest. These source assumptions may breakdown for ionosphere sources near the equator and poles and very near lightning strikes.
- The measured magnetic fields exhibit multiple azimuths or polarizations. For full solution of the MT/AMT impedance Tensor, the direction of the surface horizontal magnetic field vector must exhibit at least two distinct azimuths or polarizations over the observation period in each frequency band. A change in source or direction to the source is not required, just a change in the azimuth or polarization of the observed field. Observing multiple polarizations in measurements during a standard length occupation period is rarely a problem.
- Earth materials behave as ohmic conductors rather than dielectrics over the frequency ranges employed. In other words time-varying electric currents (displacement currents) arising from earth material dielectric permittivity and macroscopic polarization effects (graphite coated fractures) are negligible in comparison with conduction currents at a given frequency and can be assumed to be zero in modeling. This assumption has two implications: the electric and magnetic fields induced in the earth are controlled by diffusion rather than electromagnetic wave propagation theory; and the earth can be modeled as an ohmic conductor, i.e. Ohm's law is obeyed: $j = \sigma E$ where j is current density in amps per square meter, σ is conductivity in siemens per meter, and E is the electrical field in volts per meter.
- Magnetic permeability's of the earth materials are well approximated by free-space permeability. This is a good approximation except over the most highly magnetic deposits.
- Surface normal or vertical electric current flow and electric fields at the earth's surface are zero. This is a very good approximation. Due to the high air-earth resistivity contrast, induced currents must flow surface parallel, so vertical currents and the vertical electric field are zero at the surface.
- Local measured electric fields are divergence free, which is equivalent to requiring that there are no electric current sources or drains (active electrodes) contributing to the magnetic and electric field measurements. This assumption can breakdown momentarily during lightning strikes within a few km of the measurements or near points of artificial current injection.

In the MT and AMT methods, the electric and magnetic fields generated by the electromagnetic sources discussed above are measured over a range of frequencies. The common recording range is 8000 Hz to 10^{-3} Hz. Regardless of the frequency the MT source field geometry is assumed to be planar. The electric field signal is sensed as a potential difference between two separated non-polarizable porous electrodes, connected by insulated wire to the receiver. The magnetic fields are detected using mu-metal cored induction magnetic field antennas. Different arrays can be used in the field to collect MT data, two examples of which are presented below in Figure D2. These include tensor and scalar setups:

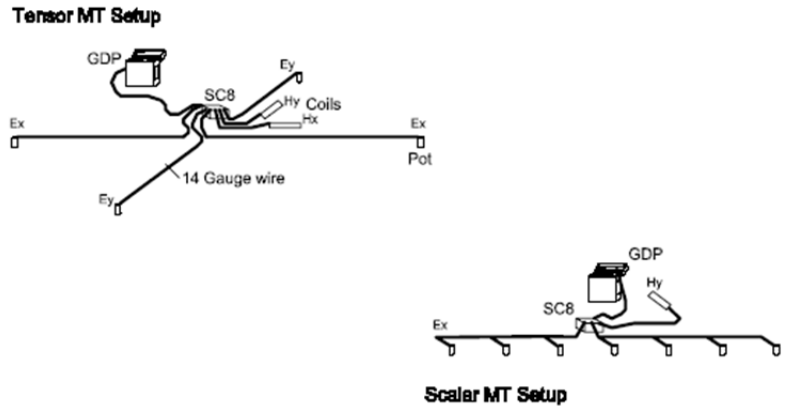

Figure D2. Tensor and scalar MT sensor setups.

The first step in the use of magnetotelluric information is to calculate impedance estimates for each pair if electric and magnetic fields. The scalar impedance, Z, is defined by E/H. This impedance can then be used to calculate the apparent resistivity:

$$\rho_{xy} = \frac{1}{5f}\left|\frac{Ex}{Hy}\right|^2 \text{ (ohm - meters)}$$

and phase:

$$\phi_{xy} = \arctan\left(\frac{\text{imag}(Z_{xy})}{\text{real}(Z_{xy})}\right),$$

where E_x is measured in mV/km and H_y is in nT.

The full impedance tensor $\overline{\overline{\mathbf{Z}}}$ relates horizontal electric and magnetic field components as

$$\begin{bmatrix} E_x \\ E_y \end{bmatrix} = \begin{bmatrix} Z_{xx} & Z_{xy} \\ Z_{yx} & Z_{yy} \end{bmatrix} \cdot \begin{bmatrix} H_x \\ H_Y \end{bmatrix}$$

or equivalently

$$E_x = Z_{xx} \cdot H_x + Z_{xy} \cdot H_y \text{ and } E_y = Z_{yx} \cdot H_x + Z_{yy} \cdot H_y .$$

The MT method is well suited for studying complicated geological environments because the electric and magnetic relations are sensitive to vertical and horizontal variations in resistivity. The method is capable of establishing whether the EM fields are responding to subsurface terranes of effectively 1-, 2-, or 3-dimensions. In a horizontally layered (1-D) earth diagonal impedance elements Z_{xx} and Z_{yy} are zero and the off diagonal terms are equal in magnitude and are related by $Z_{xy} = -Z_{yx}$. The impedance tensor Z is directionally independent in a 1-D earth. If resistivity decreases with depth, phase measurements will increase over 45^o; if resistivity increases with depth, phase measurements will dip below 45^o. An additional indicator of a 1-D earth is when the ratio H_z/H_x (Tipper) is a small number. H_z measured at the earth's surface should be zero for a 1-D earth.

For a 2-D earth, the diagonal elements of the impedance tensor are zero if sensors are aligned parallel and perpendicular to the structural strike, and in that case the off-diagonal elements correspond to the impedances of the two principal coupling modes, which are known as transverse electric (TE) and transverse magnetic (TM). For a y-directed strike direction, Z_{yx} (electric field parallel and magnetic field perpendicular to strike) would be the TE mode, and Z_{xy} (electric field perpendicular and magnetic field parallel to strike) would be the TM mode. If the dominant strike direction is unclear or unknown, Z_{xx} and Z_{yy} will be non-zero, but it is possible to apply mathematical rotation to make them zero (or nearly zero) and thus define the TE and TM directions. Mode identification is important to direct interpretational processing. Both 1-D and 2-D inversion algorithms require the identification and input of data in the TE and TM modes.

In a 2-D environment, inversion on the TM mode is usually superior to TE mode inversion, since the TM mode is more sensitive to lateral conductivity changes than is the TE mode. Wannamaker et al. (1984) has demonstrated that inversion of the 2-D TM mode in many

circumstances can be a suitable approximation to model data in a 3-D environment. However, 2-D inversions of 3-D electrical structures can sometimes produce conductivity artifacts. In particular, conductivities can be estimated too low, and conductive blobs or dike-like bodies may appear in the 2-D inversion model. This same effect can be caused by electrical anisotropy. In addition, charges can build up on vertical conductivity contacts, and this can produce significant frequency independent static shifts, which appear as offsets in the apparent resistivity curves. If not identified and corrected, static shifts can lead to order-of-magnitude inaccuracies in the inverted model.

Data are often collected in an orientation that is not aligned to geological strike of the target structure. Data at Mt Spurr were acquired with a consistent orientation of sensors with $x = 90^o$, i.e. due east. For a 3-D earth, pure TE and TM modes do not exist, and the simplicity of analysis by mode separation is reduced. In this case, all components of Z are present, and can have similar magnitudes.

Tipper

The vertical component of the magnetic field H_z is linearly related to the horizontal components by the relation

$$H_z = T_x H_x + T_y H_y.$$

In general, all quantities in the above equation are complex and frequency dependent. The quantities T_x and T_y are called tippers because they have the effect of tipping the horizontal components of the H fields slightly into the vertical plane, creating a usually small H_z component.

H_z is generated by lateral gradients in conductivity or sharp conductivity discontinuities, and quantities derived from H_z are therefore important in assessing 2-D or 3-D MT environments. Tipper magnitude |T| is defined as $\mathrm{sqrt}(|T_x|^2 + |T_y|^2)$, and is directly proportional to the lateral conductivity gradient. In a purely layered earth, there are no lateral gradients, thus $H_z = 0$, as are the tipper components and tipper magnitude.

In a 2-D earth, the tipper is associated with only the TE mode, and T_y and T_x have the same phases, so that and T_y/T_x is a real number. In this case, it is possible to determine the strike direction of a 2-D contact by computing ϕ where

$$\phi = \arctan (T_y/T_x) .$$

This quantity is referred to as tipper strike.

It is also possible to infer the conductive vs the resistive side of a contact by analyzing the tipper magnitude and phase across the contact.

In a 3-D earth, the phases of T_x and T_y are different, and more complicated definitions for ϕ are required. One definition involves finding the value of ϕ that maximizes the cross-power of horizontal and vertical components. In this way a dominant strike direction may be found under favorable conditions.

Tipper magnitudes and directions can be combined to make induction arrow maps. Induction arrows can be used to infer the presence or absence of lateral conductivity gradients, and can be used to identify 3-D conductors in the earth as they will point toward the conductor (or away from it, depending on convention used).

APPENDIX G: Geomagnetic Indices

```
Daily Geomagnetic Data     2010_DGD.txt
:Issued: 1900 UT 07 Jan 2011
#
#    Prepared  by  the  U.S.  Dept.  of  Commerce,  NOAA,  Space  Weather
Prediction Center
#
#                    2010 Daily Geomagnetic Data

                    Middle Latitude    High Latitude      Estimated
                  - Fredericksburg  ---- College ----     Planetary ---
Date         A      K-indices         A      K-indices     A      K-indices
2010 10 01     0  0 1 0 0 0 0 0 0    0  0 0 0 0 0 0 0 0    3  1 0 0 0 2 1 1 1
2010 10 02     0  0 0 0 0 0 1 0 0    0  0 0 0 0 0 0 0 0    2  0 0 0 0 2 1 1 1
2010 10 03     1  1 1 0 1 0 0 0 0    0  0 0 0 1 0 0 0 0    3  1 0 0 1 1 1 0 1
2010 10 04     2  0 0 0 0 1 1 1 1    0  0 0 0 0 1 0 0 0    3  0 0 0 0 2 1 1 2
2010 10 05     6  1 2 3 2 2 1 1 0   12  2 0 4 4 4 2 0 0    6  1 2 3 2 1 2 1 1
2010 10 06     5  1 0 2 2 3 1 1 1   13  0 0 3 4 5 2 1 0    8  1 0 2 2 3 2 3 1
2010 10 07     2  1 1 1 0 1 1 0 1   10  0 0 4 4 4 0 0 0    4  1 2 1 1 1 1 0 1
2010 10 08     3  2 1 0 1 1 1 0 1    5  3 1 1 3 0 0 1 0    4  3 1 1 1 0 1 0 1
2010 10 09     3  1 1 1 1 1 2 1 0    4  0 0 0 4 0 1 1 0    4  1 1 1 1 1 1 0 1
2010 10 10     1  0 0 0 0 1 0 0 1    3  0 0 0 2 3 0 0 1    2  0 0 0 0 1 0 0 1
2010 10 11    10  1 2 2 3 4 2 2 2   49  0 0 4 6 6 7 5 3   20  1 2 3 4 5 4 3 2
2010 10 12     7  3 2 2 1 2 1 1 2   15  2 3 3 3 4 4 1 2   10  3 3 3 1 2 3 2 2
2010 10 13     3  1 1 1 1 0 1 1 1    4  2 1 1 2 2 1 0 0    4  2 1 2 1 1 1 1 1
2010 10 14     0  1 0 0 0 0 0 0 0    0  0 0 0 0 0 0 0 0    2  1 0 0 0 0 0 0 1
2010 10 15     3  0 1 0 1 1 1 1 2    3  0 0 0 1 3 0 1 0    5  0 1 0 1 1 1 3 1
2010 10 16     3  1 1 1 0 1 1 2 1    5  1 0 1 0 2 3 1 2    6  1 2 1 0 1 1 3 2
2010 10 17    10  2 3 4 2 1 1 2 2   22  2 2 6 5 4 1 1 1   11  2 3 4 3 1 0 2 3
2010 10 18     3  2 0 0 1 0 0 1 2    4  1 0 1 3 1 0 1 2    5  2 0 0 1 1 1 2 3
2010 10 19     7  2 2 2 1 2 1 3 1    7  2 3 3 3 1 0 0 1    5  2 2 2 1 1 0 0 2
2010 10 20     3  2 0 0 1 2 0 1 0    5  1 1 0 1 4 0 0 0    4  2 0 0 1 2 0 1 1
2010 10 21     1  1 0 0 0 1 1 0 0    2  1 0 0 0 2 1 0 0    3  1 0 0 0 2 1 1 1
2010 10 22     4  0 1 2 1 1 1 2 2    5  0 0 3 2 2 1 1 1    6  0 1 2 1 1 2 2 3
2010 10 23    16  4 2 3 3 3 3 2 4   40  2 3 4 6 7 4 2 3   23  3 2 4 4 5 4 2 4
2010 10 24    10  3 3 2 2 2 2 3 1   24  3 4 3 5 5 3 3 2   14  3 4 2 3 3 2 4 1
2010 10 25     4  1 1 1 1 2 1 2 1    9  1 1 2 3 4 2 1 2    6  2 1 1 1 2 1 3 1
2010 10 26     6  3 1 2 2 1 1 2 1    7  2 1 2 2 1 2 3 2    8  3 2 2 2 1 2 2 2
2010 10 27     3  0 1 1 1 1 1 2 1    2  1 1 0 1 1 0 1 0    4  1 1 1 0 1 0 2 2
2010 10 28     2  0 0 0 1 1 1 1 0    4  1 0 0 3 2 1 1 0    3  0 0 0 0 1 1 1 1
2010 10 29     2  1 1 1 0 1 0 0 0    2  1 0 0 0 2 2 0 0    3  1 1 0 0 1 2 0 0
2010 10 30     2  0 0 0 1 1 1 0 1    0  0 0 0 0 0 1 0 0    2  0 0 0 1 1 2 0 0
2010 10 31     4  0 2 1 2 2 1 1 1    1  0 0 0 0 1 0 1 0    3  0 2 0 1 2 0 0 1
2010 11 01     2  0 0 1 0 2 0 1 0    0  0 0 0 0 0 0 0 0    2  0 1 1 0 1 0 0 1
2010 11 02     1  0 0 1 1 1 0 0 0    2  0 0 2 2 1 0 0 0    2  0 0 1 1 1 1 0 0
2010 11 03     2  1 1 1 1 1 0 1 0    6  0 0 2 2 4 1 1 0    4  1 1 1 1 1 1 1 1
2010 11 04     2  1 1 0 1 1 1 0 1    7  0 0 1 4 4 0 0 0    3  1 1 0 1 2 0 0 1
2010 11 05     2  0 0 1 1 1 2 1 0    4  0 0 2 3 2 0 0 0    2  0 0 1 1 1 1 0 0
2010 11 06     1  0 0 0 0 0 2 0 0    0  0 0 0 1 0 0 0 0    1  0 0 0 0 0 1 0 1
2010 11 07     1  1 0 0 0 1 0 1 0    1  0 0 0 0 0 0 1 1    1  1 0 0 0 0 0 1 0
2010 11 08     2  0 0 1 1 2 1 1 0    3  0 0 0 1 3 1 1 0    3  0 0 1 0 2 2 1 1
2010 11 09     1  0 2 0 0 0 0 0 0    1  0 0 1 1 1 0 0 0    3  1 2 1 1 0 0 0 0
2010 11 10     3  0 0 0 0 0 1 2 3    1  0 0 1 0 0 0 1 1    4  0 0 0 0 0 1 2 3

SOURCE
http://www.swpc.noaa.gov/ftpdir/indices/old_indices/2010_DGD.txt
```

APPENDIX H: .AVG File Structures

```
$Rx.GdpStn=450
$Rx.Stn=450
$Rx.Length=100 m
$Rx.Cmp=Zxy
Z.mwgt, Z.pwgt, Freq,   Tx.Amp, Z.mag,  Z.phz,   ARes.mag, SRes,   Z.%err, Z.perr, ARes.%err, Coher
1,      1,      0.125,  *,      14.674, -2323.3, 344.5,    344.5,  8.2,    166.2,  16.5,      0.89
1,      1,      0.1875, *,      16.713, -2377.5, 297.95,   297.95, 8.2,    165.3,  16.4,      0.85
1,      1,      0.25,   *,      16.649, -2460.8, 221.74,   221.74, 5.9,    118.5,  11.8,      0.9
1,      1,      0.375,  *,      19.129, -2573.2, 195.16,   195.16, 2.7,    53.4,   5.3,       0.95
1,      1,      0.5,    *,      21.656, -2677.9, 187.59,   187.59, 2.7,    53.9,   5.4,       0.98
1,      1,      0.75,   *,      23.043, -2649.2, 141.6,    141.6,  9.8,    196.9,  19.6,      0.98
1,      1,      1,      *,      23.739, -2729.4, 112.71,   112.71, 1.4,    27.1,   2.7,       0.99
1,      1,      1.5,    *,      27.166, -2725.9, 98.396,   98.396, 2.6,    52.5,   5.2,       0.97
1,      1,      2,      *,      27.301, -2709.9, 74.536,   74.536, 2.5,    50.2,   5,         0.97
1,      1,      3,      *,      28.885, -2659,   55.624,   55.624, 9.4,    188.9,  18.8,      0.97
1,      1,      4,      *,      31.581, -2600.7, 49.869,   49.869, 12.8,   257.5,  25.5,      0.98
1,      1,      6,      *,      36.457, -2476.8, 44.305,   44.305, 0.8,    15.7,   1.6,       0.99
1,      1,      8,      *,      42.918, -2458.7, 46.05,    46.05,  0.4,    9,      0.9,       1
```

Sample AMT/MT .AVG File

Z.mwgt: Electric field weight, -1 indicates polarity flip.
Z.pwgt: Magnetic field weight, -1 indicates polarity flip.
Freq: Frequency (Hertz).
Tx.Amp: Square wave current (amperes), none in AMT/MT.
Z.mag: Impedance magnitude (km/sec).
Ares.mag: Cagniard apparent resistivity magnitude (ohm-m).
SRes: Static-corrected apparent resistivity added by Astatic (ohm-m).
Z%err: Relative |Z| error (%).
Z.perr: Phase(Z) error (mrad).
Ares.%err: Relative apparent resistivity error (%).
Coher: Coherence, or spectral ratio, of cross-correlated electric and magnetic fields (dimensionless), where 1 denotes perfect signal coherence between the fields.

\ ASTATIC v3.50m updated data on 26/01/10

$ ASPACE= 100 m

$ XMTR= 0

Skp,	Station,	Freq,	Comp,	Amps,	Resistivity,	Phase,	%Rho,	sPhz,	TMARES/SRES,	Coher
2,	450,	0.125,	Zxy,	*,	344.5,	-2323.3,	16.5,	166.2,	344.5,	0.89
2,	450,	0.1875,	Zxy,	*,	297.95,	-2377.5,	16.4,	165.3,	297.95,	0.85
2,	450,	0.25,	Zxy,	*,	221.74,	-2460.8,	11.8,	118.5,	221.74,	0.9
2,	450,	0.375,	Zxy,	*,	195.16,	-2573.2,	5.3,	53.4,	195.16,	0.95
2,	450,	0.5,	Zxy,	*,	187.59,	-2677.9,	5.4,	53.9,	187.59,	0.98
2,	450,	0.75,	Zxy,	*,	141.6,	-2649.2,	19.6,	196.9,	141.6,	0.98
2,	450,	1,	Zxy,	*,	112.71,	-2729.4,	2.7,	27.1,	112.71,	0.99
2,	450,	1.5,	Zxy,	*,	98.396,	-2725.9,	5.2,	52.5,	98.396,	0.97
2,	450,	2,	Zxy,	*,	74.536,	-2709.9,	5,	50.2,	74.536,	0.97
2,	450,	3,	Zxy,	*,	55.624,	-2659,	18.8,	188.9,	55.624,	0.97
2,	450,	4,	Zxy,	*,	49.869,	-2600.7,	25.5,	257.5,	49.869,	0.98
2,	450,	6,	Zxy,	*,	44.305,	-2476.8,	1.6,	15.7,	44.305,	0.99
2,	450,	8,	Zxy,	*,	46.05,	-2458.7,	0.9,	9,	46.05,	1

Sample Legacy .AVGo File

Skp: Skip flag, 1=data not used, 2=data used.
Station: Receiver station location.
Freq: Frequency (Hertz).
Comp: Components measured.
Amps: Square wave current (amperes), none in AMT/MT.
Resistivity: Cagniard resistivity (ohm-meters).
Phase: Impedance phase = (E-phase – H-phase) (milliradians).
%Rho: Statistical variation of magnitude values from averaged data blocks
100 * Standard deviation/ Average Rho (percent).
sPhz: Standard deviation of the phase values (milliradians).
TMARES/SRES: Static-corrected resistivity (ohm-meters). No corrections applied for this survey (TMARES/SRES= Resistivity column).
Coher: Coherence, or spectral ratio, of cross-correlated electric and magnetic fields (dimensionless), where 1 denotes perfect signal.